Structural window design for in-plane seismic strengthening

Numerical predictions of strengthening unreinforced masonry structures in Groningen

Master Thesis

Arthur de Groot

TU Delft

Structural window design for in-plane seismic strengthening

by

Arthur de Groot

In partial fulfilment of the requirement for the degree of

Master of Science

in Building Engineering,
faculty of Civil Engineering and Geosciences at Delft University of Technology,

to be defended publicly on Tuesday, July 2th, 2019.

Thesis committee:	Prof. ir. R. Nijsse	Committee chair
	Prof. dr. ir. J.G. Rots	
	dr. ir. H.R. Schipper	
	ir. P.A. Korswagen Eguren	Daily supervisor

An electronic version of this thesis will be available at http://repository.tudelft.nl/.

TU Delft

Preface

This thesis is written to conclude the Master Building Engineering at the faculty of Civil Engineering and Geosciences at Delft University of Technology. The research was conducted under guidance and supervision of my graduation committee at Delft University of Technology. This thesis would not have been possible without them and I would like to express my gratitude for their support and guidance.

To start at where it all began, I would like to thank Rob Nijsse for his suggestion to investigate this special research topic. It has been very interesting to explore the unconventional possibilities of applying structural glass in the field of seismic engineering. Secondly, I would like to thank Paul Korswagen for his accessibility and scientific view. I very much appreciated his flexibility and commitment to meet more frequently whenever needed. The meetings with you provided me valuable in-depth guidance regarding the research setup and (numerical) challenges I faced throughout my thesis. Furthermore, I would like to express my gratitude to Jan Rots for his endless enthusiasm and his help to get in contact with Centrum Veilig Wonen. It has been great to get more insight into their view on the strengthening operation and I was very happy to have had the opportunity to present intermediate results of my research at their engineering department. Finally, I would like to thank Roel Schipper for his open-minded and hands-on design approach. His guidance helped me with the design of the structural window and I truly appreciate his readiness to listen and to think in possibilities.

Lastly, I would like to thank my family and friends for their support and encouragement. In particular, I would like thank Anne for her unconditional support and valuable suggestions on the design of numeruous images in the report and the design of the report as a whole.

Enjoy reading!

Arthur de Groot
Delft, July 2019

Summary

In recent decades, gas production has caused numerous human-induced shallow earthquakes in the province of Groningen, The Netherlands. The buildings in this area were not designed for these unexpected earthquake loads and have shown to be vulnerable. As a result, a share of the existing building stock requires strengthening. However, current strengthening measures are considered to be time-consuming, expensive, and a great hindrance to the residents. Consequently, the question rises whether unconventional strengthening measures can offer relatively simple and quick-to-implement alternatives.

The buildings in Groningen are typically composed of relatively slender load-bearing walls of unreinforced masonry. This results in a very limited seismic capacity. In addition, the seismic capacity is often significantly reduced by the presence of large windows in the load-bearing walls. Conventionally, these windows are completely neglected in structural calculations. This thesis researches if replacing existing windows by structural windows could provide an effective strengthening alternative.

The objective of this thesis is to investigate the influence of the structural window on the in-plane seismic performance of unreinforced masonry structures. This thesis focusses specifically on a masonry wall and a residential terraced house (Dutch: ”Rijtjeshuis”). The latter has been selected because it is the most common building typology, and it often has relatively large windows in its façade walls. Therefore, a structural window is expected to be the most effective for this building typology. The scope of this thesis is limited to only one type of terraced house with two rigid floors, masonry spandrels, and two large windows in the façade wall.

The structural window design aims to increase the in-plane seismic force capacity of an existing masonry structure by utilising the glass pane as a structural element. The structural window is designed to be composed of a timber frame, a semi-rigid adhesive, and a double glazing unit. The structural adhesive is made of Sikaflex-252 and has a thickness of 5mm. The structural layer of the double glazing unit has a thickness of 20mm and is composed of two laminated annealed glass panes with equal thickness. The prefabricated structural window is placed in-plane with the existing load-bearing inner leaf of the cavity wall. The prefabricated structural window is connected to the existing structure by an injection mortar joint, which fills a gap of up to 25mm at all edges of the structural window.

The potential of the structural window is investigated in various numerical studies, using DIANA FEA 10.2 These numerical studies are split into validation studies and seismic strengthening predictions. An overview of the numerical studies is given in figure 1. In the validation studies, results from numerical models are compared to and validated against experimental results reported in literature. Subsequently, the potential of the structural window is assessed by seismic strengthening predictions that combine and extrapolate the validation studies. In the strengthening predictions, the seismic performance of the strengthened masonry structures is compared to the corresponding unstrengthened structure that leaves gaps at the location of the windows. Moreover, the influence of the window size and the inclusion of window sections that can be openened is adressed in the strengthening predictions of the masonry wall and terraced house.

The capacity curve of the structures is determined by adopting a one-directional monotonic pushover loading scheme. The capacity curves are compared to the seismic demand of a ”weak” and ”strong” earthquake at an ”average” and ”extreme” location. The city of Groningen and Appingedam are selected as locations based on the spatial distribution of terraced houses and the PGA contour map. Furthermore, the ”weak” and ”strong” earthquakes are defined as earthquakes with return periods of 95 and 2475 years, respectively. The seismic demand of these earthquakes is given in an acceleration-displacement response spectrum that is retrieved from an online webtool of the NEN.

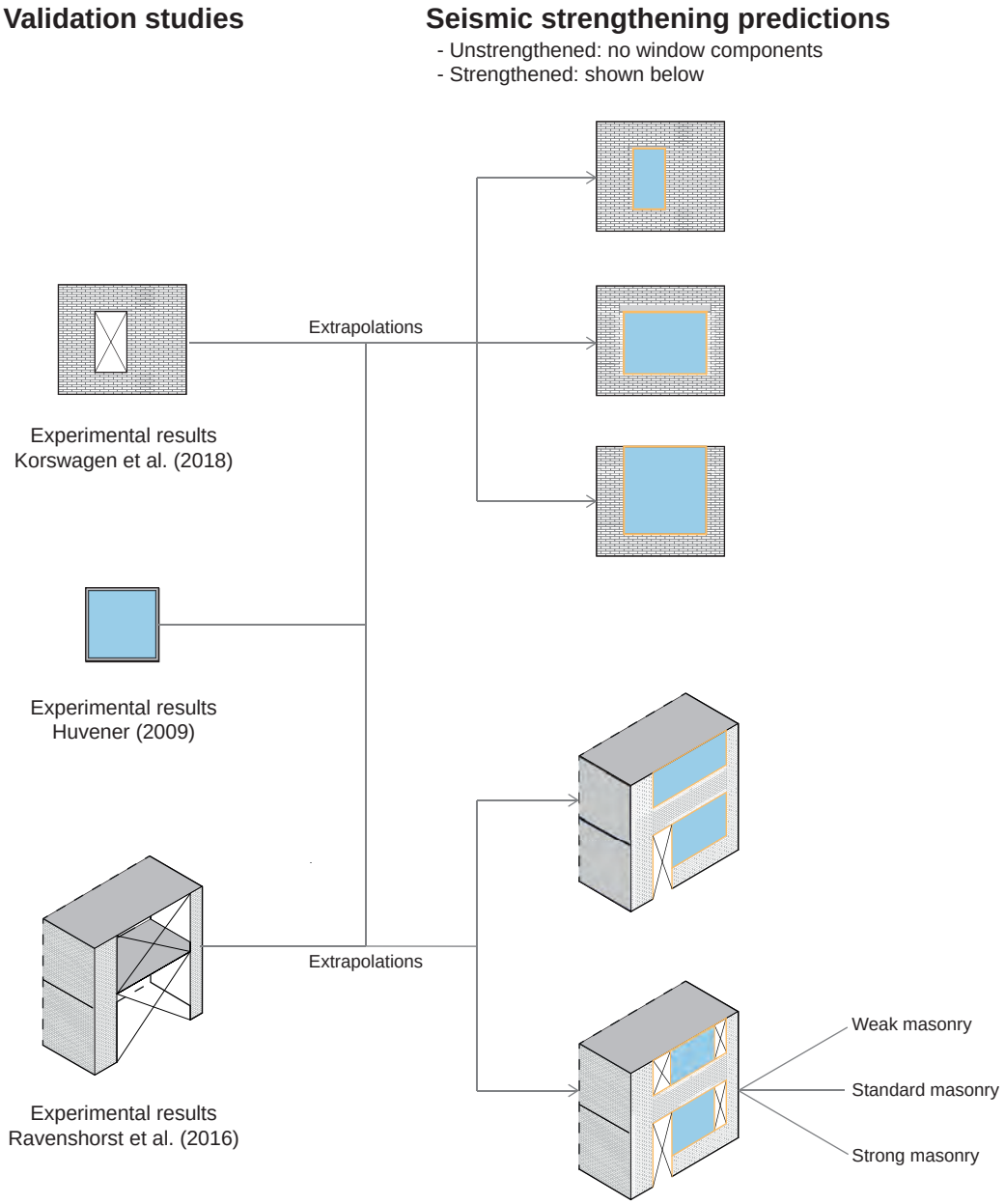

Figure 1: Overview of the numerical studies split into validation studies and seismic strengthening predictions. It is pointed out that only the strengthened masonry structures are shown for the strengthening predictions.

The seismic performance of the unstrengthened and strengthened masonry structure is assessed by the seismic force capacity, a capacity check, and a damage evaluation of the load-bearing superstructure. Additionally, the strengthened masonry structure is checked for failure of the structural adhesive and glass pane. The capacity check is performed for the strong earthquake (NC limit state), while the damage evaluation is performed for the more frequent weak earthquake (DL limit state). The damage evaluation addresses three damage characteristics: the maximum crack width, the number of finite elements with a crack width between 0.1mm and 1mm (damage category 1), and the number of finite elements with a crack width between 1mm and 5mm (damage category 2).

All numerical models solely include the load-bearing superstructure and are composed of 2D continuum finite elements. Moreover, only the front half of the terraced house is modelled, assuming line symmetry in the geometry. Furthermore, it is assumed that all floor/wall connections are fully rigid, except for the anchor connection between the first floor and façade wall. The masonry elements are modelled adopting the macro-modelling approach, i.e. as one smeared composite continuum without

an explicit definition of brick/mortar interfaces. The adopted engineering masonry model incorporates orthotropic and nonlinear material behaviour under tension, compression and shear loading. Strength degradation under repeated loading is not included in this masonry material model.

The numerical predictions of the masonry wall and terraced house indicate that a structural window improves the in-plane seismic performance of the masonry structures significantly. It is found that strengthening not only increases the seismic force capacity, but also reduces the expected damage.

The strengthened masonry walls reach 137%, 300% and 367% of the seismic force capacity of the corresponding unstrengthened wall, depending on the window size. The largest increase in seismic force capacity is found for the case with the largest window size. Moreover, the predictions reveal that the window size mainly influences the seismic force capacity of the unstrengthened wall, while the influence on the strengthened wall is limited.

The strengthened terraced house with openable window sections reaches 205% of the seismic force capacity of the unstrengthened terraced house. It is found that the presence of openable window sections primarily reduces the increase in seismic force capacity, while the reduction of expected damage is relatively unaffected. The strengthened terraced house that utilises the full window area as structural window even reaches 240% of the seismic force capacity of the unstrengthened terraced house. Nevertheless, it is observed that the capacity of the unstrengthened terraced house already is sufficient to withstand the two strong earthquakes. Furthermore, it was found that the strengthening measure greatly affects the composition of the seismic demand. The measure reduces the seismic deformation demand, while it increases the seismic force demand. The stress levels in the glass pane are expected to remain well below the stress levels that were found at the onset of glass cracking. A sensitivity analysis showed that weaker or stronger masonry properties barely influenced the stress levels in the glass pane. In contrast, local failure of the structural adhesive is expected to occur at the corners of the structural window for the two strong earthquakes. For the two weak earthquakes, the structural adhesive is expected to behave elastically.

The numerical predictions are promising. Therefore, it is recommended to validate the numerical strengthening predictions with an experimental testing campaign. It is suggested to adopt a step-wise and pragmatic approach with prototype testing from a small to a large scale, and from a monotonic to a cyclic loading scheme. The assessment of the seismic performance under cyclic loading conditions is an important next step that addresses the residual capacity after multiple earthquakes and the influence of pre-damage. Secondly, it is recommended to improve the numerical model of the terraced house by including the back half of the terraced house, adopting a masonry material model that includes strength degradation under repeated loading, and specifying detailed properties of the floor/wall connections that were assumed to be rigid. Additionally, it was found that the strengthening measure affects the composition of the seismic demand. Therefore, it is recommended to extend the damage evaluation by including connected (non-)structural elements, e.g. the outer leaf of the cavity wall and foundation elements. Furthermore, the design of the structural window focused on the structural performance. It is recommended to improve the performance on traditional requirements of a window, e.g. thermal insulation, water tightness and durability. Lastly, future studies could address variations within the terraced house building typology (e.g. different window sizes and different opening patterns) or other building typologies (e.g. detached and semi-detached houses).

List of symbols

Symbol	Definition	Unit
E_x	Young's modulus parallel to bed-joints	N/mm^2
E_y	Young's modulus perpendicular to bed-joints	N/mm^2
G_{xy}	shear modulus	N/mm^2
f_t	tensile strength	N/mm^2
G_f^I	facture energy	N/m
f_c	compressive strength	N/mm^2
G_c	compressive facture energy	N/m
c	cohesion	N/mm^2
ϕ	friction angle	rad
G_f^{II}	shear energy	N/m
d_a	activation displacement (glass/frame contact)	mm

Acronyms

Abbreviation	Definition
PGA	peak ground acceleration
URM	unreinforced masonry
NC	near collapse
SD	significant damage
DL	damage limitation
TLC	top left corner
TRC	top right corner
BLC	bottom left corner
BRC	bottom right corner
ADRS	acceleration-displacement response spectrum
LE	linear elastic
NLE	nonlinear elastic
Tr	return period
PU	polyurethane
DSF	deformation scaling factor
CS	calcium silicate
EMM	engineering masonry model
CVW	centrum veilig wonen
CoV	coefficient of variation
OWS	openable window sections

Contents

1

Introduction

1.1. Context

Human-induced earthquakes in Groningen

In 1963, gas production started in the province of Groningen, the Netherlands. In recent decades, numerous human-induced shallow earthquakes that are caused by the gas production were experienced in the Groningen area. After the first human-induced earthquake in 1991, the total number of earthquakes currently exceeds 1,000. Figure 1.1 gives an overview of the occurrence of different earthquake magnitudes. Most earthquakes have a local magnitude below 1.5 and are barely noticeable. However, this innocent character was lost when an earthquake with a magnitude of 3.6 hit Huizinge in August 2012. This earthquake caused substantial damage to numerous buildings and social unrest in the Groningen area. At the time of writing (June, 2019), this earthquake remains to be the strongest earthquake that has been recorded in Groningen area. [1] However, current seismic hazard calculations even include a maximum expected magnitude of 5.0. [2]

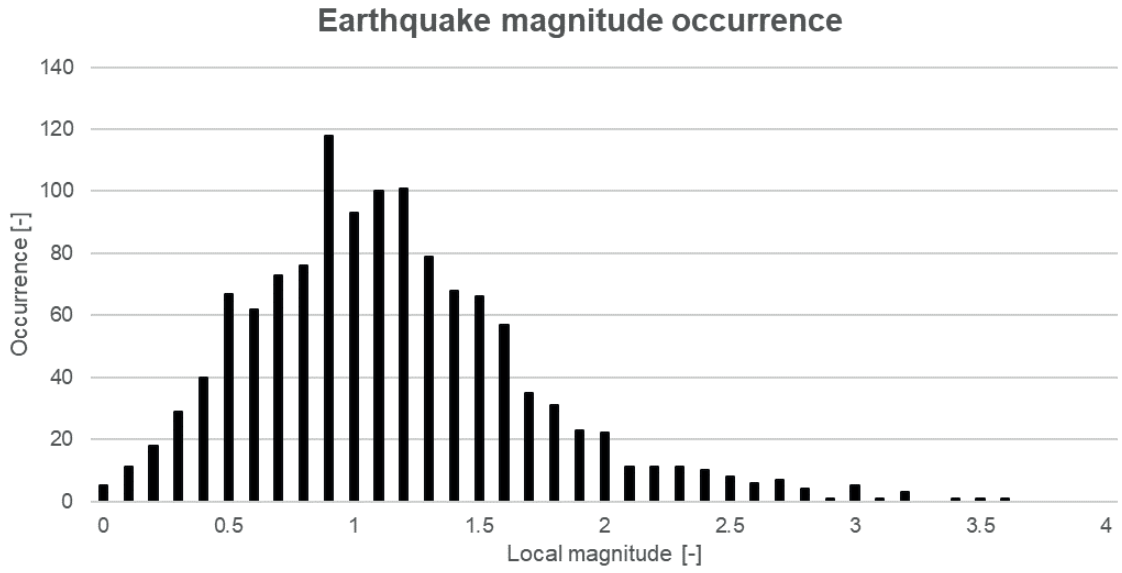

Figure 1.1: Distribution of earthquake local magnitude until August 2018 in the Groningen area based on [1].

Figure 1.2 shows the outline of the Groningen gas field and the most recent seismic hazard map of the KNMI from June 2017.[1] The contour plot indicates a maximum expected peak ground acceleration of 0.24g with a return period of 475 years.

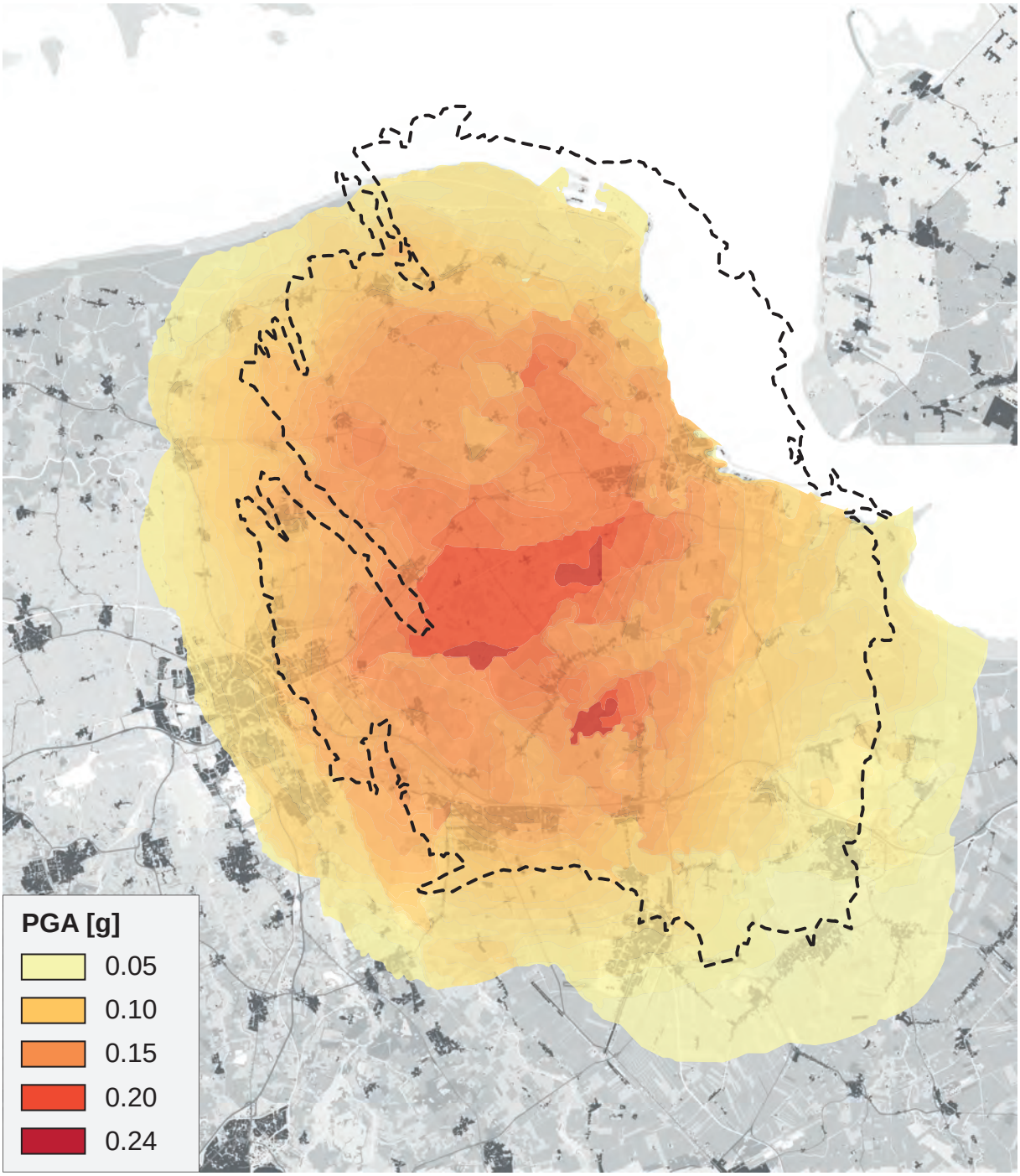

Figure 1.2: Outline of Groningen gas field and maximum PGA with Tr=475 years based on [2].

[1] Update: the most recent seismic hazard map currently dates from October 2018 and can be found at [3].

Status quo

In March 2018, the Dutch government has decided to significantly reduce the gas production from the Groningen gas field. Figure 1.3 shows that the gas production is gradually decreased to 0 in 2030.

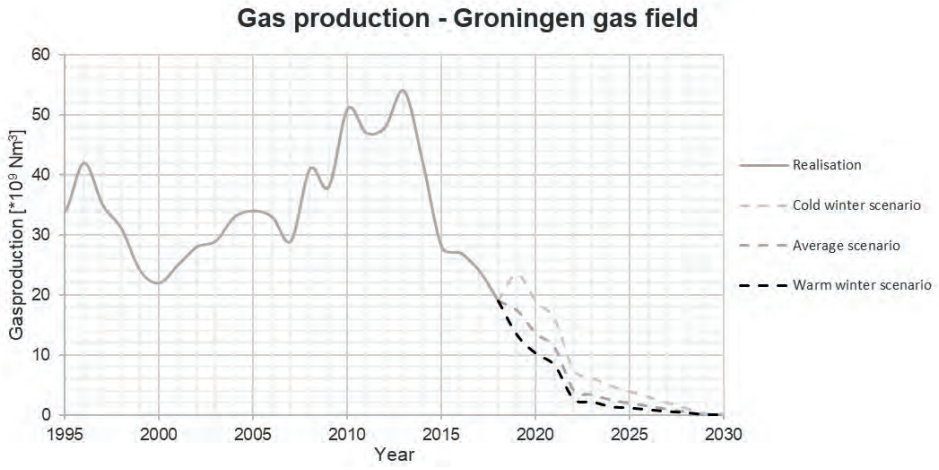

Figure 1.3: Realisation (1995-2018) and prediction (2018-2030) gas production in Groningen for different winter scenarios. [4, 5]

This gas production reduction is expected to lower the maximum PGA in the Groningen area. Nonetheless, the maximum expected local magnitude for the Groningen area remained 5.0. [6] Consequently, it is expected that a significant number of buildings in the Groningen area require strengthening.

Seismic strengthening

The buildings in the Groningen area typically have a load-bearing structure of unreinforced masonry and prove to be vulnerable to these unexpected earthquake loads. As a result, seismic strengthening of part of the existing building stock in the Groningen area is required. A total number of 22,000 buildings has been scheduled for inspection. At the end of 2018, almost 10,000 buildings were inspected of which 3,352 buildings required strengthening measures. However, only 421 buildings have been strengthened until the end of 2018. [7]

Specifically, the stability of residential terraced houses proves to be problematic. Additionally, the terraced house is the most frequently found building typology in the Groningen area. [8] Contractors often choose for very radical and time-consuming strengthening measures for these terraced houses. Figure 1.4 shows two examples of strengthening measures that have been applied to terraced houses in the Groningen area.

Figure 1.4: Strengthening of terraced houses in longitudinal direction with a steel frame inside the cavity [9] or a steel supporting structure at the end wall. [10]

Both solutions prove to be very time-consuming and expensive. For example, the steel frame inside the cavity of the cavity wall requires removal of the outer leaf before the steel frame can be placed. This stage is shown in figure 1.5. Furthermore, this solution requires extending the existing foundation elements and rebuilding the outer leaf. As a result, these conventional strengthening measures for the terraced houses cause a great hindrance to the residents. Therefore, some residents of terraced houses prefer a new building to retrofitting of the existing building. [11] Consequently, the question rises whether relatively simple and quick-to-implement strengthening measures can offer adequate alternatives.

Figure 1.5: Stripped terraced house with the outer leaf removed before placing the steel frame in the cavity. [10]

Structural modelling

It has been noticed that the interaction between the main load-bearing structure and windows is neglected both in literature, and earthquake engineering practice. In literature, only research is found in which either the window [12, 13] or masonry structure [14–16] is considered separately. In earthquake engineering practice, structural models only contain the main load-bearing structure leaving openings at the location of windows. [17] Consequently, these openings are of interest for potential strengthening measures. This hypothesis is summarized in figure 1.6.

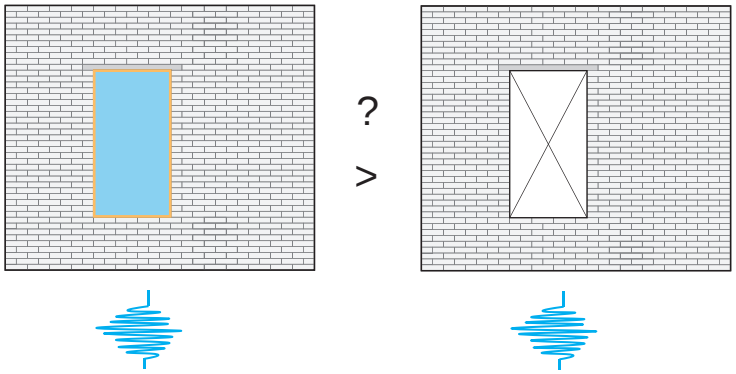

Figure 1.6: Could a structural window improve the in-plane seismic performance of unreinforced masonry structures?

1.2. Objectives

This thesis aims to assess the influence and potential of windows on the in-plane seismic performance of unreinforced masonry (URM) structures. The research will focus on seismic strengthening of existing unreinforced masonry structures in the Groningen area with a structurally designed window. The seismic performance of strengthened URM structures will be compared with unstrengthened URM structures. The unstrengthened URM structures leave an opening at the location of the window, while the strengthened URM structures incorporate the structural window.

Main question

The main question is formulated as follows:

"How could a structural window design improve the in-plane seismic performance of unreinforced masonry structures?"

Sub questions

The sub questions are structured in three parts:
Part I: Literature review
Part II: Structural window design
Part III: Numerical modelling and assessment

Part I: Literature review

1. How can the seismic performance of unreinforced masonry structures (including structural windows) be assessed?
2. What are conventional seismic retrofit strategies and how could these be incorporated in a structural window design?

Part II: Structural window design

3. Which additional requirements, both functional and practical, should be incorporated in the design of a structural window?
4. What are the components of the designed structural window and how can these be modelled?

Part III: Numerical modelling and assessment

5. What is the influence of the designed structural window on the in-plane seismic performance of unreinforced masonry structures on the scale of a structural element, i.e. an URM wall?
- *a. Damage limitation limit state*
- *b. Near collapse limit state*

6. What is the influence of window size on the structural potential of the designed structural window?
7. What is the influence of the designed structural window on the in-plane seismic performance of unreinforced masonry structures on the scale of a structure, i.e. a terraced house?
- *a. Damage limitation limit state*
- *b. Near collapse limit state*

8. What is the influence of openable window sections on the structural potential of the designed structural window?

1.3. Methodology and outline

This thesis consists of three main parts.

Part I describes the theoretical framework of this thesis and is based on a literature review. Chapter 2 elaborates on the building stock in the Groningen area. Two locations are selected for the seismic assessment based on the spatial distribution of terraced houses, and the PGA contour map. Hereafter, the principles of the assessment of the seismic performance are outlined in chapter 3. The behaviour of URM structures under seismic loads is discussed qualitatively in chapter 4. Chapter 5 gives an overview of conventional seismic retrofitting strategies and specific measures for in-plane strengthening that are applied in the Groningen area. In chapter 6, frame-glass composite walls are discussed focussing on their behaviour under lateral load, and components. These frame-glass composite walls could potentially be applied as structural window and provide an innovative in-plane strengthening measure for URM structures.

Part II will elaborate on the design of the structural window. After the formulation of a design goal, the materialisation of the different components of the structural window is explained in chapter 8. In chapter 9, valuable feedback from conversations with seismic retrofitting experts from CVW, and an expert in renovation work is addressed.

Part III assesses the potential of the designed structural window for in-plane seismic strengthening of URM structures. This assessment is performed based on numerical studies in DIANA FEA 10.2. This part is divided into two types of studies: validation studies and seismic strengthening predictions. The validation studies are validated with experimental results found in literature and are used as a valuable starting point for the seismic strengthening predictions. An overview of the validation studies is shown in figure 1.7. The validation studies are performed adopting a step-wise approach with increasing scale and complexity at each step. First of all, a window model is validated based on experiments by Huveners [18] in chapter 11. Hereafter, numerical models of an URM wall and an URM two-storey building are validated based on experiments by Korswagen et al. [19] and Ravenshorst et al. [20] in chapter 12 and 14 respectively.

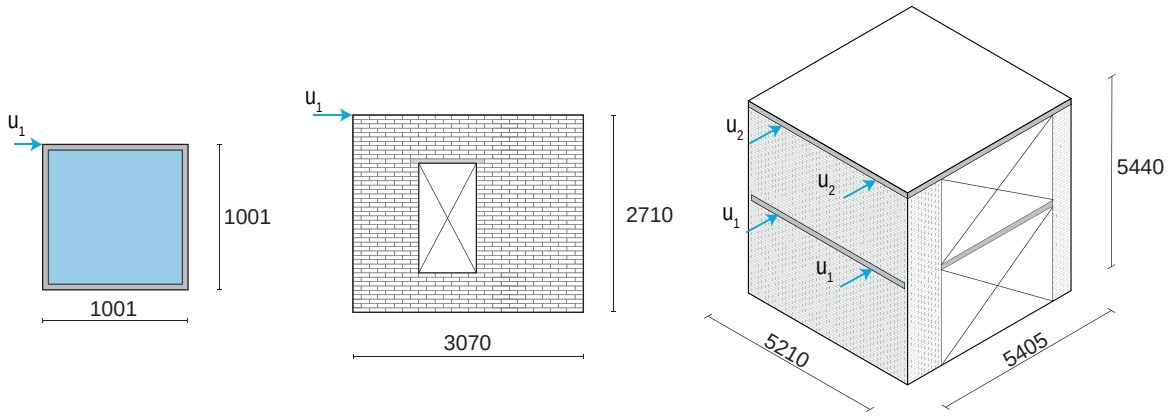

Figure 1.7: Overview of validation studies from small to large: window, URM wall, two-storey building.

In the seismic strengthening predictions, the seismic performance of strengthened models that include structural window(s) is compared to the seismic performance of unstrengthened models that leave a gap at the location of window(s). An overview of the performed seismic strengthening predictions for the URM wall is given in figure 1.8. These predictions address three different window sizes. The seismic strengthening predictions for the URM wall can be found in chapter 13. An overview of the performed seismic strengthening predictions for the terraced house is given in figure 1.9. The influence of the incorporation of ventilation possibilities is investigated by leaving gaps at part of window area. The gaps represent window area that can be opened for natural ventilation. The seismic strengthening predictions for the terraced house are discussed in chapter 15.

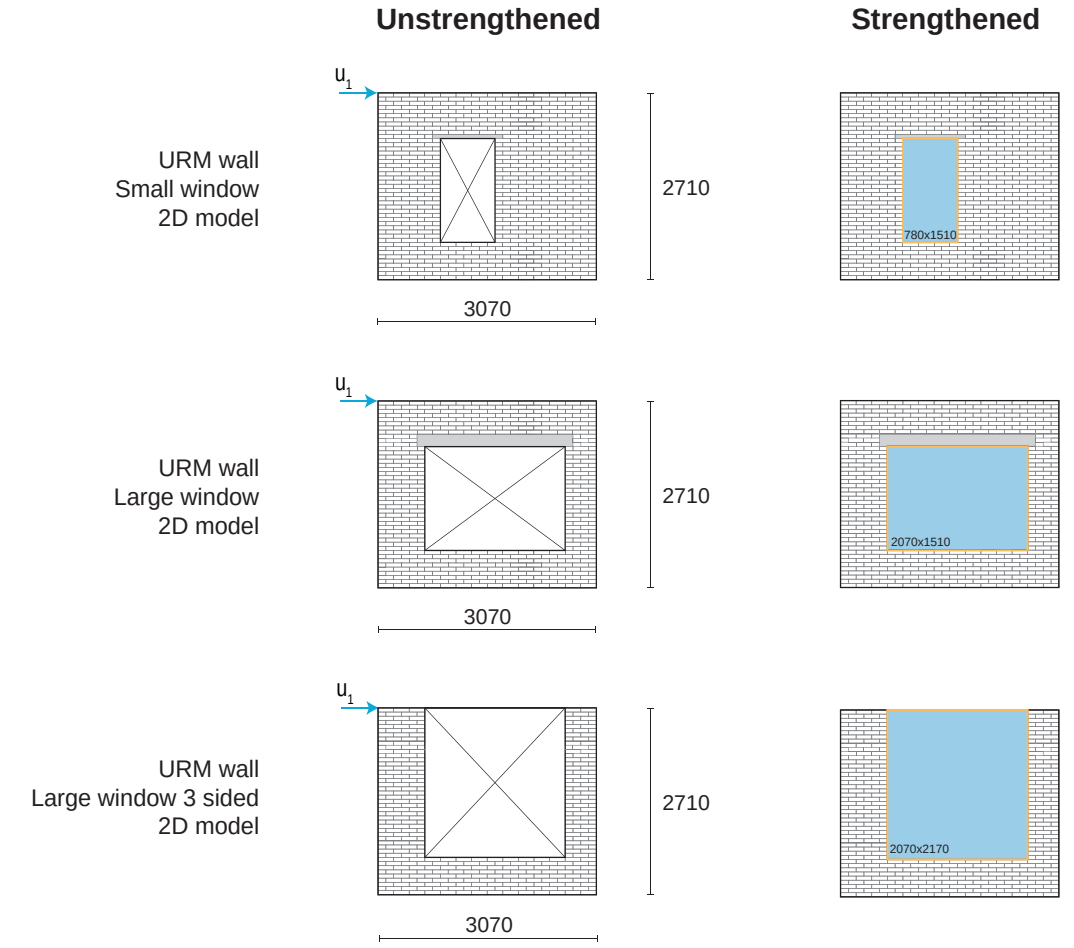

Figure 1.8: Overview of seismic strengthening predictions for the URM wall, addressing different window sizes.

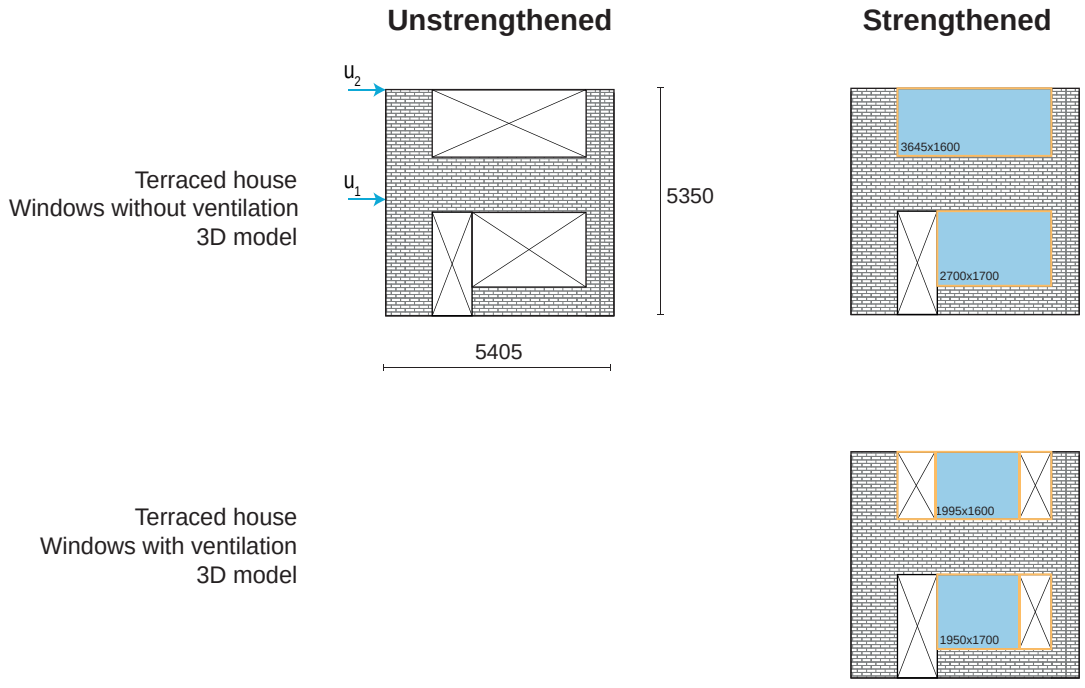

Figure 1.9: Overview of seismic strengthening predictions for the terraced house, addressing ventilation possibilities.

1.4. Scope and limitations

This thesis aims to assess the effect of a structural window on the seismic performance of the unreinforced masonry structures. However, it is impossible to address all variations found in terms of building typologies, material properties, windows, seismicity, etc. Therefore, it is chosen to focus on only one building typology in the province of Groningen.

Residential terraced houses are chosen as building typology of interest. This building typology is most frequently found in the province of Groningen and has a relatively high percentage of window area in its façade walls. Consequently, a structural window is expected to be most effective for this building typology. In addition, this thesis will be tailored to residential terraced houses that were built between 1960 and 1980. Figure 1.10 shows a typical example of a residential terraced house from 1960-1980 in the province of Groningen.

Figure 1.10: Typical example of residential terraced house from 1960-1980 in the province of Groningen. [21]

The numerical representation of the unreinforced masonry structure only includes the stability elements of the superstructure. The following elements have not been modelled explicitly:

- Roof structure.
- Outer leave of cavity walls.
- Secondary elements, e.g. non loading-bearing walls.
- Substructure, e.g. foundation elements.
- Mortar and bricks. Masonry has been modelled as one orthotropic composite continuum (macro-modelling approach).
- Back facade wall and half of the transverse walls. Only the front half of the terraced house is modelled assuming line symmetry in geometry. Thus, the front and back facade walls are assumed to be identical in terms of the location and size of the window(s) and door.

The numerical analysis of the unreinforced masonry structure focusses on the effect of the structural window on the in-plane seismic performance. The following aspects have been disregarded:

- Out-of-plane loading. The effect of the structural window on the seismic performance in the out-of-plane direction is expected to be negligible.
- Vertical seismic load. The seismic load has a vertical component. However, this component is generally significantly smaller compared to the horizontal component. Therefore, this vertical component of the seismic load is neglected.

- Strength degradation in masonry under repeated loading. The adopted material model for masonry (EMM) does not incorporate strength degradation. Therefore, a monotonic loading scheme is adopted. This is expected to give similar results to a cyclic loading scheme, while it significantly reduces computation time.
- Failure of several structural elements. Failure is only taken into account in the material model of masonry and structural adhesive because these are expected to be governing.
- Soil structure interaction. In the model, the superstructure is fully fixed at its base.

2

Building stock in the Groningen Area

2.1. Residential terraced houses

This thesis will focus on residential terraced houses of unreinforced masonry. A terraced house refers to one unit of a row of similar dwellings that share side walls. Terraced houses are also known as ”row houses”, ”townhouses” or ”rijtjeshuizen”. Arup has carried out a building typology approach for the seismic evaluation and assessment of the building stock in the study area. The study area is outlined in black in figure 2.1 and contains more than 150,000 buildings. [22]

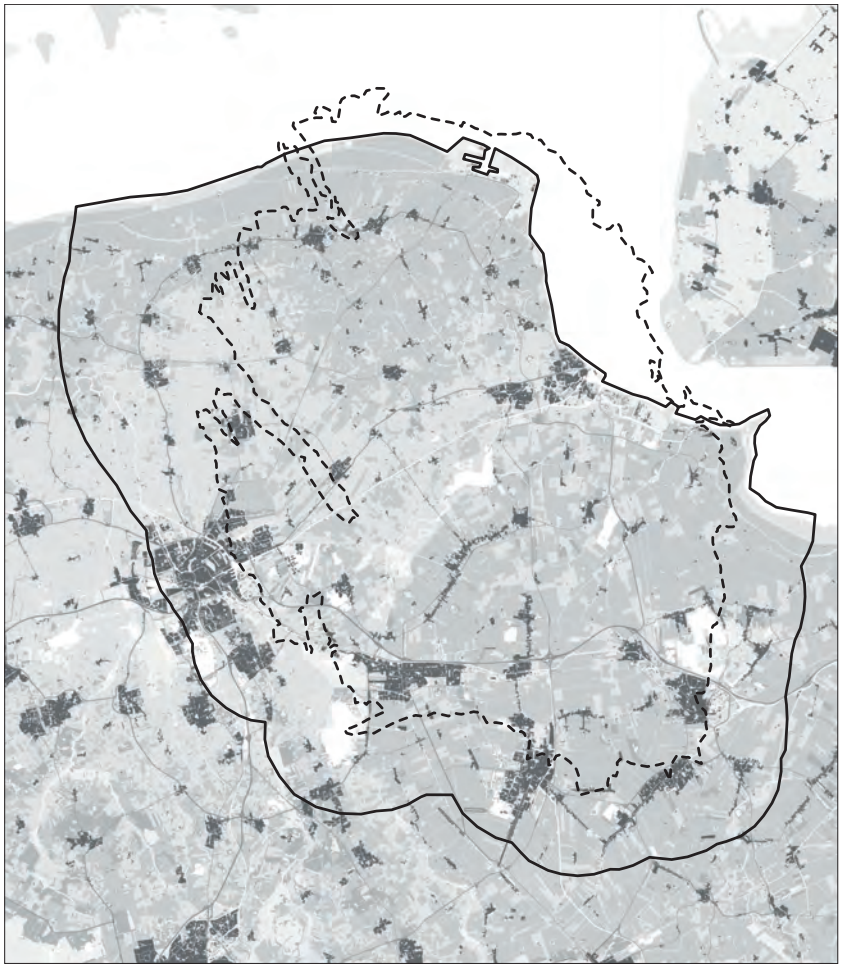

Figure 2.1: Outline of Groningen gas field and extended study area that has been adopted in this thesis based on [22].

The building stock in the study area around the Groningen field has been divided in 56 typologies. The 8 main typologies area based on building use and adjacency:

- Residential detached (RESD)
- Residential semi-detached (RESS)
- **Residential terraced (REST)**
- Residential apartment (RESA)
- Mixed residential / commercial apartment (RECA)
- Agricultural, industrial, and large commercial (AIC)
- Commercial (COMO)
- Miscellaneous (MISC)

The division of the building stock over these main typologies is shown in figure 2.2. The residential terraced house is the most common building typology representing more than 40% of the total building stock. Within the main building typologies, sub typologies are distinguished based on material, and structural system. Figure 2.2 shows that almost 90% of the buildings have a load-bearing structure made of unreinforced masonry (URM).

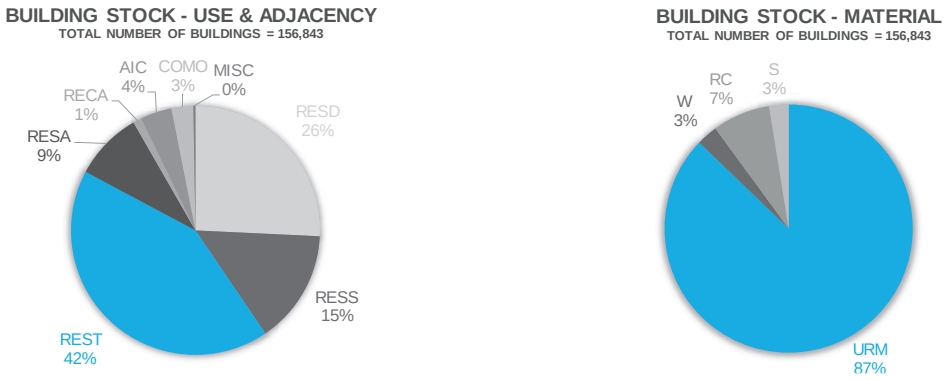

Figure 2.2: Building stock divided over main typologies (left) and material use (right) based on [8].

In addition, the residential terraced houses are of specific interest because of their clear distinction between the transverse and longitudinal directions. In contrast to detached and semi-detached houses, the terraced houses are characterized by large openings in the longitudinal direction resulting in a relatively low capacity. [23]

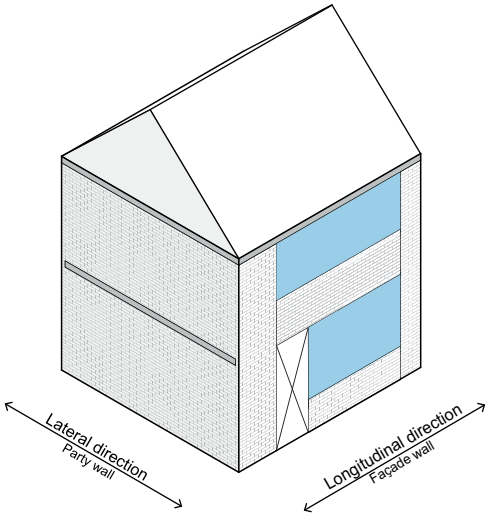

Figure 2.3: Typical terraced house with large windows in façade wall resulting in a low capacity in the longitudinal direction.

A large variety is observed in the lay-out of the front façade of residential terraced houses in the Groningen area. Typical examples of residential terraced houses in the Groningen area are shown in figure 2.4. A division into three categories is made based on the number, and size of windows in the front façade.

Category 1
Number of windows (>1m²) : 2
Window at first floor level: 1 large window

Category 2
Number of windows (>1m²) : 3
Window at first floor level: 2 windows

Category 3
Number of windows (>1m²) : 2
Window at first floor level: 1 window

Figure 2.4: Variety and classification of typical terraced houses in the Groningen area based on windows in the front façade [24].

Figure 2.5 shows that the terraced houses are unequally distributed over the study area and mainly concentrated at the boundaries of the study area. The city of Groningen and Appingedam are selected based on the spatial distribution for the seismic assessment. The city of Groningen is chosen as an average location and the Appingedam as extreme location for the seismic assessment.

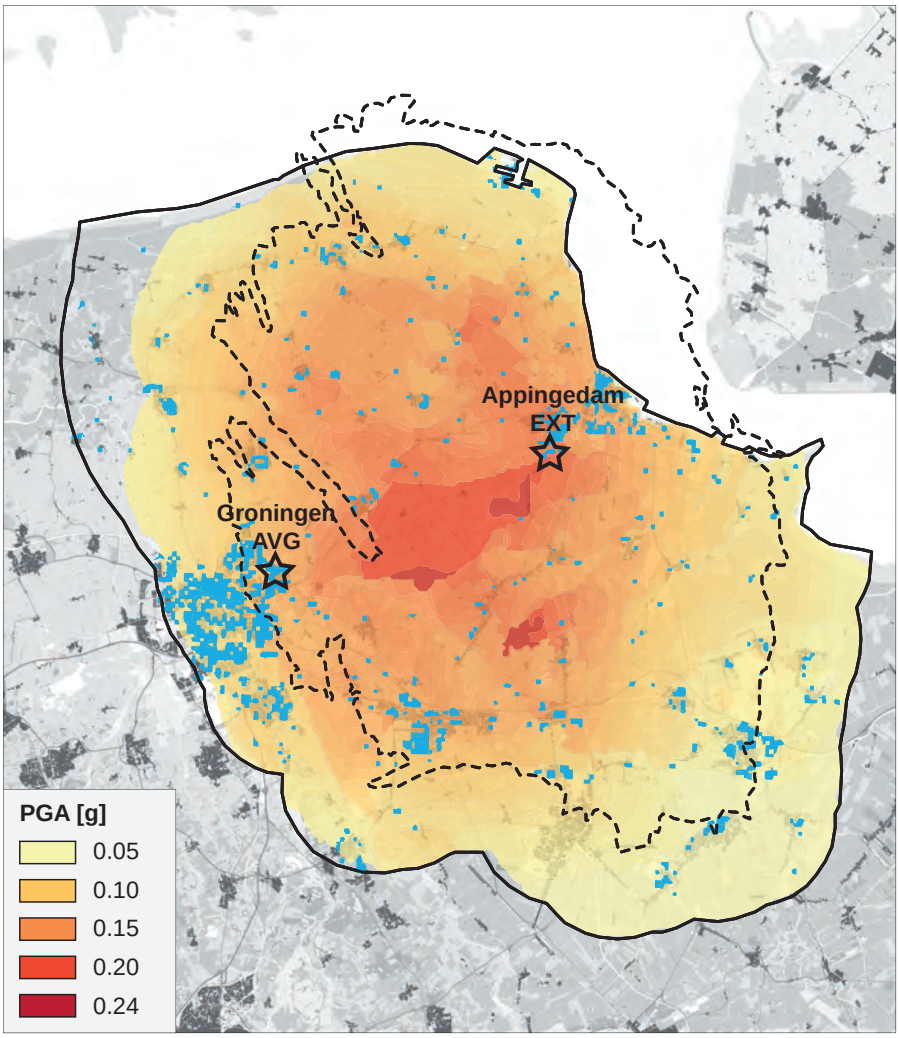

Figure 2.5: Spatial distribution of terraced houses over the study area indicated with blue dots based on Crowley et al. [8]

2.2. Conventional windows designs

Structural contribution

The influence of conventional windows on the seismic performance of unreinforced masonry structures in the Groningen area can be qualitatively assessed. First of all, the position of the stiff glass panes with respect to the load-bearing inner leaf of the cavity is of importance. Figure 2.6 schematically shows three options for the position of the window: shallow, standard and deep. It is expected that the contribution of the window to the seismic performance of the load-bearing structure can be neglected for the shallow and standard positions. This is the result of the eccentricity between the inner leaf and glass panes. For the deep positioning of the window, it is noticed that a layer of insulation is added below the window. This layer of insulation is not expected to be capable of transferring forces between inner leaf and glass pane. Based on this qualitative assessment, it is expected that the contribution of conventional windows is indeed negligible.

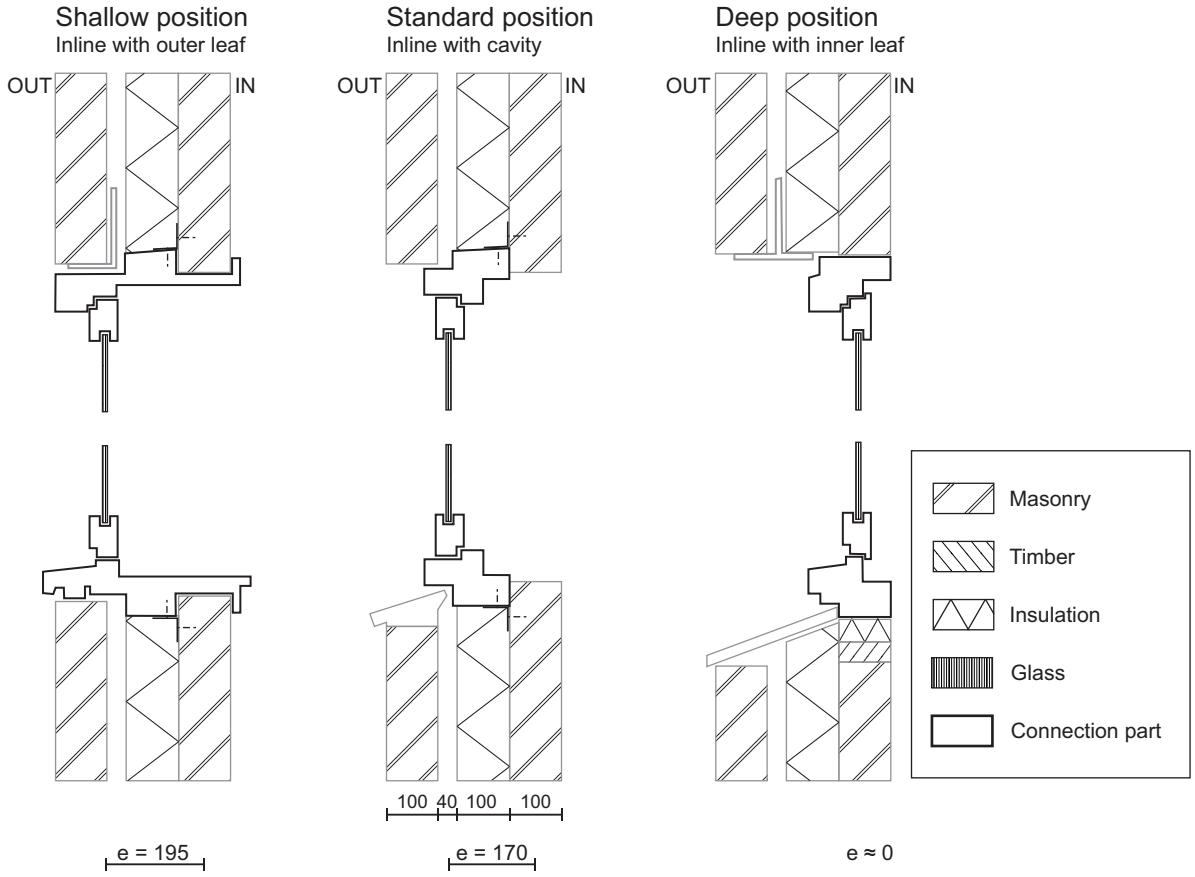

Figure 2.6: Schematization of position, and connection of the glass pane with cavity wall: shallow [25], standard [26] deep [25]

Conventional requirements

Figure 2.1 gives an overview of the requirements for conventional windows. The requirements are divided over four categories: safety, health, usability and energy. The structural safety considers wind, and user loads.

Table 2.1: Overview of requirements for conventional windows divided over four categories based on [25]

Safety	Health	Usability	Energy
Structural safety Fire safety Burglary protection	Water tightness Condensation prevention Acoustic performance Ventilation possibility Daylight admittance	Stiffness Operation Accessibility	Thermal insulation Air permeability

3

Seismic performance assessment

3.1. Calculation methods

Multiple calculation methods exist for obtaining the response of a structure under dynamic loads. The accuracy and complexity varies significantly between the different methods. There are four main calculation methods available which are differentiated based on two criteria:
- The incorporation of nonlinear material behaviour.
- The applicability for multi degree of freedom (MDOF) systems.

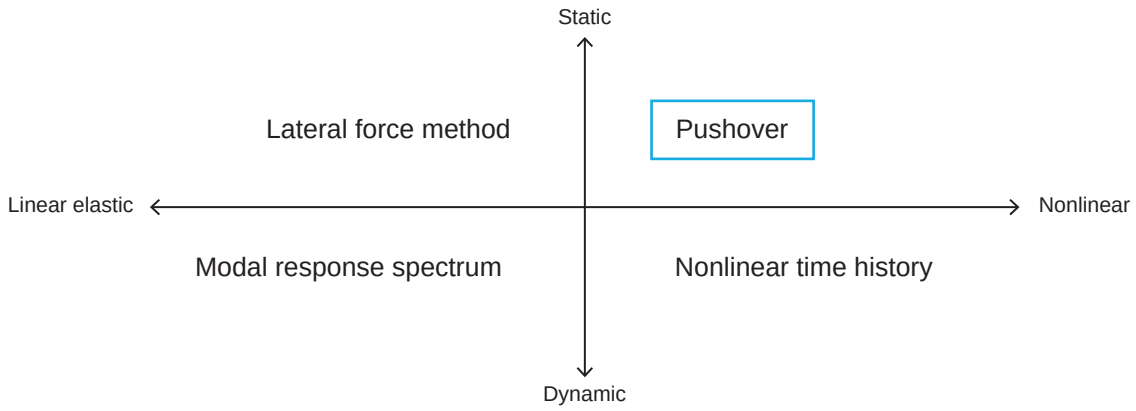

Figure 3.1: Overview of the four main calculation methods used in earthquake engineering.

Linear elastic methods are not designed to accurately calculate the nonlinear behaviour of a structure under ”large” loads, but to make quick and conservative calculations possible. This makes them inadequate for the aim of this research. Nonlinear methods are required to get insight into the actual behaviour of a structure under ”large” loads. Figure 3.1 shows that there are two calculation methods possible: pushover or nonlinear time history. The nonlinear time history yields the most accurate results, but this comes at a price. This calculation method is time consuming and requires multiple calculations with different ground motions. The NPR recommends to use 11 sets of ground motions to assess the NC limit state. [17] Consequently, the pushover method is preferred for a structure that can be considered ”simple”. The dynamic response of simple structures is governed by its fundamental vibration mode. This feature allows for the simplification of transforming the structure to a generalized single degree of freedom system. Terraced houses generally allow for this simplification. Therefore, the pushover method is adopted in this thesis.

3.2. Limit states

In earthquake engineering a differentiation is made between three limit states according to which a structure can be calculated. These limit states are related to the degree of damage to the load-bearing structure. A description of each limit state in given in NPR9998. [17]

- Near collapse (NC) limit state: calculation with a earthquake that has a return period of 2475 years. This corresponds to chance of occurrence of 2% in the 50-year design life of terraced houses.
- Significant damage (SD) limit state: calculation with a earthquake that has a return period of 475 years. This corresponds to chance of occurrence of 10% in the 50-year design life of terraced houses.
- Damage limitation (DL) limit state: calculation with a earthquake that has a return period of 95 years. This corresponds to chance of occurrence of 40% the 50-year design life of terraced houses.

The NC and DL limit state will be adopted to evaluate the seismic performance. The structural capacity will be assessed for a strong earthquake (Tr=2475 years), while the damage is evaluated for a weak earthquake (Tr=95 years) .

3.3. Evaluating seismic performance

There is no single criterium capable of capturing the seismic performance of a structure. The seismic capacity of a structure can be evaluated based on its force and deformation capacity. However, it should be noted that seismic demand highly depends on structural characteristics, e.g. global stiffness and mass. Therefore, the seismic performance has to be assessed based on at least these two criteria. In addition, it is important to address a third criterium: damage. Damage, i.e. cracks in masonry, does not necessarily result in the collapse of a structure, but it does negatively affect the sense of safety of the users.

Seismic capacity

The capacity curve of a structure can be obtained by either a pushover analysis or nonlinear time history analysis. The envelope of the obtained force-displacement diagram, also referred to as the back bone, gives the capacity curve of a structure. A typical shape of a capacity curve is shown in figure 3.2. It should be noted that not only the force, but also the deformation capacity is of interest. The deformation capacity is indicated by the red cross in figure 3.2.

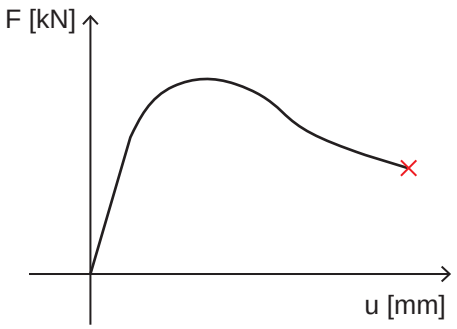

Figure 3.2: Typical shape of a capacity curve of a masonry structure with failure indicated by the red cross.

Seismic demand

The seismic demand is typically shown in an acceleration-displacement response spectrum (ADRS) and consists of two components: a deformation demand and force demand. The balance between these two components is determined by the intersection between the ADRS and the capacity curve of the considered structure. Therefore, the composition of the seismic demand also depends on structural characteristics, e.g. global stiffness (k) and mass (m).

Figure 3.3 illustrates the significant difference in the seismic demand composition for a fictitious short-period, and long-period structure. Short-period structures have a relatively low m/k ratio and are generally loaded by a relatively low deformation but high force demand. In contrast, long-period structures have a relatively high m/k ratio and are generally loaded by a relatively low force but high deformation demand.

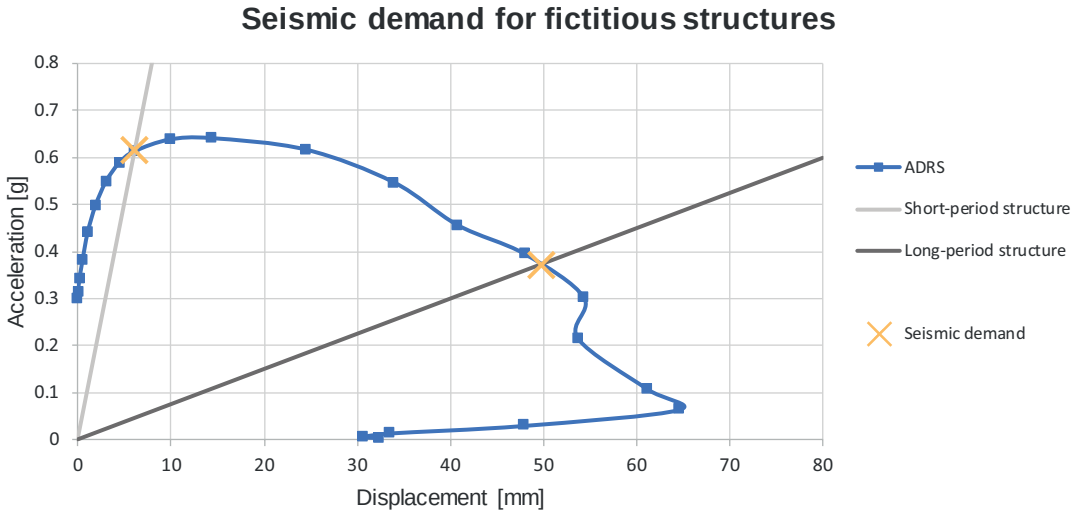

Figure 3.3: Seismic demand composition for a fictitious LE short-period and long-period structure indicated by yellow cross.

The eigen period (T) of a structure is proportional to the root of the m/k ratio. Figure 3.4 qualitatively shows the effect of changing the eigen period on the seismic demand. It is observed that period shortening and period elongation generally results in a lower and higher deformation demand respectively. In contrast, the effect of changing the eigen period on the force demand is less clear. Figure 3.4 shows that period shortening may result in a lower force demand for a short-period structure, while for a long-period structure a higher force demand can be expected.

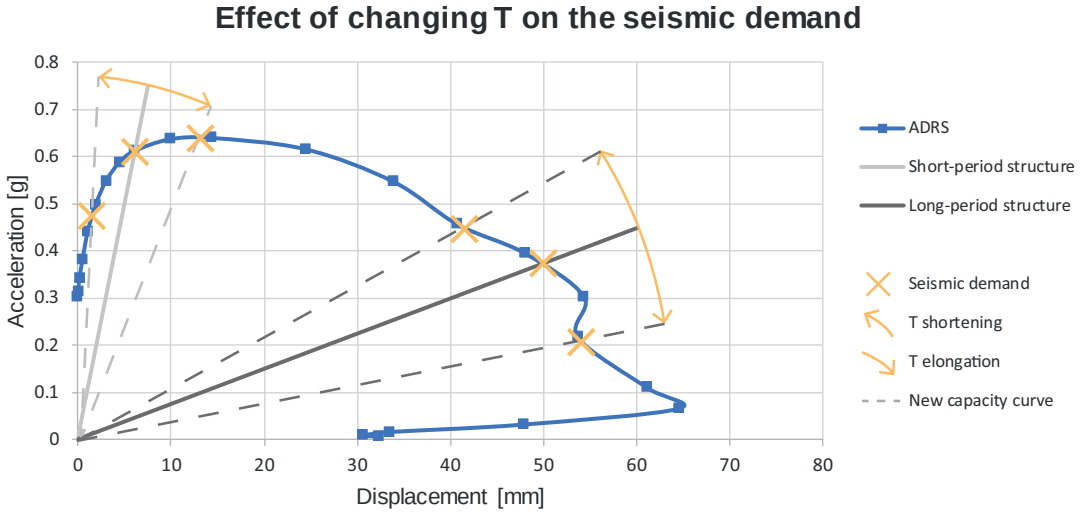

Figure 3.4: Effect of changing T for a fictitious LE long-period and short-period structure

This relation between the capacity curve and the corresponding seismic demand is of importance for the assessment of seismic retrofitting measures. The effectiveness of seismic retrofitting measures largely depend on the capacity curve of the considered structure.

An online webtool has been developed by the NEN providing response spectra for different locations in the province of Groningen. This webtool gives a prediction of the response spectrum caused by earthquakes with different return periods. [3] Figure 3.5 shows the ADRS for a ”weak” and ”strong” earthquake at the two selected locations. These weak and strong earthquake have a return period of 95 years and 2475 years respectively. This corresponds to the DL and NC limit state.

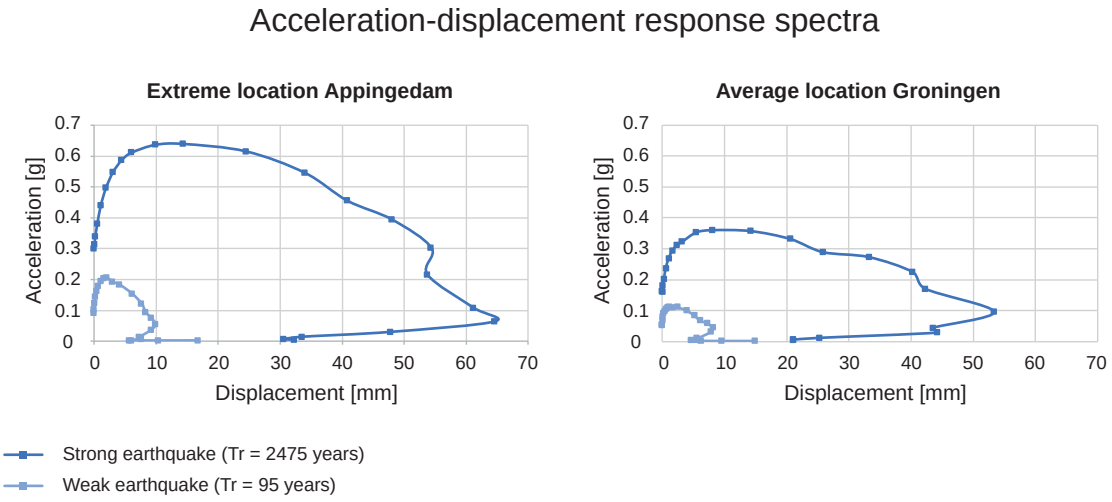

Figure 3.5: Acceleration-displacement response spectra for a ”weak” and ”strong” earthquake at the two selected locations based on [3]

It can be seen that the four earthquakes cover a wide range in seismic demand. The strong earthquake in Appingedam gives a maximum acceleration demand of $0.64g$ and a maximum deformation demand of $65mm$.[1] The weak earthquake in Groningen gives a maximum acceleration demand of $0.11g$ and a maximum deformation demand of $8mm$.

Damage

The damage to a structure is difficult to quantitatively assess. Different damage classifications system are reported in literature varying from simple, e.g. Giardina et al. [27], to more complex classification systems, e.g. Korswagen et al. [19]. Giardina et al. [27] reports damage categories for masonry structures based on the maximum crack width only. These damage categories are adopted in this thesis and are shown in table 3.1.

Table 3.1: Damage classification for masonry based on [27]

Damage category	Crack width [mm]	Classification
0	<0.1	Negligible
1	0.1 - 1.0	Very slight
2	1.0 - 5.0	Slight
3	5.0 - 15.0	Moderate
4	15.0 - 25.0	Severe
5	>25.0	Very severe

[1] Force and acceleration have been used interchangeably. These are directly proportional through the effective mass of the considered structure that is assumed to be constant (independent of the window size and the installation of the structural window).

4

Unreinforced masonry structures

4.1. Masonry terminology

Figure 4.1 gives an overview of the different components of a perforated masonry wall on the scale of the structural element and material. On both scales, elements are distinguished based on their orientation. For the structural element scale, parts of the masonry wall that orientated vertically are referred to as piers, while horizontally-orientated parts are known as spandrels. Similarly, a distinction is made between head and bed joints on the scale of the material.

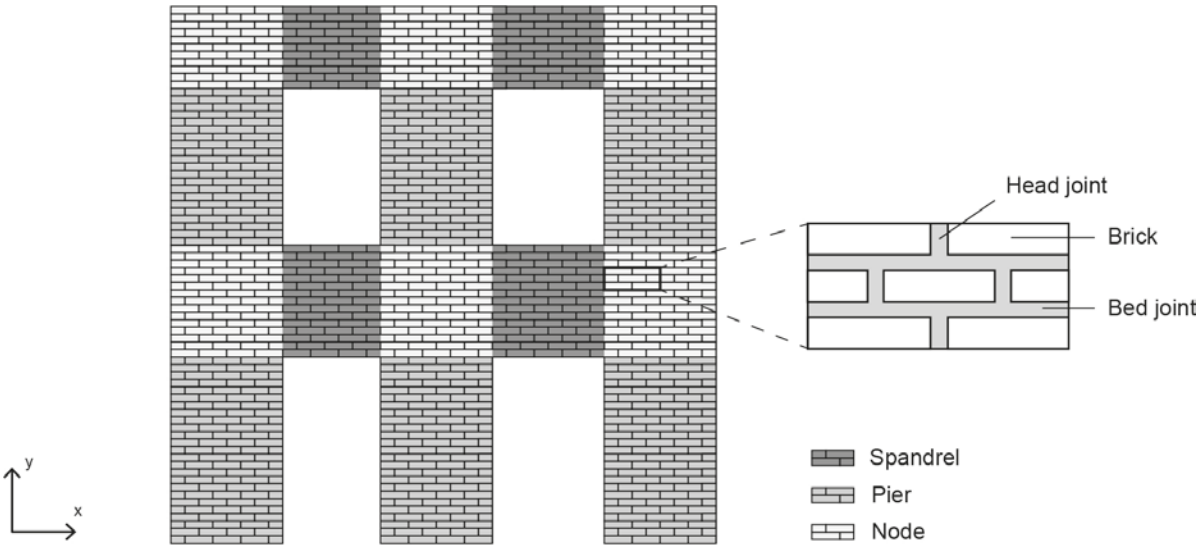

Figure 4.1: Components of a masonry wall on element and material scale based on [28]

In the Netherlands, masonry structures are typically unreinforced. This type of masonry is known to be very vulnerable to seismic loads because of its low tensile strength. However, the seismic resilience of masonry can be improved by applying confinement or reinforcement. These types of masonry are often found in regions with seismic activity. Figure 4.2 gives an overview of these commonly used types of masonry.

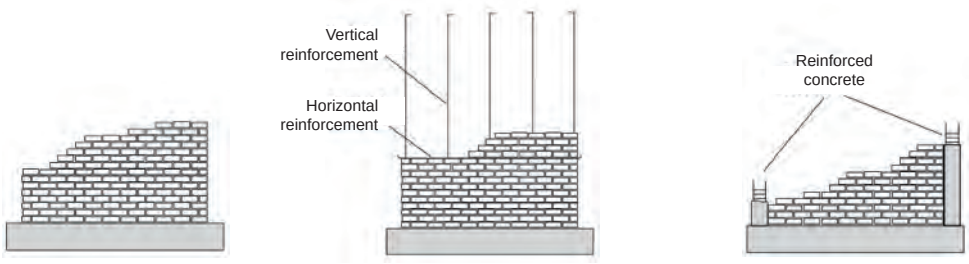

Figure 4.2: Different types of masonry based on [28]

4.2. Behaviour under seismic loads

Figure 4.3 shows a perforated boxed masonry structure under a seismic load. In this example, only one direction of seismic action is considered. It can be seen that this simplified seismic load results in a deformation at first floor level and cracking of the masonry walls.

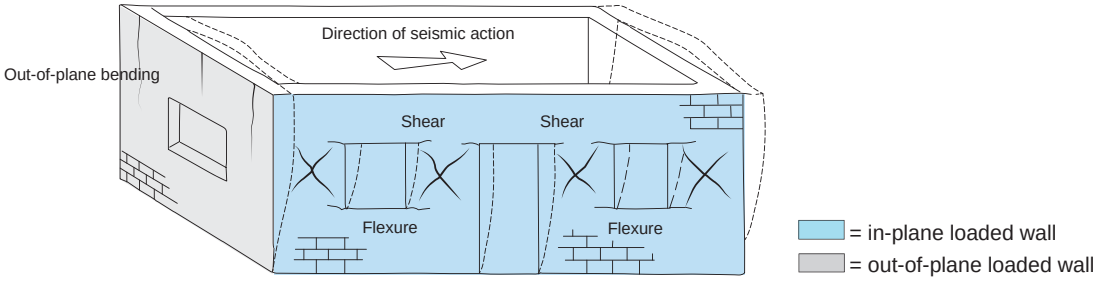

Figure 4.3: Schematization of the behaviour of an URM structure under seismic load and typical cracking patterns. [29].

In addition, it can be seen that the cracking patterns for the in-plane loaded wall are considerably different compared to the out-of-plane loaded wall. Therefore, it is important to distinguish between in-plane and out-of-plane failure mechanisms. Out-of-plane failure mechanisms are not discussed in detail within the scope of thesis. However, it should be underlined that out-of-plane failure mechanisms are typically very brittle and thus unfavourable. [30] Figure 4.3 indicates that cracks are likely to concentrate around the piers for the in-plane loaded wall. The piers of the in-plane loaded wall exhibit horizontal cracks at their top and bottom, and diagonal cracks. These cracks and their corresponding failure mechanisms are further elaborated in figure 4.4. Three main loading conditions that result in failure can be identified. Masonry either cracks, slides or crushes under tension, shear, or compression loading conditions respectively.

Furthermore, van Wijnbergen [30] underlined that the global response of an URM structure largely depends on the quality of the connections between wall and floor elements, and the in-plane stiffness of the floors. Figure 4.5 shows that the combination of flexible floors with poor connections results in large deformations at first floor level. In this case, the unfavourable out-of-plane failure mechanisms are likely to be governing. In contrast, the combination of rigid floor with tied walls and floors results in considerably less deformations at first floor level. This combination allows for box-action and the more favourable in-plane failure mechanisms are likely to be governing. Box-action is favourable because this generally results in higher seismic capacities and less brittle failure mechanisms.

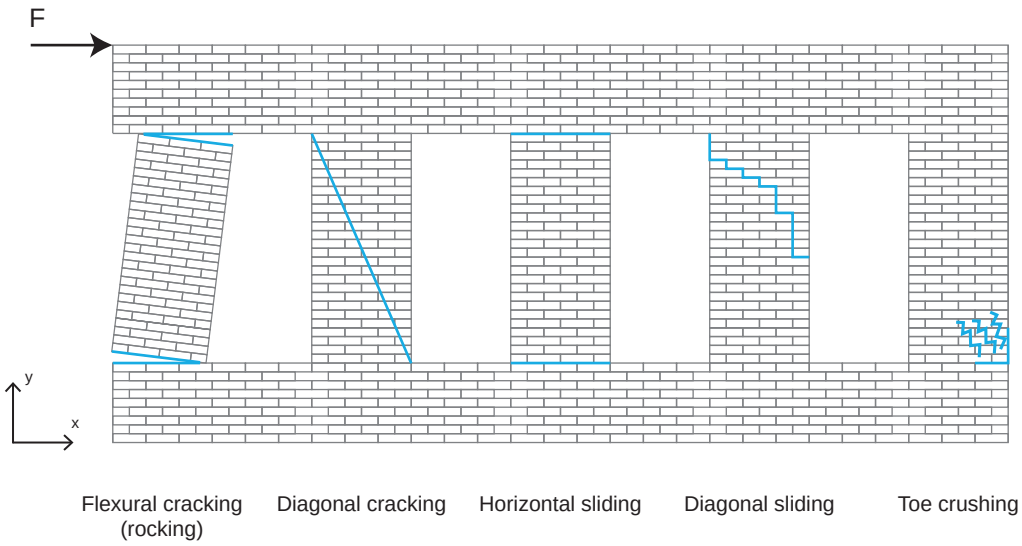

Figure 4.4: Typical in-plane failure mechanisms for masonry piers with failure planes indicated in blue based on [31].

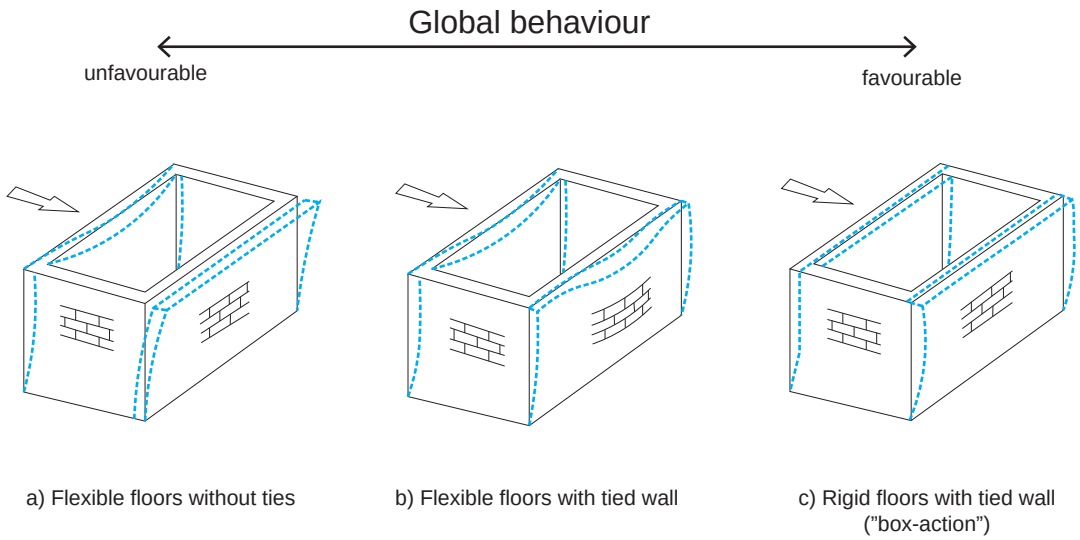

Figure 4.5: Global response of an URM structure depending the connections between structural elements and the in-plane stiffness of the first floor based on [30].

4.3. Modelling approaches

Four main modelling approaches for masonry are found in literature [32, 33]:

- **Detailed micro-modelling:** two separate continuums for both mortar and bricks with interfaces between the mortar and bricks.
- **Simplified micro-modelling:** one smeared composite continuum for mortar and bricks with interfaces at the centre of the mortar joints.
- **Macro-modelling:** one smeared composite continuum without an explicit definition of the interfaces.
- **Equivalent frame models:** a wall is schematized as a idealized frame with deformable elements representing the spandrels and piers, and rigid nodes between these elements.

The level of detail varies extremely between the different modelling approaches. The detailed micro-modelling approach is most detailed and may potentially yield results with a high accuracy but low

efficiency. In addition, the numerical model requires a proper definition of a vast amount of properties. The suitability of the micro-modelling approaches is generally considered to be limited to the scale of a structural element. On the scale of a structure, these approaches become highly uneconomical and impractical.

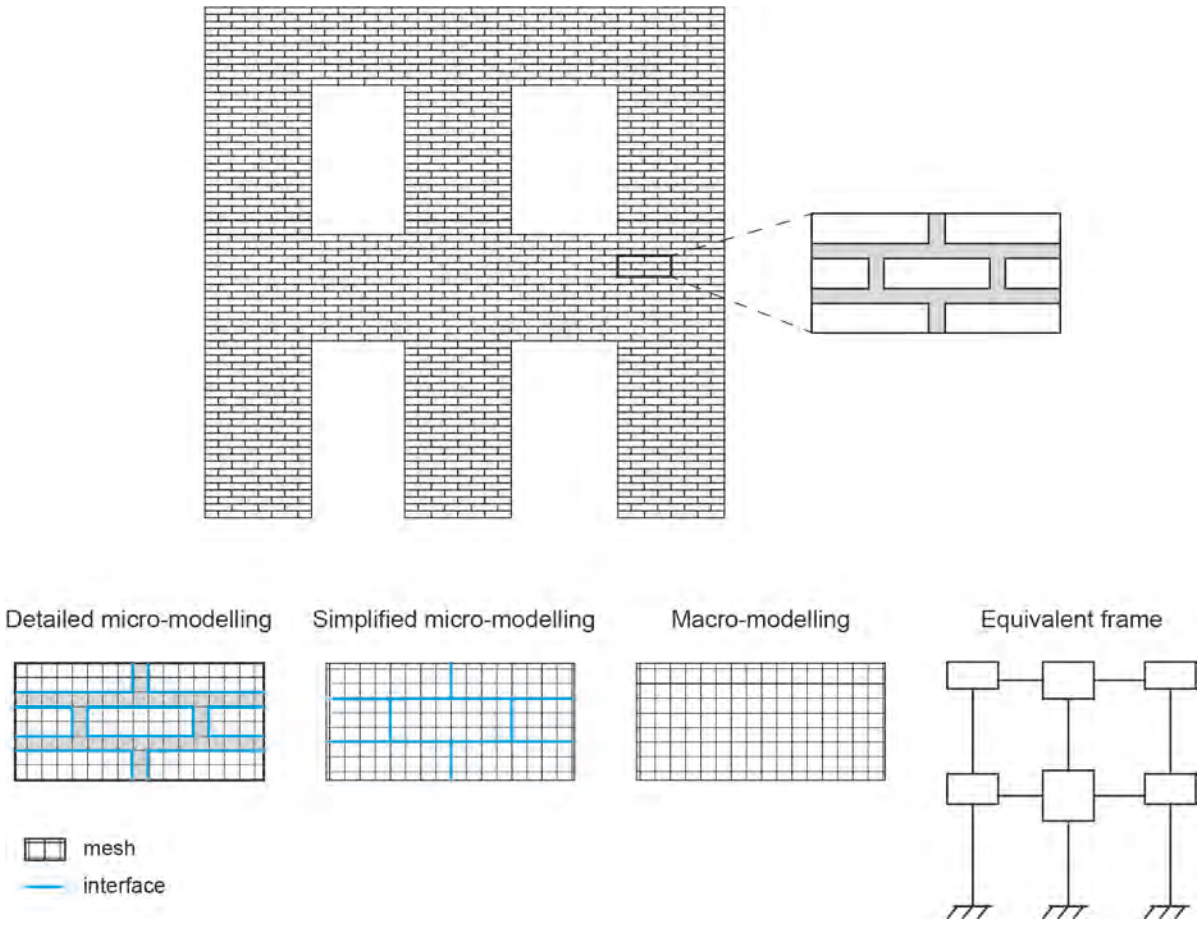

Figure 4.6: Modelling approaches based on [30].

The macro-modelling is considered to be the most balanced approach in term of accuracy and efficiency within the scope of this thesis. Therefore, the macro-modelling approach has been adopted.

4.4. Material properties

A large-scale testing campaign has been set up as a response to the human-induced seismicity in the province of Groningen. Experiments were performed to obtain structural properties of unreinforced masonry at the level of the material [34], structural elements [19, 35] and complete structures.[20] In addition, these experimental results served as an important benchmark for the validation of numerical models.

The material behaviour of masonry under tension, shear and compression loading conditions is shown in figure 4.7. These material diagrams are incorporated in the engineering masonry model (EMM) of DIANA 10.2. It should be noted that these diagrams are not drawn at the same scale. The indicative values indicate that the diagram under compression loading conditions is significantly larger compared to the diagrams under tension and shear loading conditions.

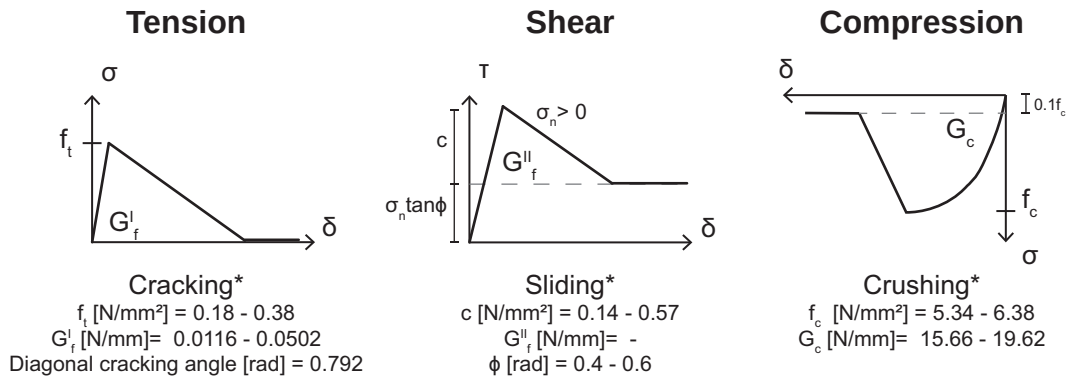

*Given values are indicative values for masonry composed with calcium-silicate bricks

Figure 4.7: Material models for macro-modelling of masonry in EMM based on [36] with indicative values based on [20, 36, 37]

Furthermore, the orthotropic nature of masonry is also incorporated in the EMM. Different properties for the elasticity and strength can be implemented. Indicative values for the elasticity properties of CS-brick masonry are given in figure 4.8. The local x-axis is orientated parallel to the bed joint, while the local y-axis is orthogonal to the bed joint.

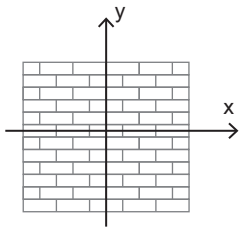

Elasticity*
E_x [N/mm²] = 2,437 - 5,267
E_y [N/mm²] = 3,495 - 6,560
G_{xy} [N/mm²] = 1,398 - 2,624

*Given values are indicative values for CS-brick masonry

Figure 4.8: Orthotropic elasticity for masonry in the EMM with indicative values for CS-brick masonry based on [20, 36].

Lastly, masonry exhibits stiffness and strength degradation under repeated loading. Figure 4.9 shows a schematization of the response of an URM structure to three repetitions of an imposed displacement indicated by u_1. It is observed that the URM structure has a reduced global stiffness and strength after each repetition. These degradation effects could vary significantly in size, e.g. Korswagen et al. [19] found a strength degradation ranging between 4% and 22%. Strength degradation behaviour under repeated loading is not incorporated in the material models of the EMM.

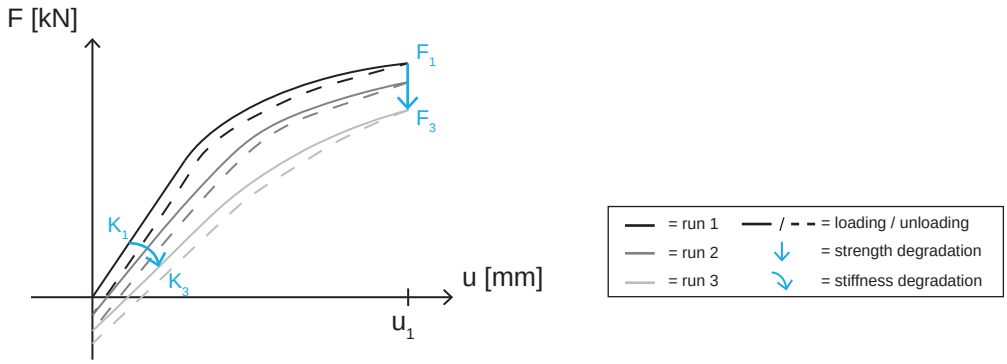

Figure 4.9: Schematization of exaggerated degradation effects observed in masonry structures under repeated loading.

Recently, the implementation of strength degradation into the engineering masonry model has been investigated by Srinidhi [38]. Srinidhi [38] implemented a degradation model in the masonry material model under tensile loading. Figure 4.10 shows the material behaviour under three load repetitions in tension indicated in blue. It can be seen that the adopted material model does not include strength degradation, while this is included in the proposal of Srinidhi [38]. However, this improved material model is not adopted in this thesis.

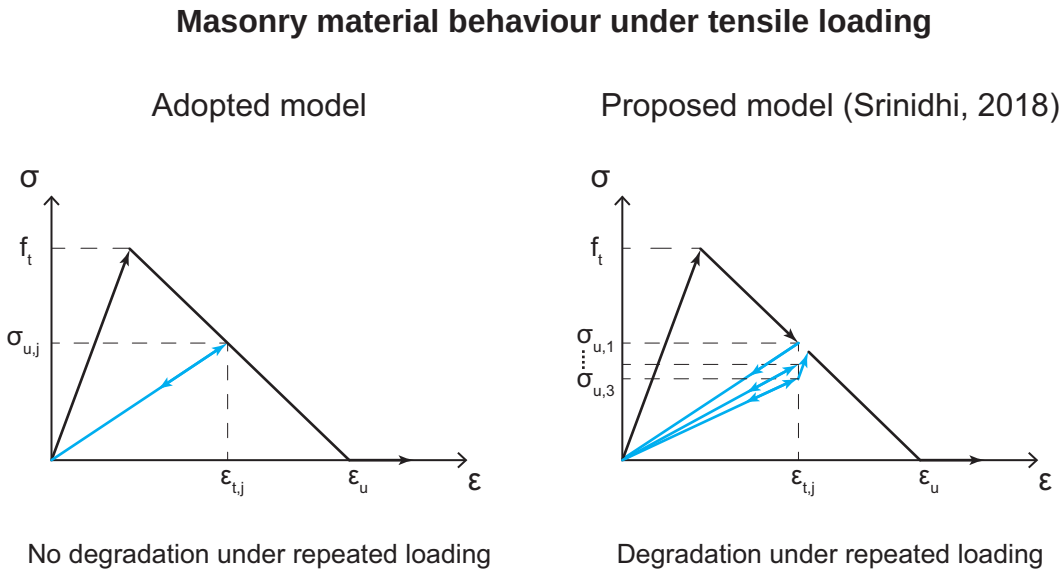

Figure 4.10: Schematisation of masonry material behaviour under four load repetitions in tension indicated in blue. Comparison of the adopted material model (left) and the proposed improved model with strength degradation (right) based on [38].

5

Seismic retrofitting

5.1. Conventional design strategies

Several retrofit design strategies reported in literature are listed below. A distinction can be made between strategies that aim to increase the capacity of the structure and strategies that aim to decrease the load acting on the structure.

Strategies that aim to increase the capacity of the structure:

- **Increase seismic deformation capacity (ductility):** the structure is capable to deform plastically and absorb energy without sudden collapse. This behaviour depends on structural material, design and detailing. [22, 30, 39]
- **Increase seismic force capacity:** the amount of energy that is absorbed by elastic deformation (reversible) increases, reducing the required plastic deformation (irreversible). [22, 30, 39, 40]
- **Increase lateral stiffness:** this reduces the deformation demand on the structure and thus requires less ductility of the critical elements. It should be noted that this has one side effect: period shortening. [30, 39, 40]
- **Improve structural integrity:** strong connections between the perpendicular walls and between walls and floors improve the structural integrity. This increases the overall lateral stiffness and strength. [22, 30, 39]
- **Local modification of components:** improving the strength, stiffness or ductility of components or connections could offer an economical strengthening solution. [22, 30, 40]
- **Reduce irregularities in plan and elevation:** irregularities in plan result in unwanted torsional forces, while irregularities in elevation result in force concentrations. [22, 30, 39, 40]

Strategies that aim to decrease the load acting on the structure:

- **Supplementary energy dissipation (i.e. damping):** additional damping can be introduced by passive energy dissipating systems, e.g. tuned mass dampers or tuned liquid dampers. [22, 30, 40]
- **Seismic base isolation:** isolation of the superstructure from its foundation by means of bearings results in significant reductions of seismic forces and deformation demands. [22, 40]
- **Decrease building mass:** an earthquake introduces inertial forces that are directly proportional to the building's mass. It should be noted that this has two side effects: period shortening and decrease of overburden load. This overburden load acts as prestress on URM walls, which increases the capacity. [22, 30, 40]

5.2. Conventional seismic retrofitting measures in Groningen

Centrum Veilig Wonen (CVW) has a central role in the strengthening operation in the Groningen area. CVW coordinates inspections and assessment of existing structures, selection of retrofitting measures, and execution of the proposed measures. Standardized retrofitting measures have been collected in a catalogue to increase the uniformity and efficiency of the strengthening operation.

The retrofitting catalogue addresses generalized retrofitting measures at structural element level. Retrofitting measures at a global level are not included in the catalogue because this often requires tailored-made solutions. The retrofitting catalogue is divided into seven categories:

- Potentially high risk building elements
- Connections
- In-plane strengthening floor and roof
- Out-of-plane strengthening of walls
- In-plane strengthening of walls
- Foundation improvements
- Changing dynamic behaviour

Figure 5.1 gives an overview of the in-plane strengthening measures for a wall given in retrofitting catalogue. It is observed that almost all strengthening measures apply an additional layer to the masonry wall. These type of measures are likely to be inadequate if there is only limited wall area available which is generally the case for the façade walls of terraced houses.

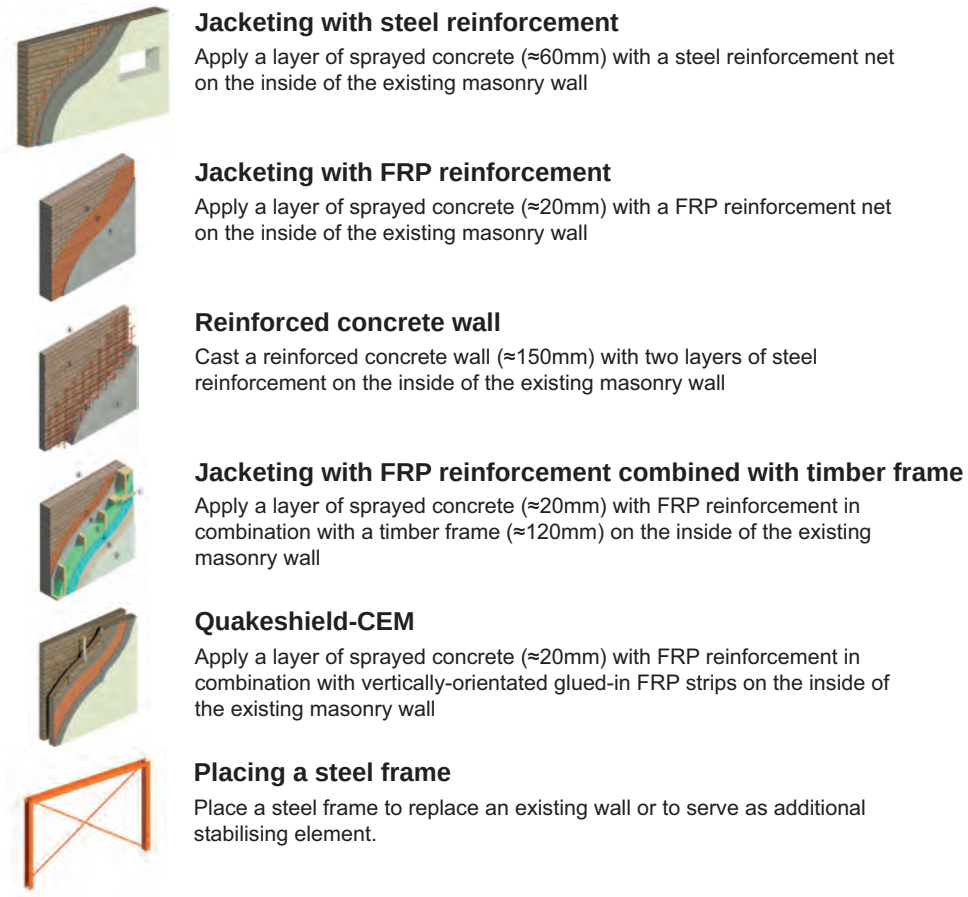

Figure 5.1: Overview of in-plane strengthening measures for walls based on [41]. All images are retrieved from [41].

Placing a steel frame is the only in-plane strengthening measure that does not apply an additional layer to the existing masonry wall. However, it can be problematic to find an appropriate location for this strengthening measure. Two solutions for applying a steel structure are shown in figure 5.2. Both solutions aim to improve the seismic capacity of the terraced house in the longitudinal direction.

Figure 5.2: Strengthening of terraced houses in longitudinal direction with a steel frame inside the cavity [9] or a steel supporting structure at the end wall. [10]

However, both solutions prove to very time-consuming and expensive. For example, the steel frame inside the cavity of the cavity wall requires removal of the outer leaf before the steel frame can be placed. This stage is shown in figure 5.3. In addition, this solution requires extending the existing foundation elements and rebuilding the outer leaf. As a result, these conventional strengthening measures for the terraced houses in the Groningen area cause a great hindrance to the residents. Therefore, some residents of terraced houses in Appingedam prefer a new building to retrofitting of the existing building. [11]

Figure 5.3: Stripped terraced house with the outer leaf removed before placing the steel frame in the cavity. [10]

5.3. Potential strategies for structural window design

The most suitable design strategies that could be incorporated in a structural window designs are: increase seismic force capacity and increase lateral stiffness. In addition, it could be possible to incorporate the supplementary energy dissipation principle by designing connection between masonry and glass.

6

Frame-glass composite walls

6.1. Introduction

Several authors studied the possibility of using glass panes as stabilising elements. Huveners et al. [42] and Ber et al. [43] presented studies into the in-plane capacity of circumferentially adhesive bonded glass panes. A frame-glass composite wall was composed by connecting a glass pane to a frame by a structural adhesive. Huveners et al. [42] and Ber et al. [43] studied a frame-glass composite wall with a steel and timber frame respectively.

The components of a frame-glass composite system are schematically shown in figure 6.1. The presence of the structural adhesive makes it possible to introduce forces to the glass pane and utilise the glass pane as stabilising element. Therefore, frame-glass composite walls offer an interesting design option for the structural window.

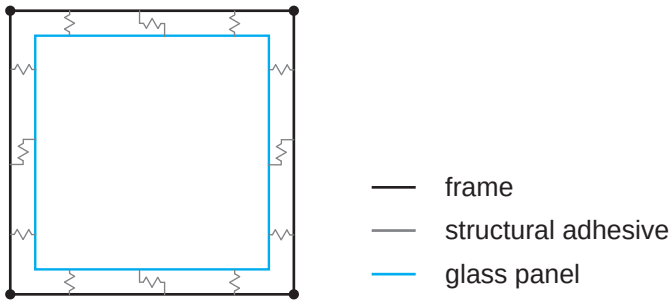

Figure 6.1: Schematisation of the components of a frame-glass composite wall.

6.2. Behaviour under lateral loads

The capacity curve of a squared frame-glass composite wall with joint type 1 is divided in two subsequent main stages which are shown in figure 6.2. The activation displacement, marked with d_a in figure 6.2, is the lateral displacement at which glass/frame contact occurs. The main stage before prior to reaching the activation displacement is referred to as pre-activation stage, while the main stage after reaching the activation displacement is referred to as the post-activation stage. Additionally, it is found in section 11.6 that both pre-activation and post-activation stage can be divided into two substages resulting in a total of four subsequent substages. The pre-activation stage can be divided in a linear elastic stage, and local adhesive tearing. The post-activation stage can be divided in frame/glass contact stage, and glass cracking.

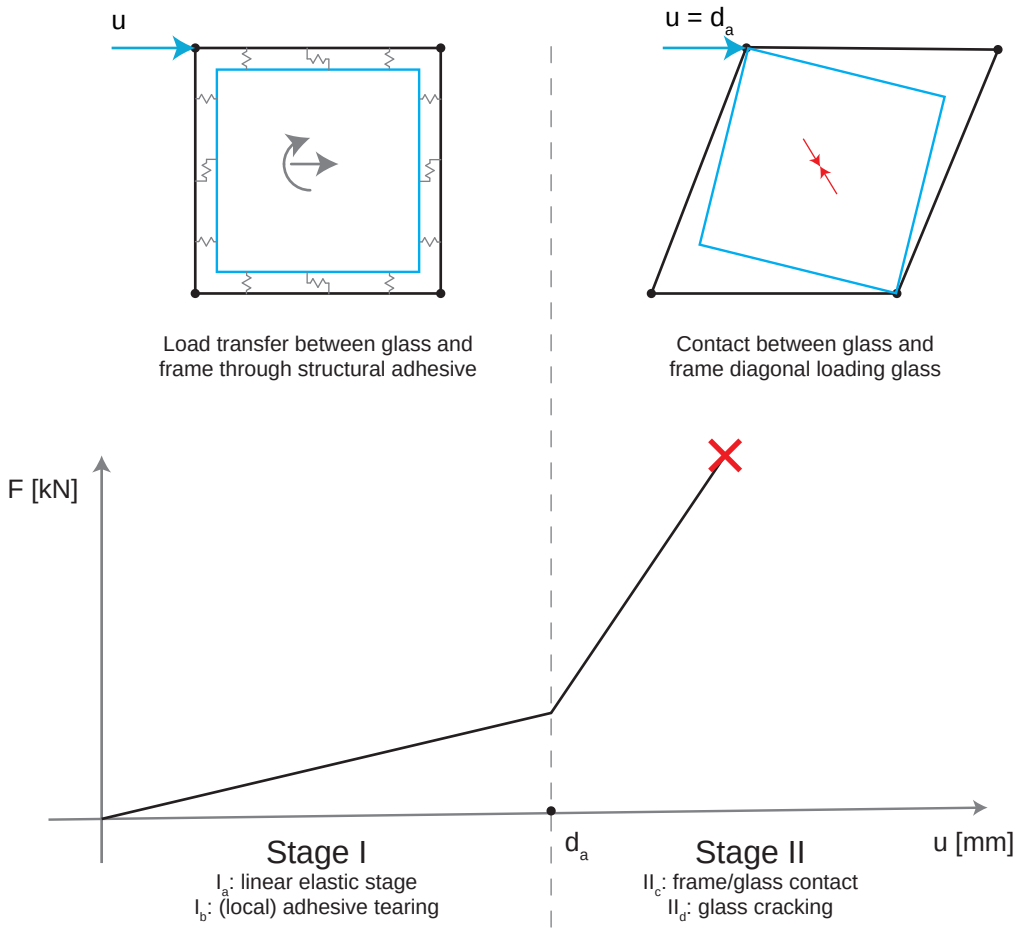

Figure 6.2: In-plane capacity curve of a squared frame-glass composite wall with joint type 1 consisting of two subsequent main stages and four subsequent substages based on [18].

The global stiffness of the frame-glass composite wall significantly increases in the post-activation stage. During this stage, the glass pane is likely to fail due to local stress concentrations at the two loaded corners. The activation displacement at which glass/frame contact occurs can be calculated analytically by equation 6.3.

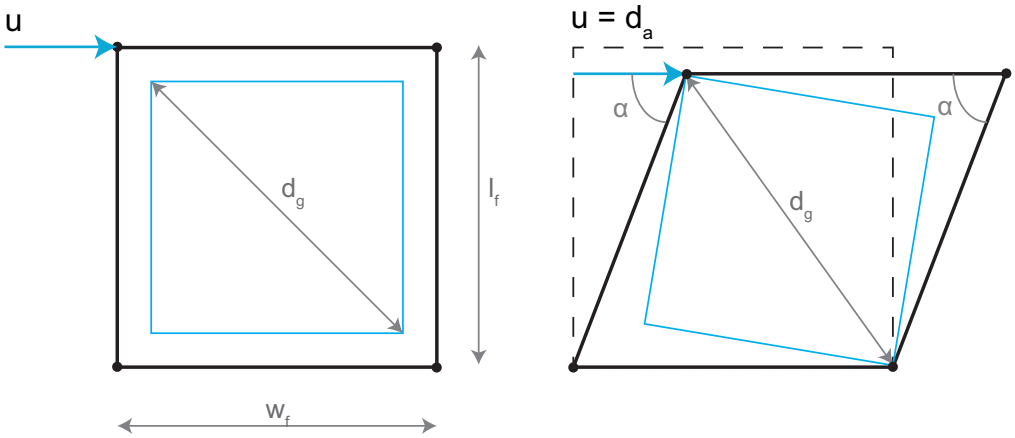

Figure 6.3: Derivation of the activation displacement.

$$d_a = l_f cos(\alpha) \tag{6.1}$$

$$d_g^2 = w_f^2 + l_f^2 - 2w_f l_f cos(\alpha) \tag{6.2}$$

Combining equation 6.1 and 6.2 gives equation 6.3.

$$d_a = \frac{l_f^2}{2w_f} + \frac{w_f^2}{2w_f} - \frac{d_g^2}{2w_f} \tag{6.3}$$

Furthermore, this simplifies to equation 6.4 if the frame-glass composite wall is squared ($w_f = l_f$).

$$d_a = l_f - \frac{d_g^2}{2l_f} \tag{6.4}$$

6.3. Structural adhesives

Ber et al. [43] underlined that the load bearing capacity and global stiffness of a frame-glass composite wall largely depends on the type of connection between the frame and glass. Important characteristics that determine the performance of the connection are the type of adhesive, durability of adhesive, joint dimensions, joint type.

Structural adhesives can be classified into three main categories based on their mechanical properties. This classification is shown in figure 6.4. In addition, it is important to underline that material properties of a structural adhesive strongly depend on loading rate, load duration and temperature. Loading rate and load duration could be of importance considering an earthquake load.

Elastic	**Semi-rigid**	**Rigid**
e.g. silicone	***e.g. PU, superflex polymers***	***e.g. epoxy, acrylate***
high flexibility low strength	medium flexibility medium strength	low flexibility high strength

Figure 6.4: Classification of structural adhesives based on their mechanical properties based on [44]

Furthermore, a differentiation is made between three joint types is shown in figure 6.5.

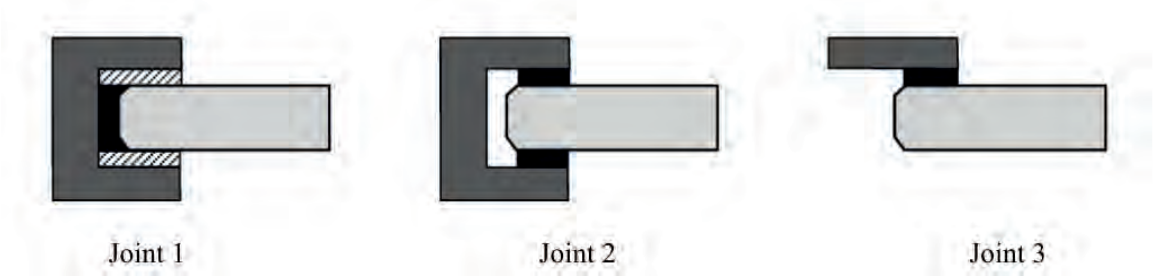

Figure 6.5: Joint types between glass pane and steel frame. [45]

6.4. Glass

Glass is a very brittle material with no plastic capacity meaning that glass might fail very suddenly. The strength of glass strongly depends on inevitable surface flaws. These surface flaws significantly reduce the tensile strength of glass, while barely affecting the compressive strength of glass. As a result, the tensile strength is almost always governing for structural applications.

The tensile strength of glass can be increased by thermal tempering. Thermal tempering creates a favourable residual stress field in the glass with tensile stresses in the core and compressive stresses at the surface. The compressive stresses at the surfaces act as prestress and prevent crack growth. However, it should be noted that thermal tempering does not only affect the tensile strength, but also the post-breakage behaviour of glass.

Figure 6.6 compares the tensile strength and post-breakage behaviour of three commonly-used glass types. These glass types have different levels of residual compressive stresses at the surfaces. Annealed glass has no residual compressive stresses at the surfaces, while fully tempered glass has most residual compressive stresses (80-170MPa) at the surfaces. Heat strengthened glass has lower residual compressive stresses (40-80MPa) at the surfaces compared to fully tempered glass as a result of a slower cooling process. [46] It is observed that thermal tempering negatively affects the post-breakage behaviour.

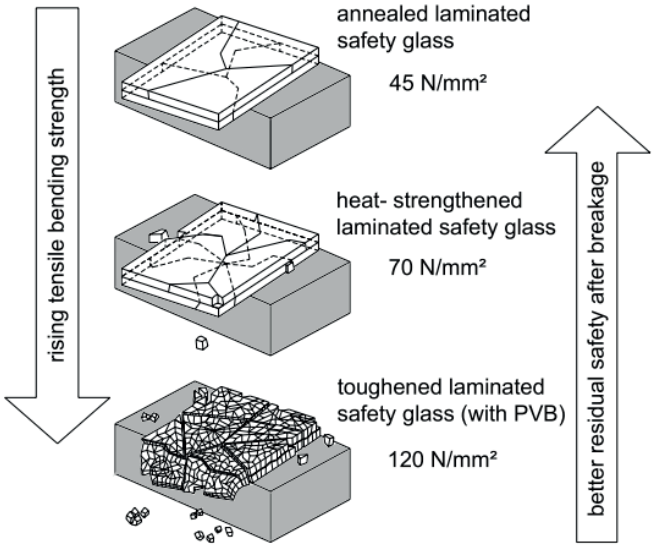

Figure 6.6: Three types of float glass with different bending tensile strength and post-breakage behaviour [47]

7

Conclusions part I

The building stock in the Groningen area consists of more than 150,000 buildings divided over eight main typologies. The residential terraced house building typology has been selected to assess the seismic potential of a structural window design. This building typology is of interest because it is the most common building typology, and it often has relatively large windows in their façade walls. The latter results in a very limited structural capacity of terraced houses in the longitudinal direction. Therefore, a structurally designed window is expected to be most effective for this building typology.

Two locations in the Groningen area have been selected based on the spatial distribution of terraced houses and the PGA contour map for the seismic assessment. The city of Groningen is chosen as an average location and Appingedam as extreme location for the seismic assessment. The pushover method is adopted to determine the seismic capacity of a considered structure. This calculation method incorporates nonlinear material behaviour and is well suited for the regular geometry often found for terraced houses. The seismic assessment will address both a capacity check and an evaluation of damage. The capacity check will be performed for a ”strong” earthquake, while the damage is evaluated for a more frequent ”weak” earthquake. The strong and weak earthquake have a return period of 2475 and 95 years respectively. The seismic demand of these earthquake are given in an acceleration-displacement response spectrum that are retrieved from an online webtool developed by the NEN.

Unreinforced masonry structures are typically very vulnerable to seismic loads mainly because of their limited tensile strength. Four main modelling approaches with varying level of detail are found in literature for masonry structures. In engineering practice, masonry structure are usually modelled adopting the equivalent frame or macro-modelling approach. Within the scope of this thesis the macro-modelling approach is considered to be most suitable and has been selected. This approach models masonry with one smeared composite continuum without an explicit definition of brick/mortar interfaces. Furthermore, the engineering masonry model will be adopted for the numerical modelling in DIANA 10.2. This material model incorporates orthotropic properties of masonry and nonlinear material behaviour under tension, compression and shear loading. However, strength degradation under repeated loading is not incorporated in this material model.

In literature, several design strategies have been reported that aim to either increase the seismic capacity of a structure or decrease the seismic demand acting upon a structure. For the strengthening operation in Groningen area, standardized retrofitting measures at the level of a structural element have been collected in a catalogue. It is noticed that most of the conventional in-plane strengthening measures for walls apply an additional layer to the exiting wall. These strengthening measures are likely to be inadequate for in-plane strengthening of the façade walls of a terraced houses that typically only have limited wall area available. Two global retrofitting measures for strengthening a terraced house in longitudinal direction have been found in literature. These global retrofitting solutions either place a steel frame in the cavity of the façade walls or a steel supporting structure at the end wall of a row of terraced houses. However, both solutions prove to very time-consuming, expensive and

causing great hindrance to the residents. Consequently, some residents of terraced houses prefer a new building to retrofitting of the existing building.

Replacing the existing windows by frame-glass composite walls could potentially provide an innovative in-plane strengthening measure for the façade walls of a terraced house. These composite walls are composed of the traditional elements of a window being a frame and glass pane. Additionally, these composite wall incorporate a structural adhesive that connects the frame with the glass pane and enables the composite wall to act as a stabilising element.

The capacity curve of squared frame-glass composite walls with joint type 1 under lateral loads consists of two subsequent main stages. These two main stages are separated by the activation displacement at which glass/frame contact occurs. After reaching the activation displacement, the global stiffness of the composite wall is significantly increased and compressive stresses rapidly increase along the diagonal of the glass pane. Ultimately, glass cracking is likely to occur at the loaded corners of the glass pane due to local peak stresses.

8

Structural window design

8.1. Design goal

The design goal of the structural window has been formulated as follows:

"Increase the in-plane seismic force capacity of an existing URM structure by utilisation of the glass panel as a structural element."

Figure 8.1 shows that utilisation of the glass pane can be achieved in two ways. The first main stage presents the safest design option and is preferred for most load conditions. In the first main stage, the glass pane is utilised by load transfer through the circumferentially adhesive bonded joint without any risks of brittle failure. In the second main stage, the glass pane is utilised by direct contact between the frame and glass. During this stage, a substantial part of the structural adhesive is torn and glass pane might fail suddenly due to local stress concentrations at the two loaded corners. Consequently, this stage is preferably prevented for most loading conditions and is only acceptable under extreme loading conditions.

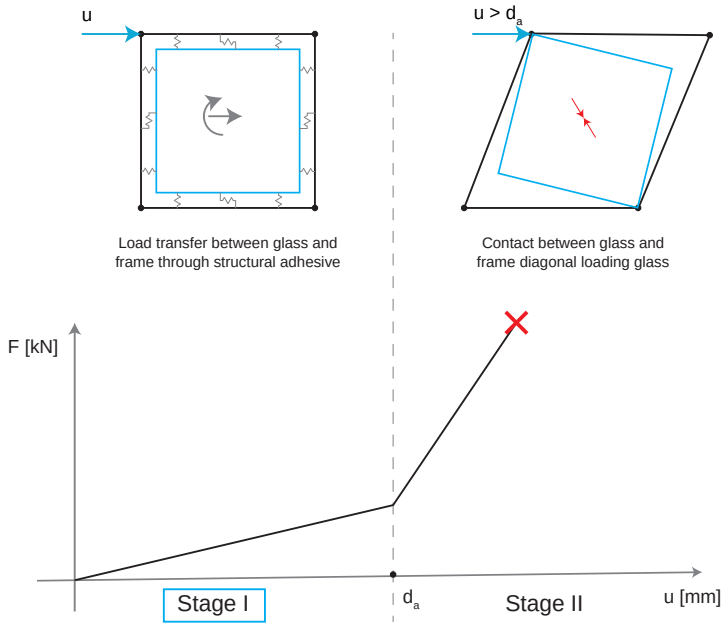

Figure 8.1: Main stage I of the capacity curve of the structural window presents the safest design option.

8.2. List of requirements

The requirements have been divided into three categories. First of all, a selection has been made from the conventional functions that were given in section 2.2. Furthermore, structural and additional requirements have to be fulfilled in order to meet the formulated design goal for the structural window that is placed into an existing structure.

The conventional functions that were qualitatively taken into account the structural window design are given in bold in figure 8.1.

Table 8.1: Selected conventional functions of windows indicated in bold.

Safety	Health	Usability	Energy
Structural safety Fire safety Burglary protection	**Water tightness** Condensation prevention Acoustic performance **Ventilation possibility** **Daylight admittance**	Stiffness Operation Accessibility	**Thermal insulation** **Air permeability**

Structural requirement:
- Allow for load transfer between load-bearing inner leaf of a masonry wall and structural glass panes.

Additional requirements:
- Compensate for irregularities in shape of existing windows.
- Minimise construction time at site.

8.3. Materialisation

The materialisation of the prefabricated structural window is shown in figure 8.2. The materialisation is explained for each component separately in the subsections.

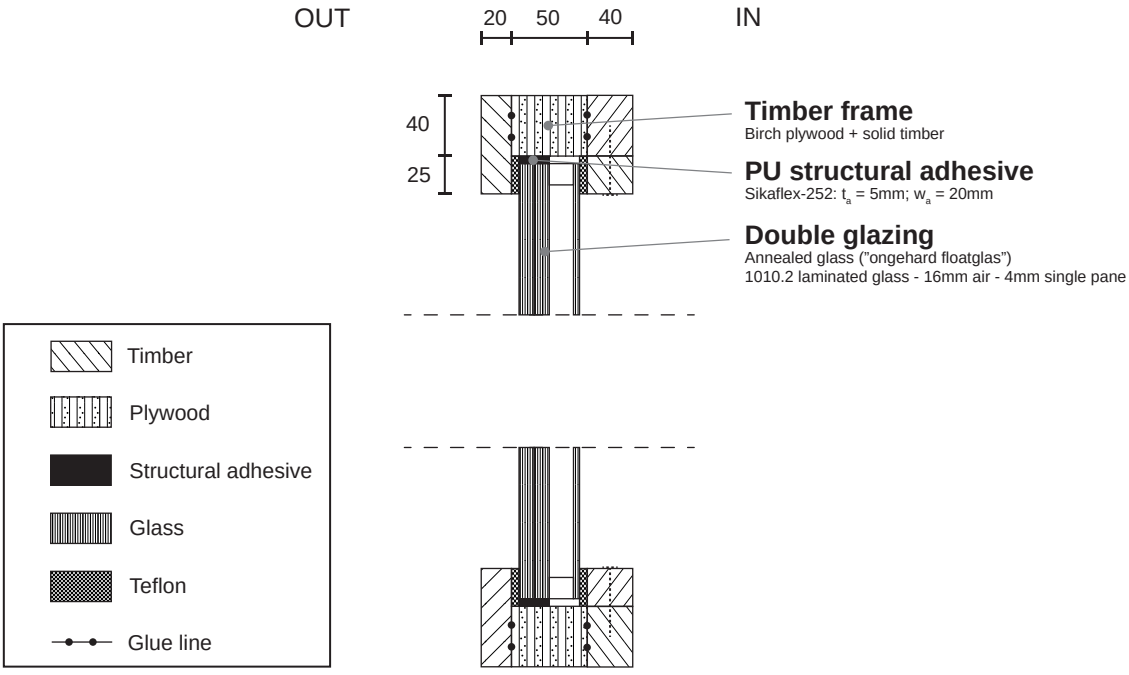

Figure 8.2: Cross section with components of the prefabricated structural window

8.3.1. Structural adhesive

An appropriate structural adhesive should have both flexibility and strength. Flexibility is required to accommodate imposed deformations, e.g. caused by thermal loads. Strength is required to transfer loads and utilise the glass pane as a structural element. Figure 8.3 shows that semi-rigid adhesives present the most balanced option in terms of flexibility and strength. Therefore, semi-rigid adhesives are selected as most suitable option. Specifically, Sikafex-252 has been chosen because of the availability of information about its structural properties. Experimental testing and information about the structural properties of this specific type of structural adhesive were reported by Huveners [18].

Elastic ***e.g. silicone***	**Semi-rigid** ***e.g. PU, superflex polymers***	**Rigid** ***e.g. epoxy, acrylate***
high flexibility low strength	medium flexibility medium strength	low flexibility high strength
Insufficient force transfer	Most suitable option	Insufficient deformation capacity

Figure 8.3: Semi-rigid adhesives present the most balanced option in terms of flexibility and strength.

8.3.2. Glass panes

Glass is a very brittle material with no plastic capacity meaning that glass might fail very suddenly. Therefore, safety and post-breakage behaviour are very important criteria when applying glass as a structural material. In addition, the glass panel should provide thermal insulation.

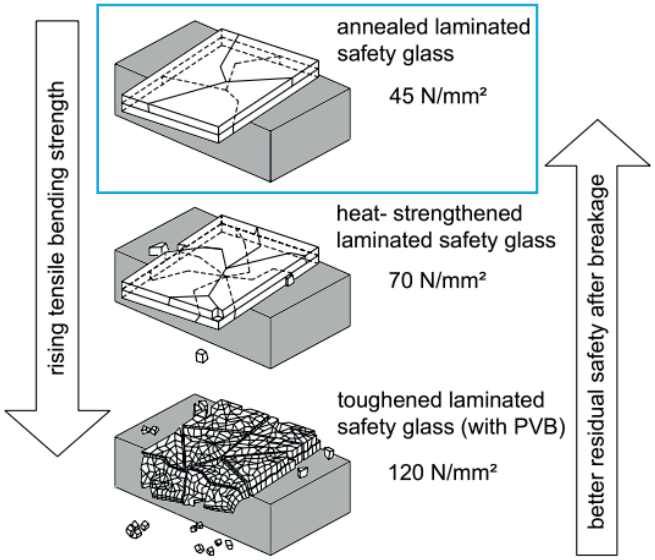

Figure 8.4: Annealed glass presents the most suitable option because of its favourable post-breakage behaviour based on [47]

Annealed glass is chosen as the most suitable option because of its favourable post-breakage behaviour. Additionally, three safety principles were adopted in the design:

- Lamination has been applied for the structural layer of the glass panel to increase ductility.
- Direct contact between glass and a hard material (e.g. steel, concrete, and masonry) is avoided by placing a timber frame between the glass panel and masonry. In addition, the adopted joint thickness of 5mm prevents timber/glass contact for most cases. In section 15.3, it is shown that direct timber/glass contact only occurs under extreme loading conditions, i.e. a strong earthquake in Appingedam.

– The flexibility of the structural adhesive allows for (thermal-)movement of the glass panes.

Lastly, double glass is required to comply with the thermal insulation requirement.

8.3.3. Frame

The frame of the structural window should provide stiffness and strength in both in-plane directions, and provide thermal insulation. Therefore, solid timber has been chosen as most suitable option for the frame. In addition, plywood has been chosen for the loaded centre part of the frame to provide sufficient stiffness in both in-plane directions. This plywood block is glued to two solid timber elements its sides. The side element at the inside is composed of two elements to allow for production of the adhesive joint.

8.4. Connection to existing structure

A proposal for the connection to an existing structure is presented in this section. However, it should be noted that this discussion merely serves as an example solution. In reality, adaptions might be required as a result of varieties in the composition, and geometry of the existing structure. Figure 8.2 shows that the prefabricated structural window is placed in-plane with the inner leaf of the cavity wall. The connection of the prefabricated structural window to the existing structure is made with an injection mortar that fills a gap of 25mm at all sides of the prefabricated structural window.

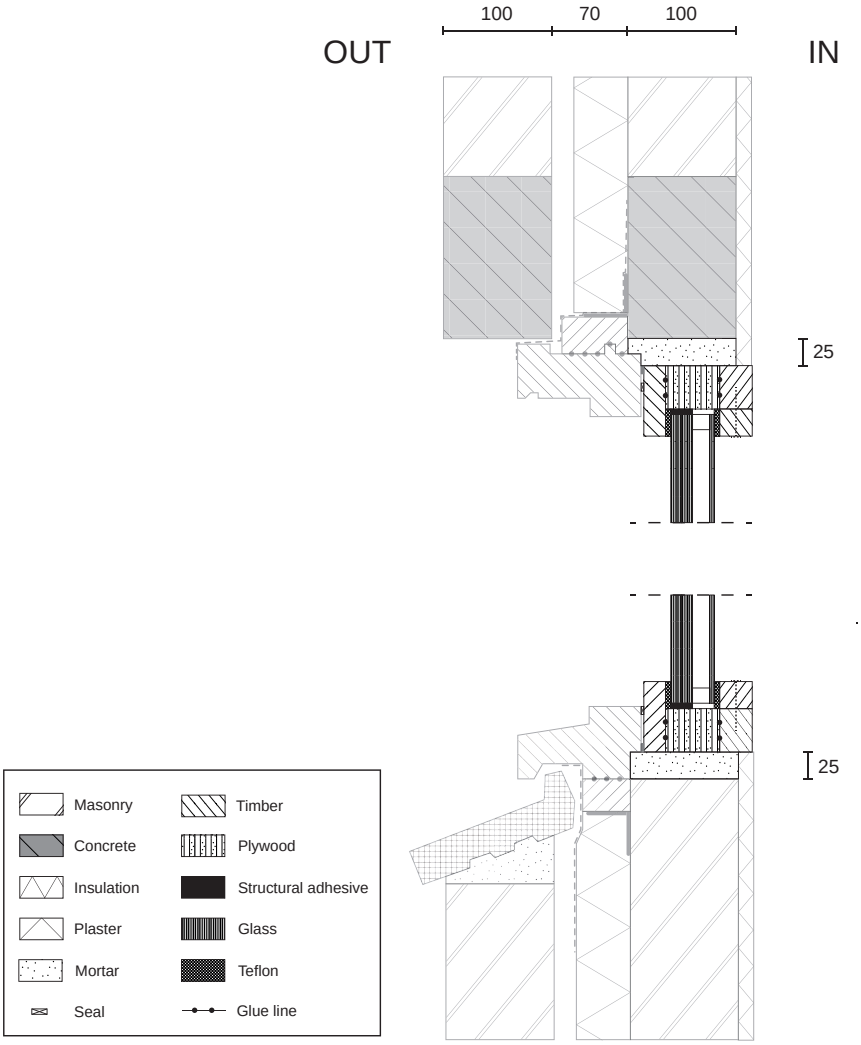

Figure 8.5: Prefabricated structural window placed into the existing structure in line with the inner leaf.

8.5. Modelling approach

The inclusion of structural windows in the numerical model in DIANA FEA 10.2 will be performed adopting two different approach. The superglue approach is quick but not very realistic, while the component approach will be more realistic but more complex.

- **Superglue approach:** The structural adhesive and timber frame are neglected. Only the glass panel is modelled by a 2D continuum that is rigidly connected to the surrounding masonry elements. This approach is expected to give an upper-bound envelop for the capacity curve of the actual strengthened structure.
- **Component approach:** All components of the structural window are modelled. The window frame is represented by beam elements, structural adhesive by a structural interface elements, and the glass panel by a 2D continuum. This approach has been reported by Huveners [18] and is expected give a realistic capacity curve of the strengthened structure.

Figure 8.6 shows an exploded view of the component approach. The connections between the glass pane, timber frame and masonry are modelled with NLE structural interface elements. The structural adhesive between the glass pane and timber frame is indicated as interface 1, while interface 2 connects the masonry wall and frame. The timber frame is composed of 4 beams with the corner nodes tied in the translational directions. Rotation around the z-axis is released at these corners simulating hinge behaviour.

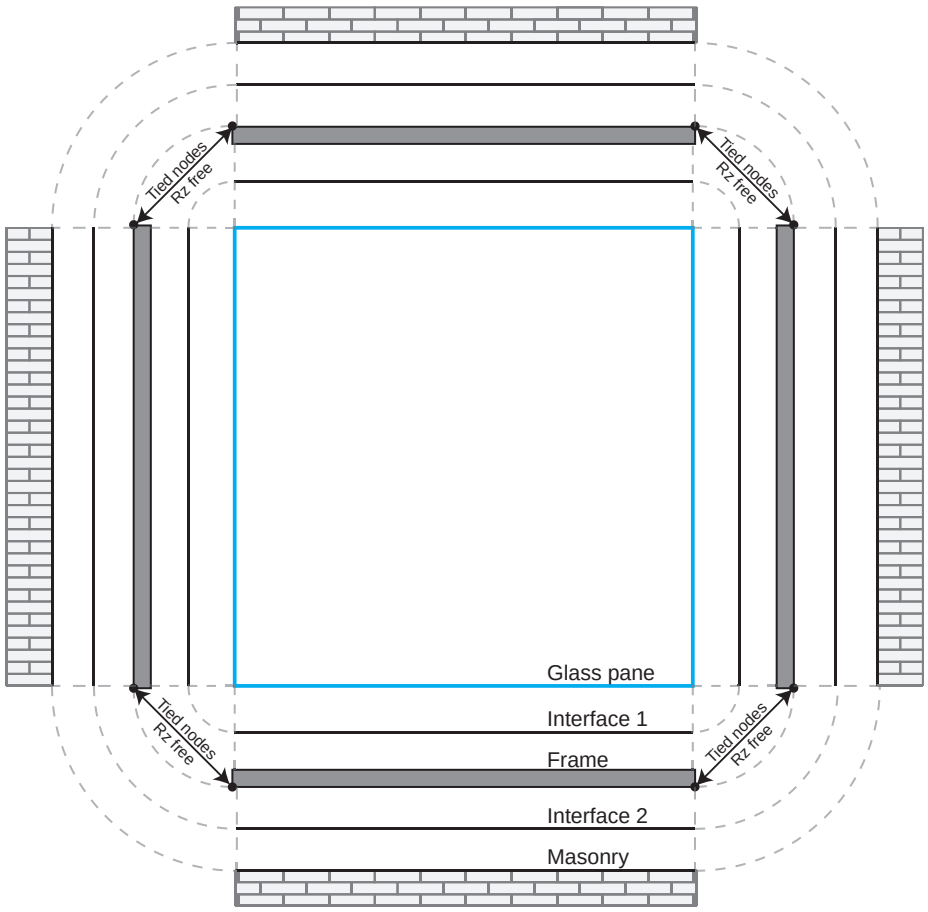

Figure 8.6: Component approach - Exploded view of the connection between masonry, frame and glass.

Figure 8.7 shows the superglue approach. In this theoretical approach this connection between the glass pane and masonry is infinitely stiff and the frame is neglected.

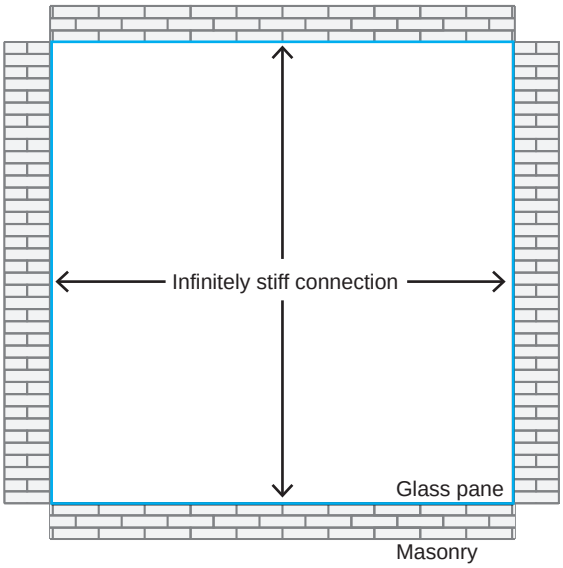

Figure 8.7: Superglue approach - rigid connection between masonry and glass pane. The structural adhesive and timber frame are not modelled.

9

Design validation

The design has been presented to seismic retrofitting experts at CVW and a renovation expert. This resulted in several suggestions to improve the practical and technical feasibility of structural window design. The suggestions are either incorporated in this thesis or its recommendations.

9.1. Feedback

Feedback based on the conversation with the seismic retrofitting experts is listed below:

- **Connected elements:** higher capacity and stiffness of the superstructure might result in higher loads to connected elements, e.g. foundation elements. Therefore, the foundation elements might become governing and might also require strengthening.
- **Ventilation:** the structural window design should incorporate ventilation possibilities in order to be a suitable and realistic strengthening measure.
- **Load duration:** the effect of the short load duration on the material properties of the structural adhesive is interesting to further investigate.
- **Production process:** the production of the prefabricated structural window could be further studied. How is the structural adhesive applied between the glass and frame?

Feedback based on the conversation with the renovation expert is listed below:

- **Installation:** the large weight of the prefabricated structural window ($\approx 60kg/m^2$) requires installation from the outside with lifting equipment, e.g. with a assembly robot with vacuum units. The vacuum units should be applied to the laminated structural layer of glass.
- **Wet connection:** a dry connection is preferred over the wet connection with injection mortar. The solution with the injection mortar joint is expected to be challenging to execute in an existing building. There is a risk for leakage.
- **Other possibilities:** it could be interesting to take other measures that improve the sustainability of the building in combination with placing a structural window. For example, the cavity wall could be filled with insulation.

9.2. Processing of feedback

The processing of the feedback is explained for each aspect separately. These are listed below:

- **Connected elements:** it is indeed found that strengthening with the structural window results in a larger seismic force demand. This effect has been discussed in chapter 15 and is incorporated in the recommendations for the seismic performance assessment. These can be found in section 17.2.
- **Ventilation:** the influence of openable window sections on the structural potential of the designed structural window has been included in this thesis and is discussed in section 15.3.

- **Load duration:** the material properties of the structural adhesive are expected to be dependent on load duration, loading rate, and loading repetitions. These dependencies were not taken into account in this thesis and have been included in the recommendations for the experimental validation steps. These can be found in section 17.2.
- **Production process:** the production process of the prefabricated structural window is not discussed in this thesis. However, examples of the production process can be found in literature, e.g. Huveners [18]
- **Installation:** The installation process of the prefabricated structural window has not been further investigated. However, this remark has been included in the recommendations for the structural window design. These can be found in section 17.2.
- **Wet connection:** A dry connection solution is expected to be challenging. It will be difficult to compensate for the irregularities in the existing building while maintaining the possibility for load transfer between masonry and frame. Therefore, the wet connection with injection mortar is preferred. However, it is recommended to further examine the practical feasibility of the wet joint focussing on the possible risk of leakage. This recommendation is adopted in the recommendations for the structural window design and can be found in section 17.2.
- **Other possibilities:** Combining the strengthening measure with other measures has not been further investigated. However, this remark has been included in the recommendations for the structural window design. These can be found in section 17.2.

10

Conclusions part II

The structural window was designed with the aim to increase the in-plane seismic force capacity of an existing URM structure by utilisation of the glass pane as a structural element. The design of the structural window aims to safely utilise the glass pane by load transfer through the circumferentially adhesive bonded joint under most loading conditions. Direct contact between the frame and glass is preferably prevented for most loading conditions and is only considered acceptable under extreme loading conditions. During this stage, a substantial part of the structural adhesive is torn and the glass panes might fail suddenly due to local stress concentrations at the two loaded corners.

The structural window is composed of a timber frame, a semi-rigid adhesive, and double glazing unit. The structural layer of the double glazing has a thickness of 20mm and is composed of two laminated annealed glass panes with equal thickness. Sikaflex-252 is applied as structural adhesive and has a thickness of 5mm. The prefabricated structural window is placed in-plane with the existing load-bearing inner leaf of the cavity wall. The connection of the prefabricated structural window to the existing structure is made with an injection mortar that fills a gap up to 25mm at all sides of the prefabricated structural window.

The technical and practical feasibility of the structural window design was validated by a presentation for seismic retrofitting experts at CVW and a renovation expert. Several suggestions were listed in chapter 9 and these have been either incorporated in this thesis or recommendations.

The structural window could be realistically modelled adopting the component approach. In this modelling approach, all components of the structural window design are modelled. Beam elements, 2D continuum elements, and nonlinear interface elements are adopted for timber frame, the glass panel, and structural adhesive respectively. The nonlinear material properties of the structural adhesive do not only incorporate adhesive failure, but also an increased stiffness at glass/frame contact. Glass/frame contact occurs when the relative normal interface displacement in the negative direction reaches the thickness of the structural adhesive.

Additionally, a theoretical upper-bound solution is obtained adopting the superglue approach for the structural window. In this approach, the structural adhesive and timber frame are neglected. Only the glass pane is modelled by a 2D continuum that is rigidly connected to the surrounding masonry elements. This approach is expected to give an upper-bound envelop for the capacity curve of the actual strengthened structure.

11

Validation window model

A 2D window model in DIANA FEA 10.2 will be validated with experimental results reported by Huveners [18]. Huveners [18] describes experiments in which the potential of steel-glass composite walls as stabilizing elements is investigated. In these experiments, a steel frame is connected to a single glass pane by a circumferentially adhesive bonded joint. The suitability of different joint types and types of structural adhesives are investigated. A monotonic in-plane load is applied at the TLC of the composite wall to obtain the capacity curve. These experiments were performed up to failure and the different governing failure mechanisms are discussed. This chapter will only consider joint type 1 with a PU joint (Sikaflex-252) across the thickness of the glass pane.

11.1. Model geometry

Figure 11.1 shows an exploded view of the build up of the window model.

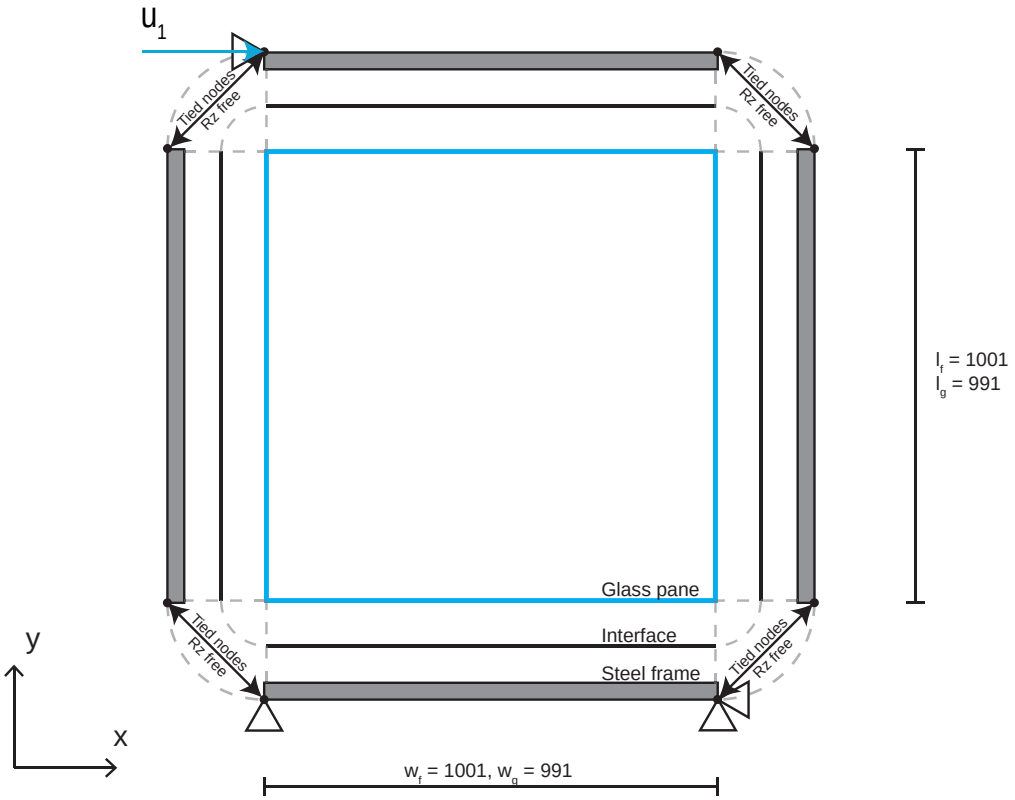

Figure 11.1: Exploded view of the computational model used for window model

The structural adhesive between the glass pane and steel frame is modelled with a NLE structural interface. The steel frame is composed of 4 beams with their nodes at the corners tied in the translational directions. The rotation around the z-axis is released for these corner nodes simulating hinge behaviour. The lateral displacement load is applied at the TLC of the steel frame.

11.2. Discretization

The glass pane is modelled with quadrilateral plane stress elements. These elements can be applied since the experiments showed that out-of-plane failure of the glass pane is not expected. The steel frame is discretized in class-III beam elements. Both the steel frame and glass pane are modelled with linear elastic material properties.

Table 11.1: Discretization into elements for glass pane and steel frame for URM wall model.

	Glass pane	**Steel frame**
Material model	Linear elastic isotropic	Linear elastic isotropic
Element type	Plane stress (CQ16M)	Class-III beams (CL9BE)
DOFs	u_x, u_y	u_x, u_y, ϕ_z
Integration scheme	2x2	2-point Gauss
Mesh size [mm]	50	50
Thickness [mm]	12	-
Cross-section [mm^2]	-	7200 (120x60)

The PU adhesive joint is modelled with nonlinear 2D line interface elements. The nonlinear behaviour is implemented based on diagrams and takes into account failure, i.e. tearing, of the joint. An overview of their element properties can be found in table 11.2. It should be noted that the reported in table 11.2 thickness corresponds to the thickness in the out-of-plane direction. The adhesive joint has a in-plane thickness of 5mm.

Table 11.2: Discretization into elements for structural adhesive.

	PU adhesive
Material model	Nonlinear elasticity
Element type	2D line interface (CL12I)
DOFs	u_x, u_y
Integration scheme	3-point Newton-Cotes
Mesh size [mm]	50
Thickness [mm]	12
NLE properties input	Diagrams

11.3. Material properties

The steel frame and glass pane are modelled with linear elastic isotropic behaviour. An overview of their properties can be found in table 11.3.

Table 11.3: Material properties for glass pane and steel frame

Property	**Parameter**	**Symbol**	**Unit**	**Glass pane**	**Steel frame**
Elasticity	Young's modulus	E	MPa	70,000	210,000
	Poisson's ratio	v	-	0.23	0.20
	Density	ρ	kg/m^3	2,400	7,800

The nonlinear diagrams of the PU adhesive are reported in Huveners [18] and are shown in figure 11.2. The LE properties of the interface are k_n = 1.2 N/mm^3 and k_s = 0.1 N/mm^3. Important points of the diagram are labelled. First of all, tearing of the adhesive joint occurs at a normal displacement of +2.5mm, a transverse displacement of -5mm, and a transverse displacement of +5mm. Secondly, a normal displacement of -5mm simulates reaching the activation displacement. The stiffness of the joint significantly increases beyond this point simulating contact between the steel frame and glass pane.

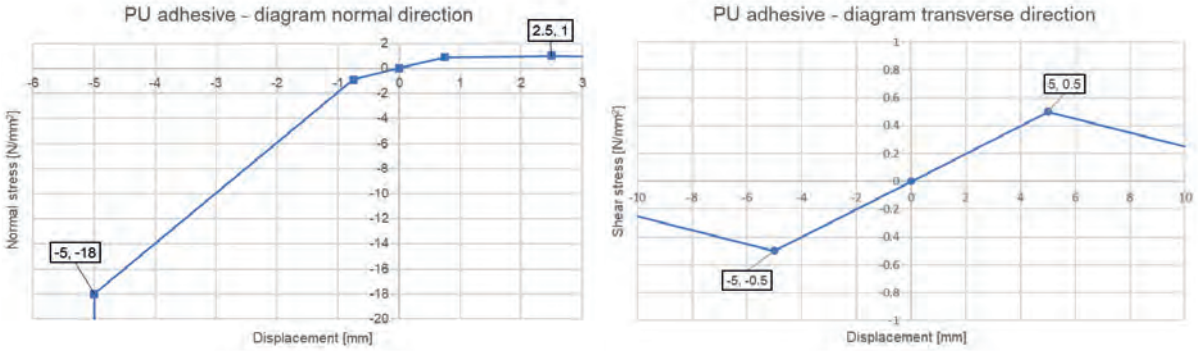

DUSTNY (u_y σ_y):
[-7.5 1,800,000; -5 -18; -0.75 -0.9; 0 0; 0.75 0.9; 2.5 1; 25 0.001]

DUSTSX (u_x τ_x)
[-50 -0.0005; -5 -0.5; 0 0; 5 0.5; 50 0.0005]

Figure 11.2: Initial diagrams adopted for the structural adhesive.

11.4. Analysis method

An overview of the applied analysis method is shown in table 11.4. Only physical nonlinearity is included.

Table 11.4: Analysis method applied for the window model

Load	Load name	Lateral displacement
	Load	40mm
	Steps	0.01(100)
Iterative procedure	Procedure	Regular Newton-Raphson
	Max. iterations	50
	Line search	No
Convergence criterium	Norm	Force & displacement
	Tolerance	0.01
	No convergence	Terminate

11.5. Results

Capacity curve

Figure 11.3 compares the obtained capacity curve of numerical model with the experimentally obtained results found in Huveners [18]. In the pre-activation stage, the capacity curve seems to match reasonably well. In the post-activation phase, the numerical result is too stiff compared to the experiments. The absence of failure in the post-activation stage can be explained by the LE properties of glass pane in the numerical model.

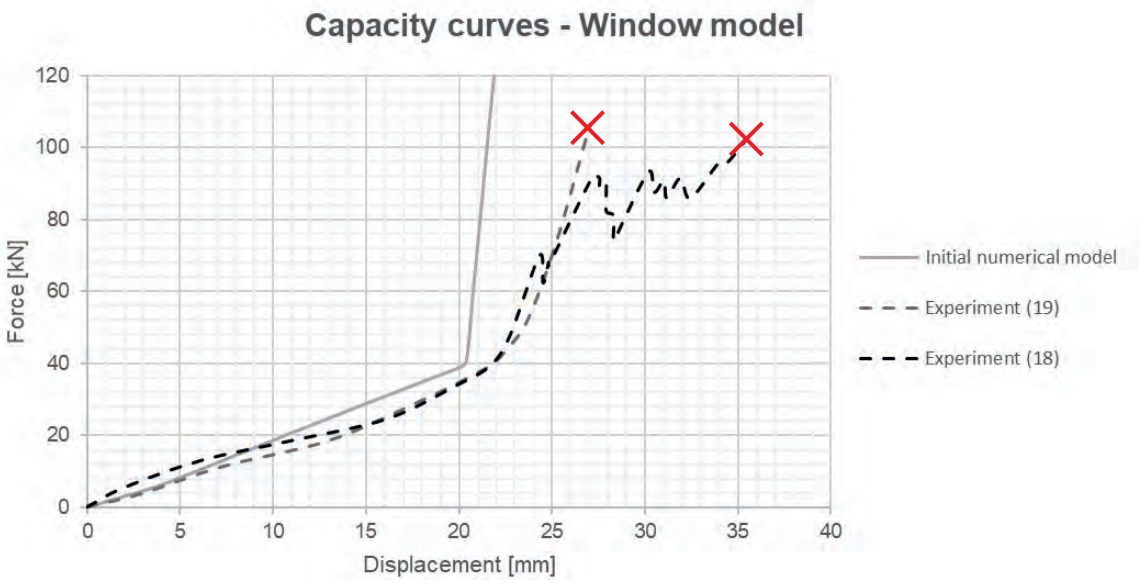

Figure 11.3: Comparison of the results of the initial window model with experimental results in Huveners [18].

Activation displacement

The numerical model predicts an activation displacement (d_a) of 20.4mm which is slightly lower compared to the experimental results. However, equation 11.1 shows that the analytically calculated d_a matches reasonably well with the numerical result. This analytical formula was derived in section 6.2

$$d_a = l_f - \frac{d_g^2}{2l_f} = 1001 - \frac{991^2 + 991^2}{2 * 1001} = 19.9mm \tag{11.1}$$

11.6. Calibration of results

Capacity curve

The numerical model is adjusted to improve the post-activation behaviour of steel-glass composite wall. The stiffness of the structural interface beyond a normal displacement of -5mm is reduced. The updated diagrams are shown in figure 11.4.

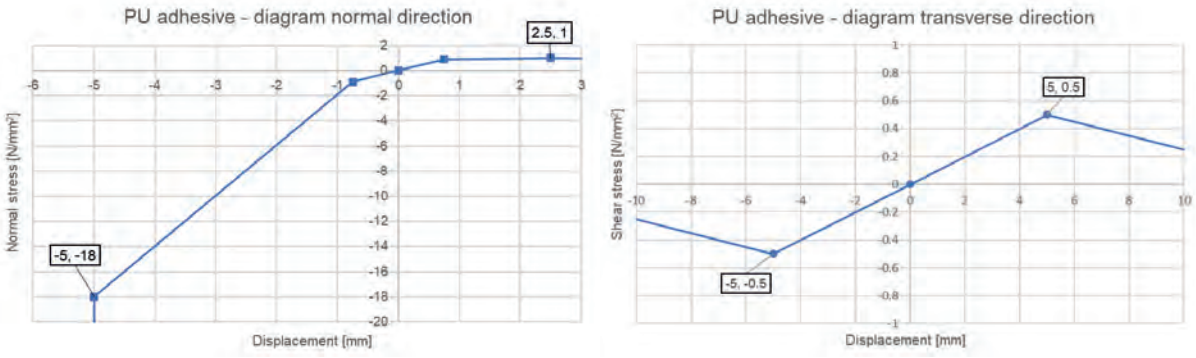

DUSTNY (u_y σ_y):
[**-10 -1200; -5.5 -50;** -5 -18; -0.75 -0.9; 0 0; 0.75 0.9; 2.5 1; 25 0.001]

DUSTSX (u_x τ_x)
[-50 -0.0005; -5 -0.5; 0 0; 5 0.5; 50 0.0005]

Figure 11.4: Updated diagrams of the structural adhesive material properties (updated values are given in bold).

Figure 11.5 compares the improved numerical results with the experiment results found in Huveners [18]. The updated post-activation stage matches reasonably well with the experimental results.

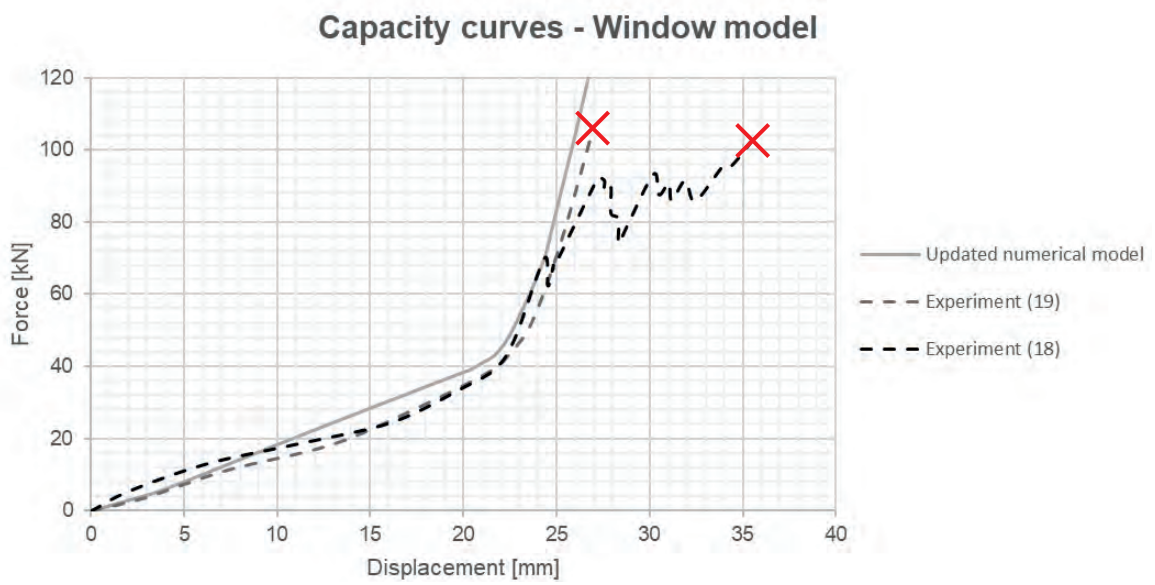

Figure 11.5: Comparison of the results of window model after post-activation calibration of interface properties.

Window capacity curve stages

It is found that the two main stages of the capacity curve of squared steel-glass composite wall that were identified in section 6.2 can be further refined. Both the pre-activation and post-activation stage can be divided into two substages resulting in a total of four subsequent substages which are shown by the colours in figure 11.6.

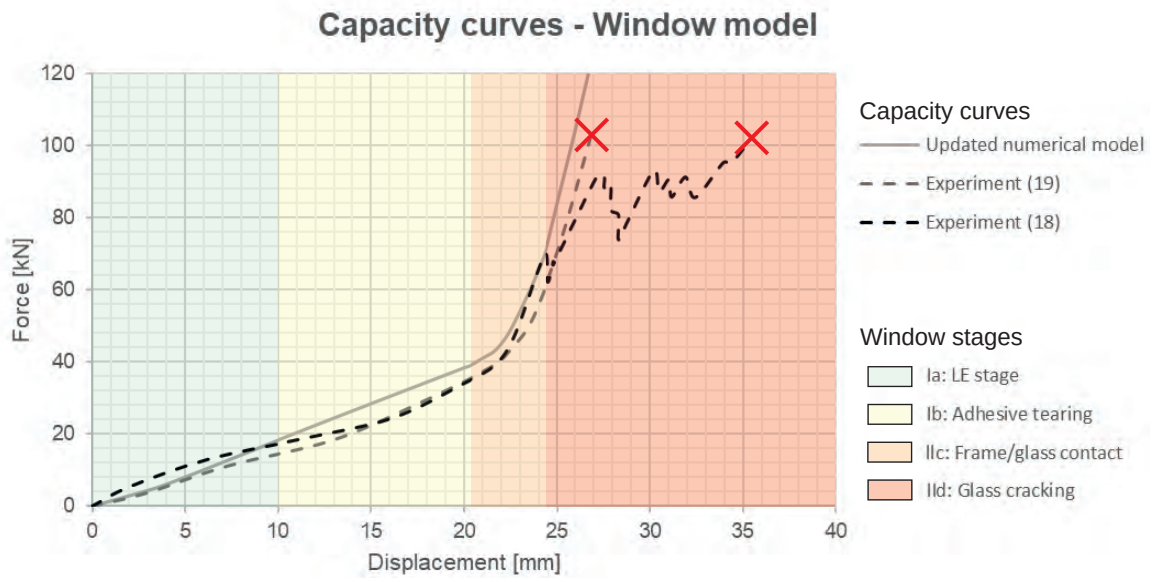

Figure 11.6: Division of the capacity curve of steel-glass composite wall into four subsequent substages.

The first substage, depicted in green, is a LE stage in which the loads are transferred through the adhesive joint without tearing of the adhesive.

The second substage starts at a lateral displacement of 10mm when the maximum relative normal interface displacements reaches +2.5mm and tearing of the adhesive is initiated. It is observed that the steel-glass composite wall has significant residual capacity beyond the initiation of adhesive tearing.

The second substage proceeds to a lateral displacement of 20.4mm and the relative normal interface

reaches a value of -5.0mm indicating that frame/glass contact occurs. The lateral displacement at which frame/glass occurs corresponds to the activation displacement. In the subsequent third substage, the global stiffness of the steel-glass composite wall increases significantly and local peak stresses develop in the glass pane at the TLC and BRC.

Lastly, in the fourth substage cracking of the glass pane initiates. Based on the experimental results, it is found that cracking of the glass pane initiates when the force capacity reaches 70kN. The numerical model reaches this force capacity at a lateral displacement of 24.4mm.

Figure 11.7 shows the numerical results for the relative normal displacement of the interface and the principle stresses in the glass pane at the transition points between the subsequent substages.

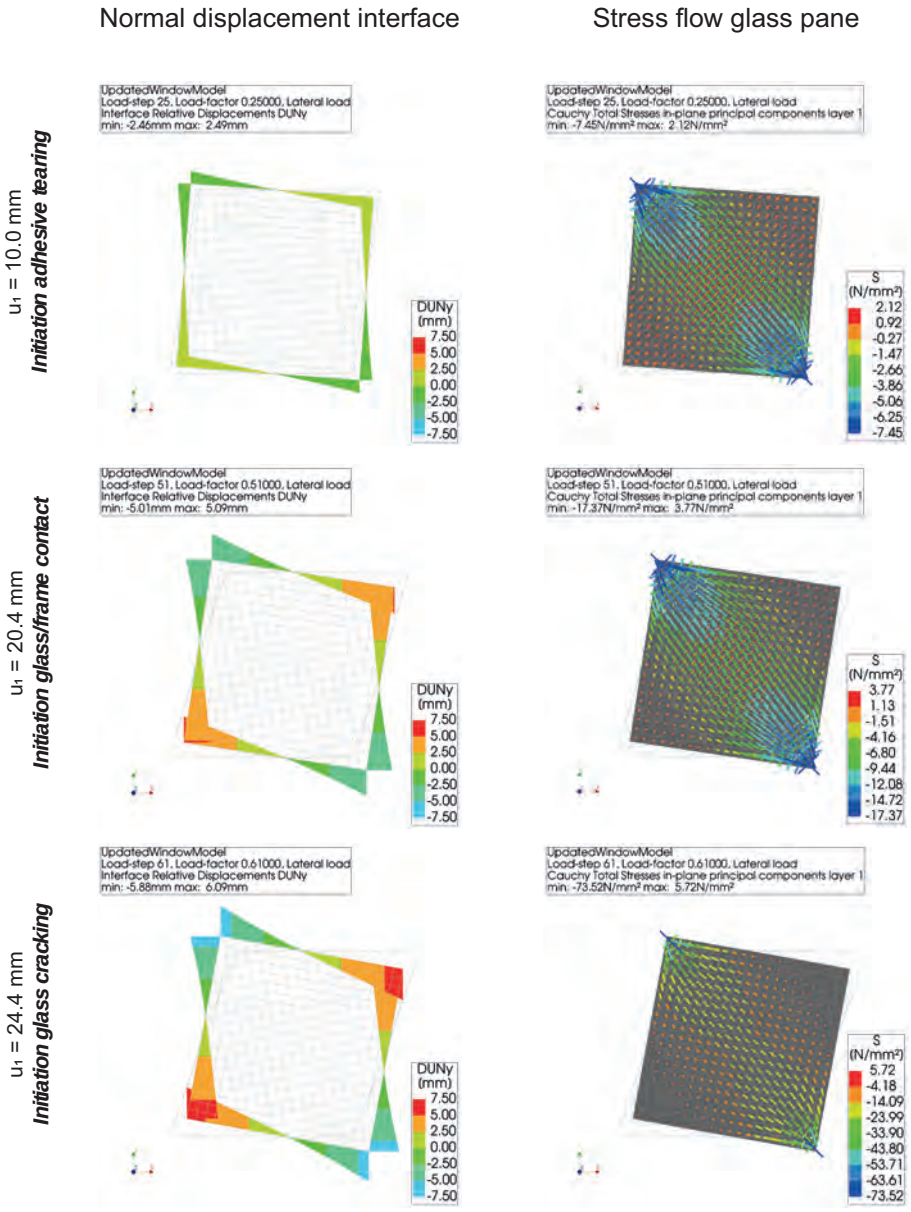

Figure 11.7: Interface normal displacement and stress flow of the window model at transition points of capacity curve. (DSF: 10)

It is observed that the interface normal displacement reach values of +2.5mm and -5.0mm at a lateral displacements of 10mm and 20.4mm respectively. Furthermore, it can be seen that at the initiation of glass cracking stress levels in the glass pane range between -73.53 N/mm^2 and +5.72 N/mm^2.

11.7. Conclusions chapter 11

The capacity curve of a steel-glass composite wall was adequately captured by a 2D finite element model in DIANA 10.2. The model only included failure of the adhesive. The steel frame, and glass pane were given LE material properties. The nonlinear material properties of the PU adhesive not only incorporated adhesive tearing, but also an increased stiffness at glass/frame contact. The nonlinear material properties of the PU adhesive were calibrated based on the experimental capacity curves reported in Huveners [18]. This calibration focussed on the shape of the capacity curve after glass/frame contact. The calibrated nonlinear material properties of the PU adhesive with a thickness of 5mm were given in figure 11.4.

Furthermore, figure 11.6 showed that the capacity curve of a squared steel-glass composite wall can be divided in four subsequent substages. This is a refinement of the two main stages that were identified in section 6.2. The transition between the substages are marked by transition points that represent the initiation of adhesive tearing, glass/frame contact, and the initiation of glass cracking subsequently. The stress levels at the initiation of glass cracking were found to be between -73.53 N/mm^2 and 5.72 N/mm^2.

12

Validation URM wall model

A 2D URM wall model in DIANA FEA 10.2 will be validated with experimental results reported by Korswagen et al. [19]. Korswagen et al. [19] describes experiments on three single-wythe walls of clay brick masonry subjected to a repetitive one directional in-plane pushover load reaching a maximum value of 1.2 mm. The single-wythe walls were built to replicate masonry properties that are found in the Dutch building stock from before 1950. The goal of this study was to investigate light damage, crack initiation and crack propagation in masonry.

12.1. Model geometry

Figure 12.1 shows the model build up. The single-wythe wall has a thickness of 100mm. The masonry wall was glued to a HEM600 and HEM300 steel beam at its top and bottom respectively. The wall is subjected to a precompression load of 12 N/mm. In addition, a displacement controlled pushover load of 4 mm is applied at the TLC of the wall.

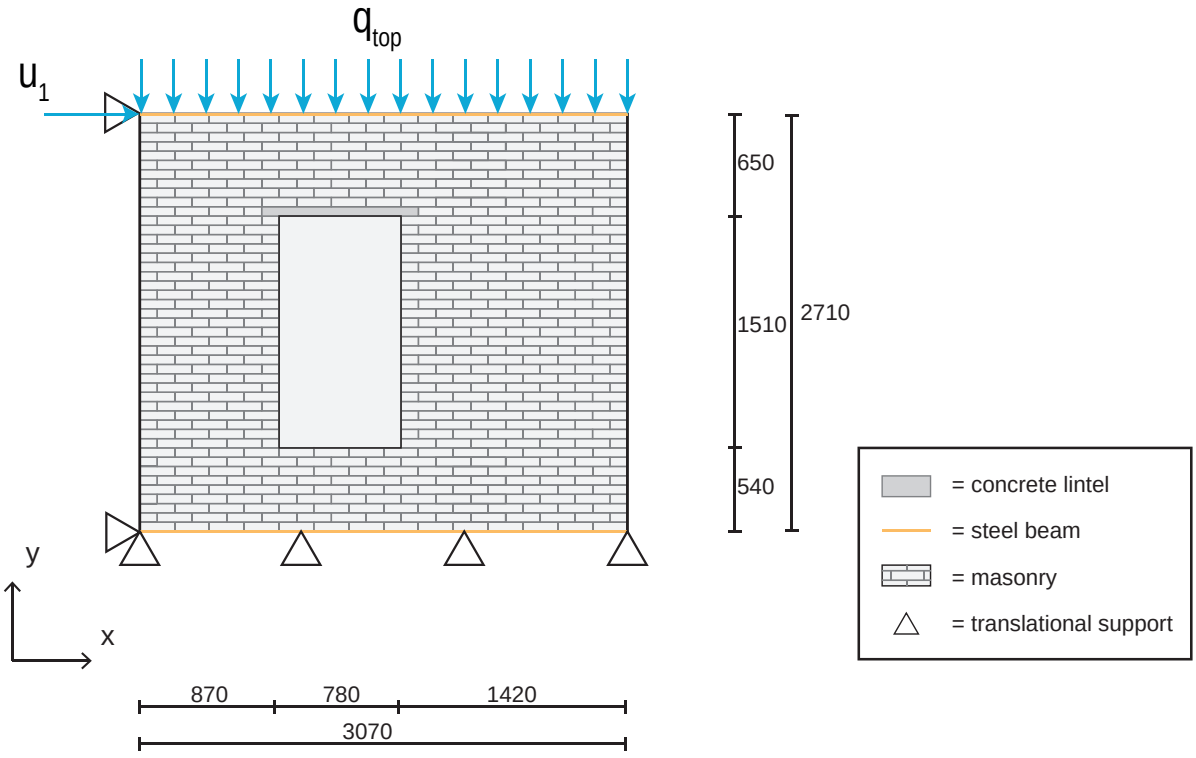

Figure 12.1: Build-up of the computional model used for the URM wall model

12.2. Discretization

The finite element model discretizes the wall into quadrilateral elements of 50mm x 50mm. Plane stress elements are adopted since out-of-plane action is expected to be negligible. The steel beams have been discretized into class-III elements. Nonlinear material behaviour is included for the masonry only, because failure is expected to occur in the masonry. An overview of the discretization into elements is given in table 12.1.

Table 12.1: Discretization into elements for the URM wall model.

	Masonry walls	**Concrete lintel**	**Steel beams**
Material model	Engineering Masonry Model	Linear elastic isotropic	Linear elastic isotropic
Element type	Plane stress (Q8MEM)	Plane stress (Q8MEM)	Class-III beams (L6BEA)
DOFs	u_x, u_y	u_x, u_y	u_x, u_y, ϕ_z
Integration scheme	2x2	2x2	1-point Gauss
Mesh size [mm]	50	50	50
Thickness [mm]	100	100	-
Cross-section [mm^2]	-	-	Top beam: HEB600 Bottom beam: HEB300

12.3. Material properties

The steel beams and concrete lintel are modelled with linear elastic isotropic behaviour. An overview of their properties can be found in table 12.2.

Table 12.2: Material properties for concrete lintel and steel beams for the URM wall model.

Property	**Parameter**	**Symbol**	**Unit**	**Concrete lintel**	**Steel beams**
Elasticity	Young's modulus	E	MPa	33,500	210,000
	Poisson's ratio	v	-	0.2	0.2
	Density	ρ	kg/m^3	2,500	7,800

.

The engineering masonry model (EMM) is adopted for the masonry taking into account nonlinear and orthotropic behaviour. This material model includes cracking, crushing and sliding failure behaviour. An overview of the material properties of the masonry can be found in table 12.3. These properties have been reported in [19].

Table 12.3: Material properties for macro-modelling of clay masonry for the URM wall model according to Korswagen et al. [19].

Property	**Parameter**	**Symbol**	**Unit**	**Value**
Elasticity	Young's modulus	E_x	MPa	2,200
		E_y	MPa	3,400
	Shear modulus	G_{xy}	MPa	1,300
	Density	ρ	kg/m^3	1,680
Cracking	Tensile strength	f_{ty}	MPa	0.10
	Tensile fracture energy	G_{ft}	N/mm	0.005
	Diagonal crack orientation	α	rad	0.792
Crushing	Compressive strength	f_c	MPa	14
	Compressive fracture energy	G_c	N/mm	20
Sliding	Cohesion	c	MPa	0.15
	Fracture energy in shear	G_{fs}	N/mm	-
	Friction angle	ϕ	rad	0.6

12.4. Analysis method

An overview of the applied analysis method is shown in table 12.4. The structural analysis consists of two load steps. The self-weight and precompression load is applied in load step 1. Secondly, the

pushover load is applied in load step 2. In contrast to the experiment, the pushover load is applied monotonically in steps of 0.04 mm in order to save computational time. In addition, the wall is loaded with a larger pushover load compared to the experiment. Only physical nonlinearity is included.

Table 12.4: Analysis method applied for URM wall validation model.

Loadstep 1	**Load**	Load name	Self-weight + precompression
		Load	12 N/mm
		Steps	1.0
	Iterative procedure	Procedure	Regular Newton-Raphson
		Max. iterations	100
		Line search	Yes
	Convergence criterium	Norm	Either force or displacement
		Tolerance	0.01
		No convergence	Terminate
Loadstep 2	**Load**	Load name	Pushover load
		Load	4 mm
		Steps	0.01 (100)
	Iterative procedure	Procedure	Regular Newton-Raphson
		Max. iterations	50
		Line search	Yes
	Convergence criterium	Norm	Either force or displacement
		Tolerance	0.01
		No convergence	Continue

12.5. Results

Capacity curve

Figure 12.2 shows that the obtained capacity curve is well in line with results in reported Korswagen et al. [19]. Both the initial stiffness and force capacity are adequately captured by the numerical model. It should be noted that the results shown from Korswagen et al. [19] are not those from the experiment, but from the calibrated numerical model used in that report.

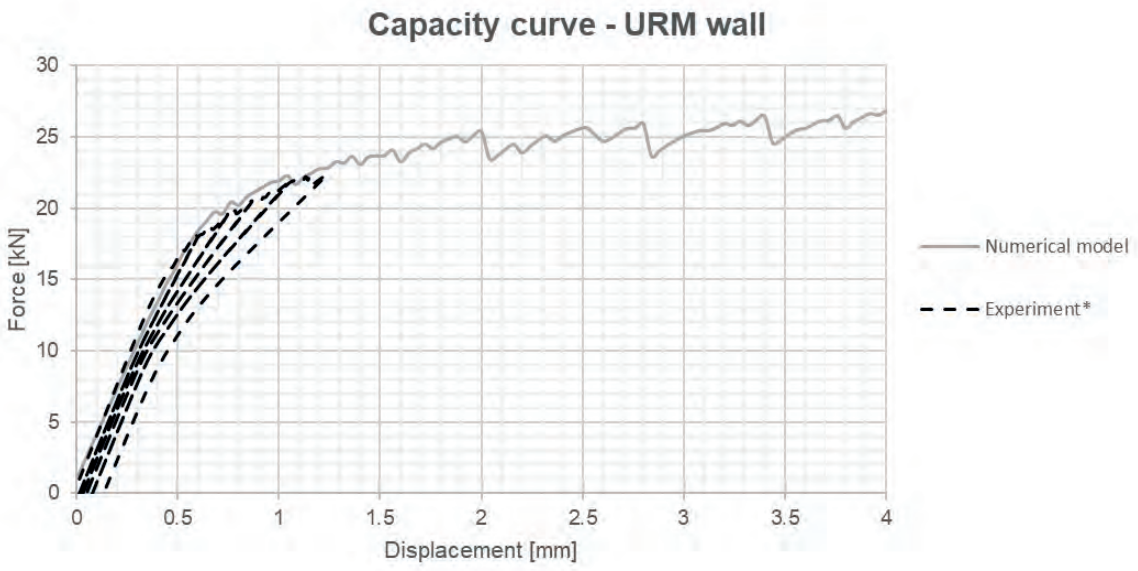

Figure 12.2: Comparison of results with (numerical) results reported in [19]. * = experimental results are from calibrated numerical model used in [19].

Crack patterns

Figure 12.3 gives a closer look into the results obtained by the numerical model. The stress flow and cracks at a lateral displacement of 0.64mm, 1.20mm and 4.00mm. These points mark the end of the LE stage, the maximum displacement applied in the experiment, and the maximum displacement applied in the numerical model respectively. The damage categories given in section 3.3 have been adopted in the contour plot of the crack widths. It can be observed that the two piers are showing the rocking failure behaviour with damage concentrating at the top and bottom of the two piers. In addition, diagonal/vertical cracks are observed in the wide pier.

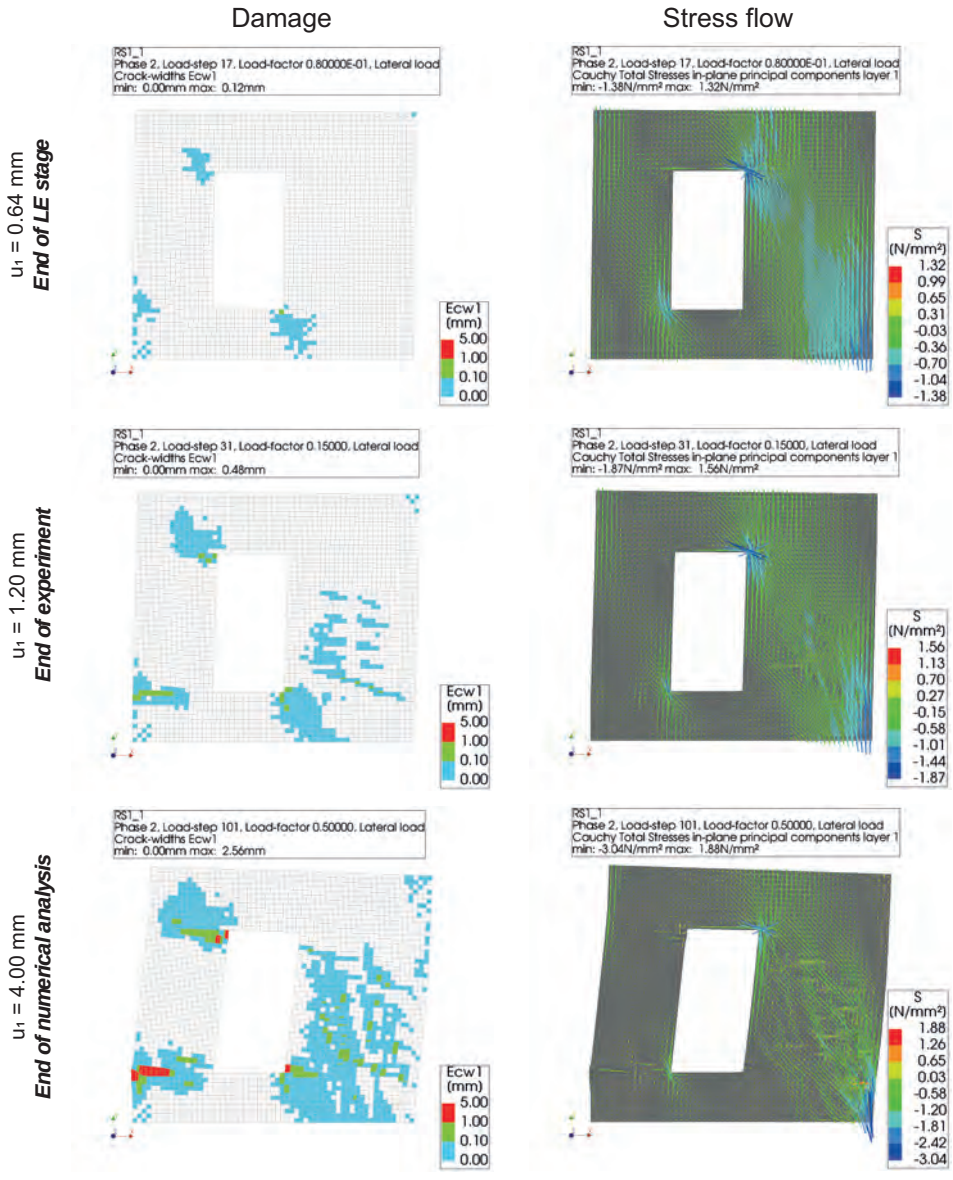

Figure 12.3: Damage evolution and stress flow of the numerical model for the URM wall. (DSF: 50)

The crack pattern observed at $u_1 = 1.2mm$ in the numerical model has been compared with the crack patterns observed in the experiments in figure 12.4. All experimental results show a governing rocking failure mechanism with crack concentrations at the top and bottom of the two piers. However, a variety is observed in the exact crack patterns of the different masonry walls. The rocking failure mechanism was adequately capatured by the numerical model, but the exact crack patterns do not match any of the experimental results.

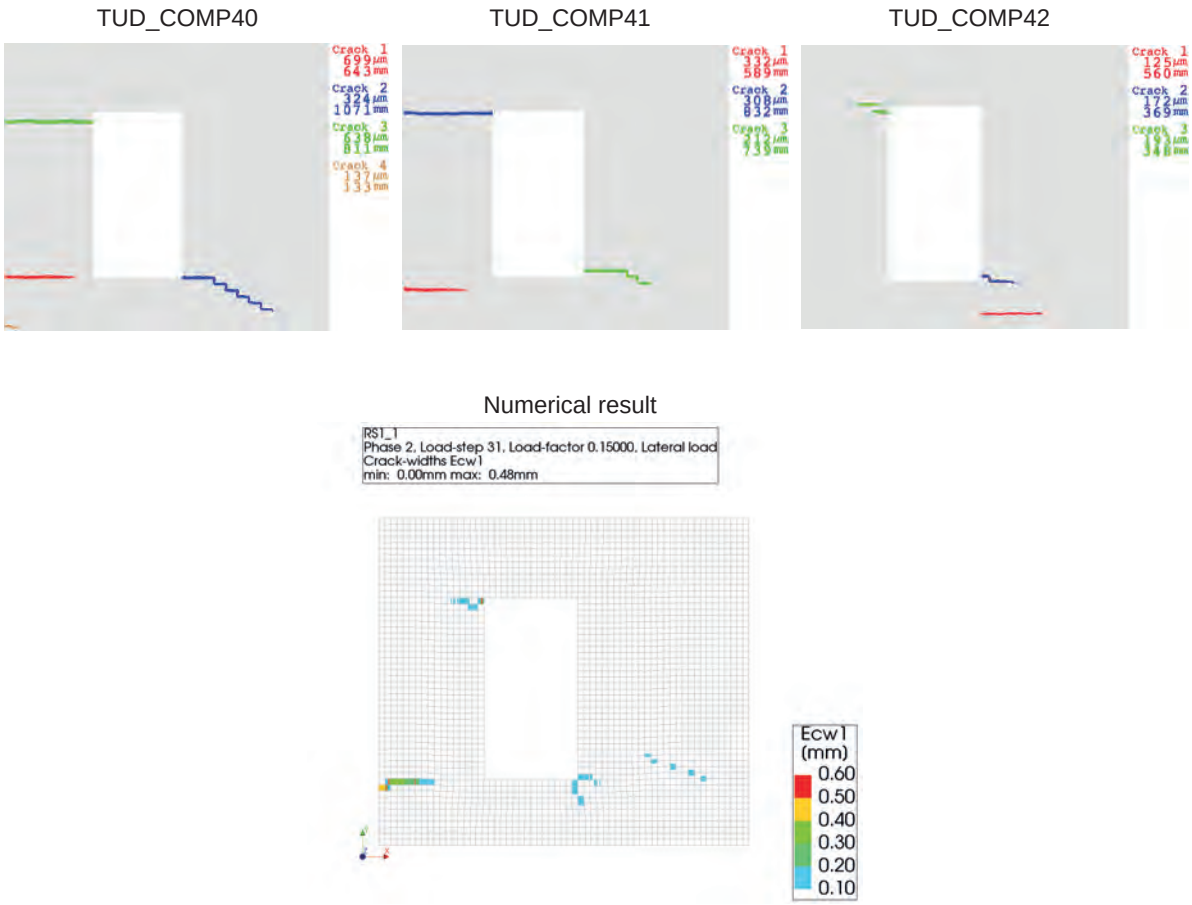

Figure 12.4: Comparison of crack patterns observed in the experiment (P. Korswagen, personal communication, March 28, 2019) and numerical model for the URM wall ($u_1 = 1.2mm$). For the numerical model results outside limits are hidden.

Different suggestions for improving the damage characteristics of the numerical model are listed below:
- Adopt a (detailed) micro-modelling technique for the masonry walls.
- Adopt 3D solid elements or 2D shell elements instead of 2D plane stress elements.
- Adopt a material model that includes cyclic damage accumulation and apply a repetitive loading scheme instead of a monotonic loading scheme.

Despite the clear differences in terms of damage characteristics, implementation of these suggestions is considered to be outside of the scope and aim of this thesis. The numerical model is considered to be acceptable for the purpose of this study.

12.6. Conclusions chapter 12

The capacity curve of a single-wythe wall of clay brick masonry was adequately captured by a 2D finite element model in DIANA 10.2. In addition, the governing rocking failure mechanism with crack concentrations at the top and bottom of the two piers is observed in both the experiment and numerical model. However, the exact crack patterns and corresponding crack widths prove to be difficult to capture correctly. These damage characteristics are likely to improve by adopting a more detailed modelling approach (e.g. 2D shell elements, 3D solid elements or micro-modelling) for the masonry. However, this is considered to be outside of the scope and aim of this thesis.

It is concluded that the numerical model setup provides a good starting point for variation studies in which a structural window is included in the numerical model.

13

Seismic strengthening predictions URM wall

The seismic strengthening predictions of the URM wall combines the validated window model with validated URM wall model and extrapolates the results. In this chapter, numerical results for strengthened models are compared with unstrengthened models. The unstrengthened models leave an opening at the location of the window, while the strengthened models incorporate the designed structural window adopting the component approach. Additionally, a theoretical upper-bound solution is obtained adopting the superglue approach for the structural window. Three cases with different window sizes are considered. For all cases, the full window area is utilised for the designed structural window leaving no gaps for ventilation. The URM wall is assumed to be a stability element present in both the front and back façade of a single-storey building with an effective mass of $16,000kg$. The URM wall is subjected to a one-directional monotonic pushover loading scheme. The seismic performance assessment addresses the capacity curve, window stages, and damage characteristics.

13.1. General settings

The properties of the validated URM wall model are adopted. Additional settings required for the inclusion of a structural window are given in this section. The properties of the components of structural window and the use of a phased structural analysis are discussed. These settings are the same for all of the three considered cases.

Additional finite elements

The glass pane and timber frame are both modelled with LE elements. An overview of their properties is given in table 13.1.

Table 13.1: Discretization into elements for glass pane and timber frame

	Glass pane	**Timber frame**
Material model	Linear elastic isotropic	Linear elastic isotropic
Element type	Plane stress (Q8MEM)	Class-III beams (L6BEA)
DOFs	u_x, u_y	u_x, u_y, ϕ_z
Integration scheme	2x2	1-point Gauss
Mesh size [mm]	50	50
Thickness [mm]	20	-
Cross-section [mm^2]	-	2,000 (50x40)

.

The component approach requires structural interfaces between frame/glass (interface 1) and masonry/frame (interface 2). Both interfaces are modelled with nonlinear 2D line interface elements. An overview of their properties is given in table 13.2.

Table 13.2: Discretization into elements for interfaces between frame/glass and masonry/frame

	Interface 1	**Interface 2**
Material model	Nonlinear elasticity	Nonlinear elasticity
Element type	2D line interface (L8IF)	2D line interface (L8IF)
DOFs	u_x, u_y	u_x, u_y
Integration scheme	2-point Newton-Cotes	2-point Newton-Cotes
Mesh size [mm]	50	50
Thickness [mm]	20	100
NLE properties input	diagrams	diagrams

.

Additional material properties

The LE material properties of the glass and the birch plywood are given in table 13.3.

Table 13.3: Material properties for glass pane and timber frame

Property	**Parameter**	**Symbol**	**Unit**	**Glass pane**	**Birch plywood**
Elasticity	Young's modulus	E	MPa	70,000	9,000
	Poisson's ratio	v	-	0.23	0.40
	Density	ρ	kg/m^3	2,400	680

.

Interface 1 represents a PU adhesive with a thickness of 5mm between the glass and frame. The NLE diagrams for this interface are according to the diagrams given in section 11.6 and are not repeated in this section.

Interface 2 represents an injection mortar connection between the masonry and frame. The NLE diagrams for this interface are given in figure 13.1. The properties of this interface are related to those of the adjacent masonry elements. The stiffness of these adjacent masonry elements is calculated in equation 13.1 and 13.2.

$$k_n = \frac{E}{l} = \frac{3400}{50} \approx 70 N/mm^3 \tag{13.1}$$

$$k_t = \frac{G}{l} = \frac{1300}{50} \approx 25 N/mm^3 \tag{13.2}$$

The normal stiffness of the interface is chosen to be large in the compressive direction ($\approx 100 * k_n$), while small in the tensile direction ($\approx 0.01 * k_n$) compared to the normal stiffness of the masonry elements. The shear stiffness of the interface in both directions is chosen to be comparable to the shear stiffness ($\approx k_t$) of the masonry elements. Failure of interface 2 is not included since failure of the adjacent masonry is assumed to be governing. Failure of the adjacent masonry element automatically limits the stress that is transferred by interface 2.

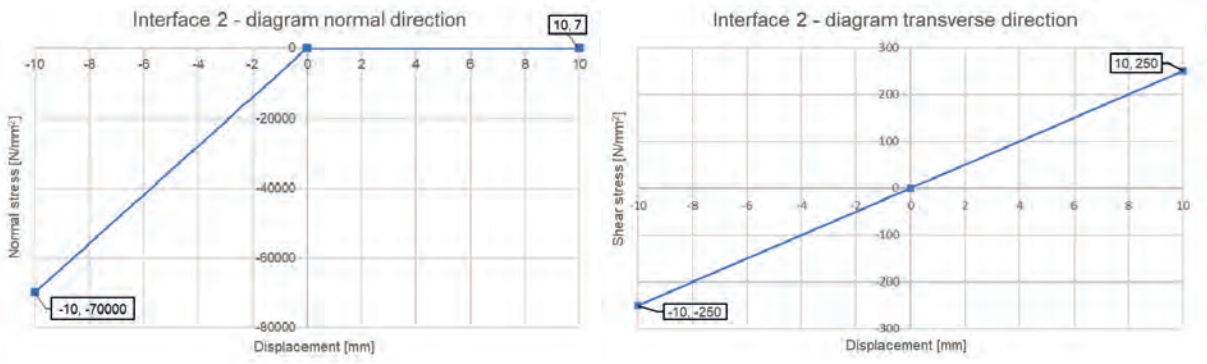

DUSTNY (u_y σ_y):
[-10 -70,000; 0 0; 10 7]

DUSTSX (u_x τ_x)
[-10 -250; 0 0; 10 250]

Figure 13.1: Assumed diagrams for the the masonry/frame connection.

Phased analysis

In all analyses the precompression and self-weight are first applied on the geometries of the masonry wall, lintel, top beam, and bottom beam only. Hereafter, the components of the structural window are added to the model in the second phase of the structural analysis to calculate the response to the pushover load. This phased analysis is necessary to take into account the self-weight and precompression load correctly. In the first phase, the structural window should not be loaded and the window components should not affect the stresses in the masonry since the structural window is placed into an existing structure. A total pushover load of $8mm$ is chosen. This value is expected to give sufficient insight into the capacity curve and failure mechanisms. A larger value is not preferred as this may result in convergence problems.

Table 13.4: Analysis method applied for seismic strengthening predictions of the URM wall models.

Phase 1 **Masonry structure only**	**Load steps**	Load name	Self-weight + precompression
		Load	12 N/mm
		Steps	1.0
	Iterative procedure	Procedure	Regular Newton-Raphson
		Max. iterations	100
		Line search	Yes
	Convergence criterium	Norm	Either force or displacement
		Tolerance	0.01
		No convergence	Terminate
Phase 2 **Complete model**	**Start steps**	Start step	Use load of previous phase
	Load steps	Load name	Pushover load
		Load	8 mm
		Steps	0.005(200)
	Iterative procedure	Procedure	Regular Newton-Raphson
		Max. iterations	50
		Line search	Yes
	Convergence criterium	Norm	Either force or displacement
		Tolerance	0.01
		No convergence	Continue

13.2. Small window

Model geometry

Figure 13.2 shows the build-up for computational model of the URM wall with a small window. In this case, the window area covers 14% of the total façade area. Results for the unstrengthened wall are compared with the strengthened wall, and the theoretical upper bound model. For the strengthened wall and theoretical upper bound model, the structural window is placed adopting the component and superglue approach respectively.

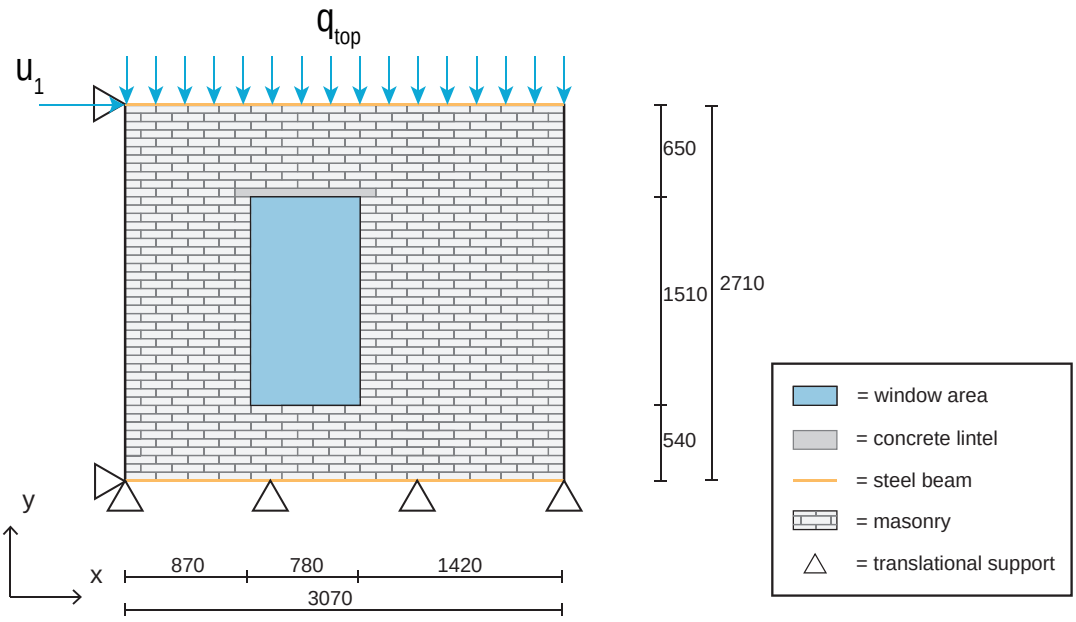

Figure 13.2: Build-up of the computational model used for the URM wall with a small window

Capacity curve

Figure 13.3 shows the obtained capacity curves for the URM wall with small window. At a displacement of 8mm, the strengthened wall has reached 137% of the seismic force capacity of the unstrengthened wall. This is close to the theoretical upper bound model that has 146% of the seismic force capacity of the unstrengthened wall. It is observed that the initial stiffness is increased for the theoretical upper bound model compared to the unstrengthened wall, while this is barely the case for the strengthened wall. For the strengthened wall, the contribution of the structural window increases with increasing lateral displacements. At the end of the LE stage, around 0.8mm, the capacity curve of the strengthened wall is close to the unstrengthened wall, while at the end of the analysis, at 8mm, it is closer to the theoretical upper bound model.

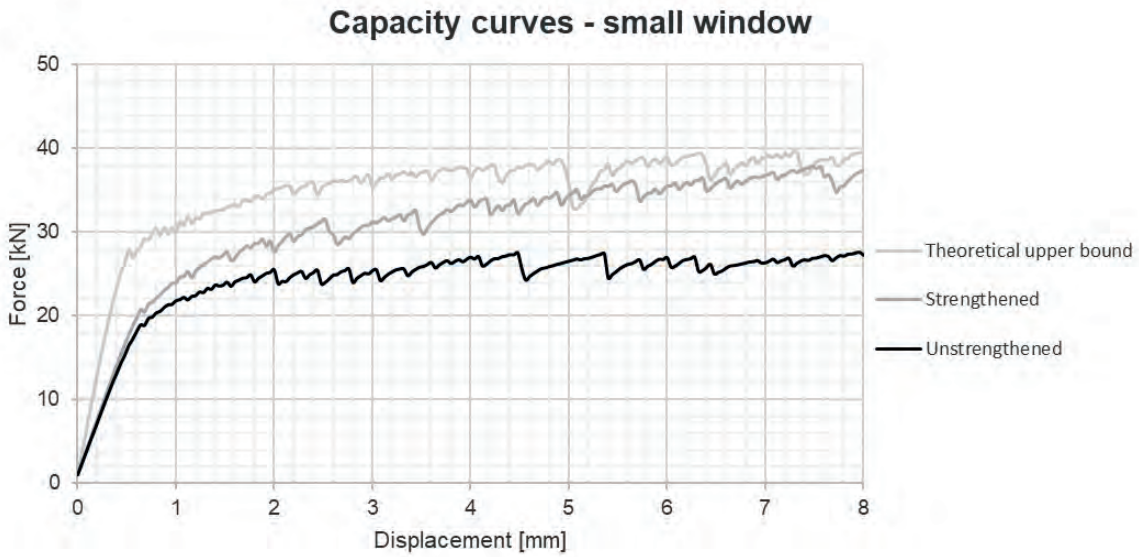

Figure 13.3: Capacity curves of seismic strengthening predictions for the URM wall with small window

Window stages

Figure 13.4 projects the window substages from section 11.6 on the capacity curve of the strengthened wall. It can be seen that the structural window remains in the first substage for the complete analysis up to a lateral displacement 8mm. This indicates that loads are transferred through the adhesive joint without tearing of the adhesive. In addition, no failure of the glass is expected for the analysis.

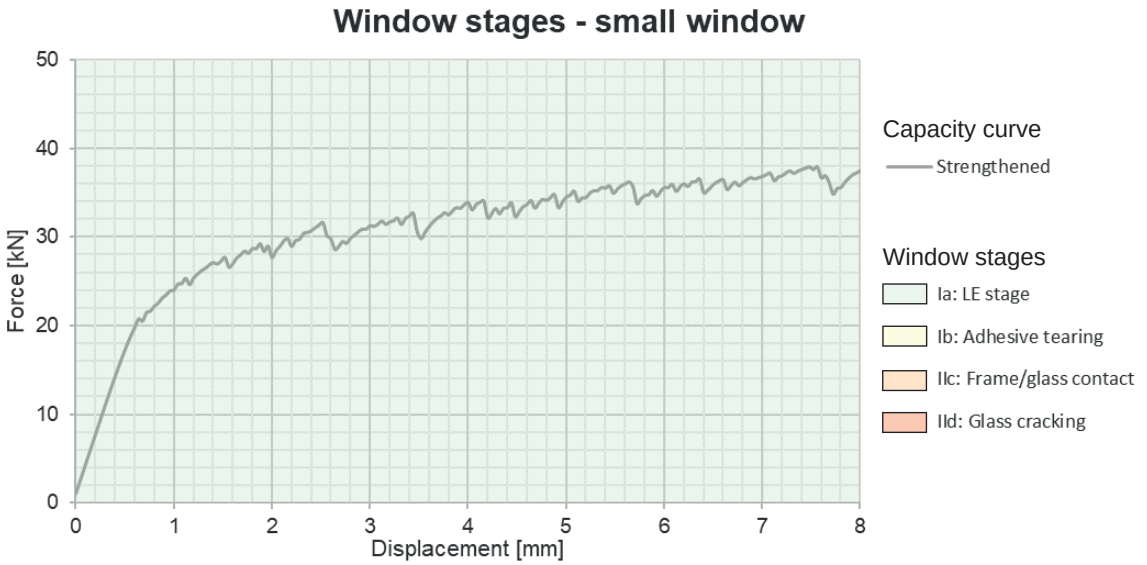

Figure 13.4: Projection of the window substages on the capacity curve of the strengthened URM wall with a small window.

Crack patterns

The crack patterns give insight into the failure mechanism that occurs. The cracks at the final step of the numerical analysis, i.e. a lateral displacement of 8mm, are compared for the unstrengthened wall, strengthened wall, and the theoretical upper bound model in figure 13.5.

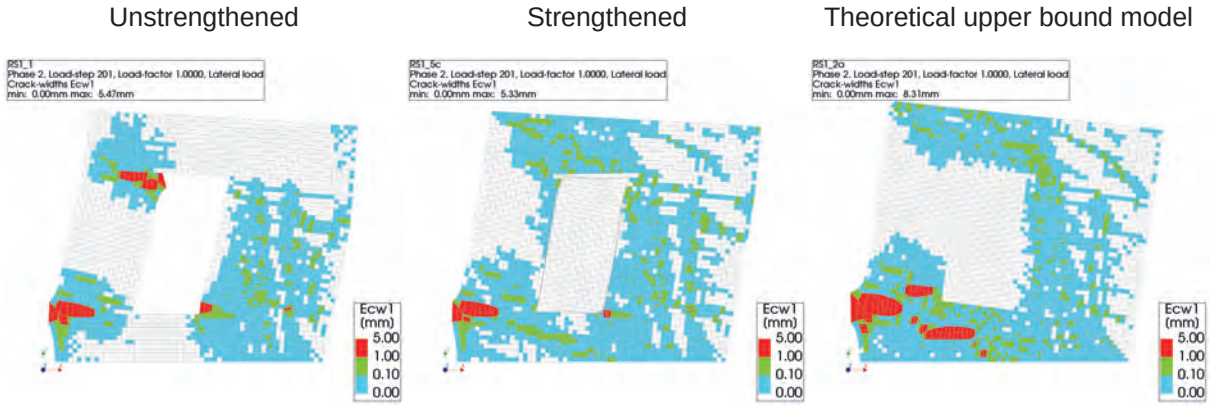

Figure 13.5: Crack patterns at a lateral displacement of 8mm for the URM wall with a small window case. (DSF = 50)

It is observed that the inclusion of the structural window affects the failure mechanism. The structural window seems to make collaboration between the piers possible. As a result, concentrated cracks mainly develop in the bottom left corner instead of two cracks, at the bottom of both piers. The maximum crack width for the theoretical upper bound model is significantly larger compared to the unstrengthened wall, while the strengthened wall results in a comparable maximum crack width at a lateral displacement of 8mm. In addition, the total number of cracked elements is larger for the strengthened wall, and theoretical upper bound model compared to the unstrengthened wall.

Of course, it should be kept in mind that the seismic deformation demand depends on structural characteristics. The capacity curves show that these characteristics are different for the three models. Therefore, this comparison does not give any insight into the damage that is expected as a result of a certain earthquake. The seismic performance including an evaluation of the expected damage as a result of different earthquakes is discussed in the next subsection.

Seismic performance

Based on the assumed effective mass of $16,000kg$ the seismic performance can be evaluated for a single-storey house. The seismic performance is evaluated for two locations: Groningen and Appingedam. This evaluation will compare the results for unstrengthened and strengthened wall. The theoretical upper bound model is disregarded as this model only served a theoretical purpose.

Average location - Groningen

The capacity curves of the unstrengthened and strengthened wall are plotted against the ADRS of a weak and strong earthquake in figure 13.6. It is observed that both walls have sufficient capacity for the strong earthquake. Nonetheless, the unstrengthened wall has very limited structural surplus to withstand the strong earthquake.

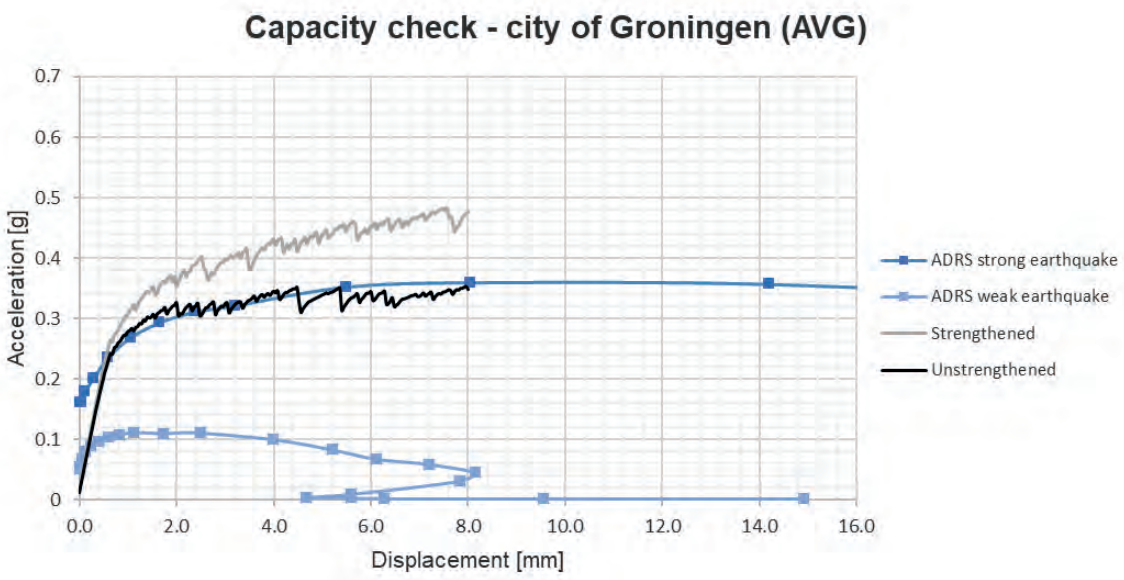

Figure 13.6: Average location - ADRS and obtained capacities for the URM wall with a small window.

A closer look is given to the expected damage as a result of a weak earthquake. First of all, the seismic deformation demand is determined by the intersection between the ADRS of the weak earthquake and the capacity curve. For both walls, this intersection is found in the LE stage of the capacity curve. Therefore, little damage is expected. The expected damage as a result of the weak earthquake is evaluated by three damage characteristics: the maximum expected crack width, the number of elements in damage category 1, and the number of elements in damage category 2. Figure 13.7 compares these damage characteristics for the two walls.

The effect of the structural window on the seismic performance of an URM wall with a small window located in the city of Groningen can be concluded.

Based on figure 13.6, it can be concluded that strengthening with the structural window has a positive effect on the seismic force capacity. The contribution of the structural window to the total seismic force capacity increases with increasing imposed lateral displacements. At a lateral displacement of 8mm, the strengthened wall reaches 137% of the seismic force capacity of the unstrengthened wall. However, both the unstrengthened and strengthened wall showed sufficient capacity to withstand a strong earthquake. Based on figure 13.7, it can be concluded that strengthening

with the structural window has no effect on the expected damage resulting from a weak earthquake. Both walls are expected to remain practically undamaged as a result of the weak earthquake. The maximum expected crack width of 0.02mm is negligible.

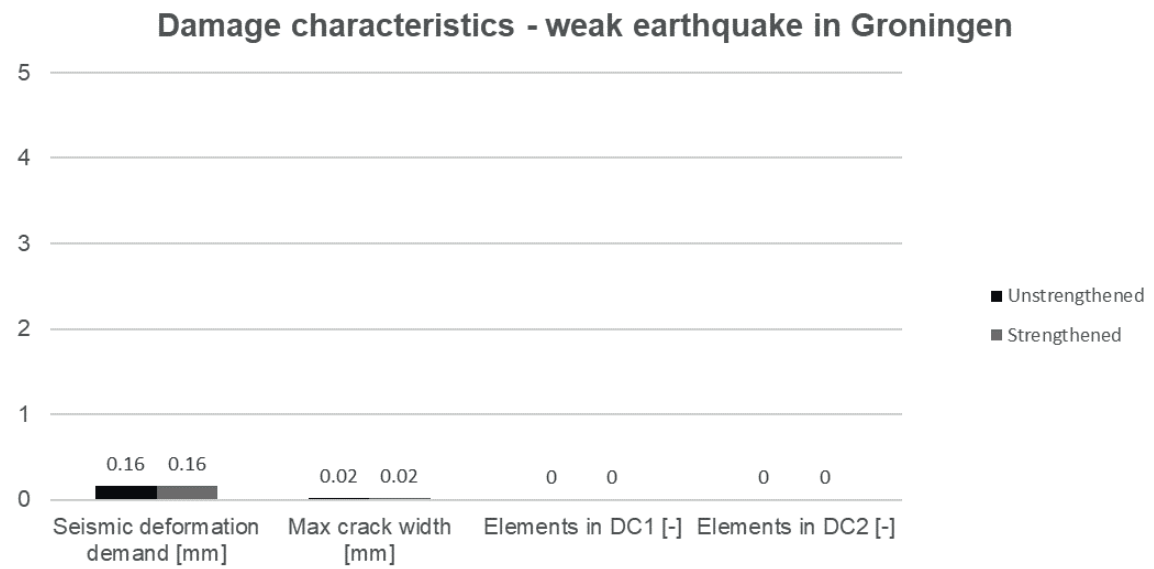

Figure 13.7: Average location - Damage analysis for the URM wall with a small window.

Extreme location - Appingedam

The capacity curves are plotted against the ADRS of a weak and strong earthquake in figure 13.8. It is observed that both models have sufficient capacity for a weak earthquake. However, both model show insufficient capacity to withstand a strong earthquake.

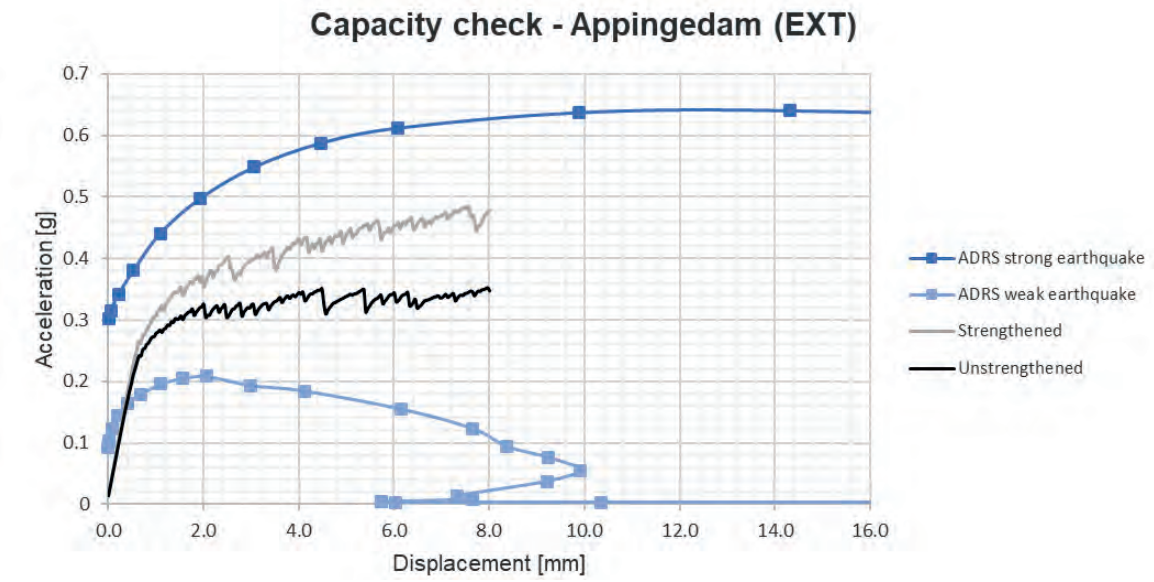

Figure 13.8: Extreme location - ADRS and obtained capacities for the URM wall with a small window.

Figure 13.9 gives an overview of the expected damage as a result of a weak earthquake in Appingedam. For both models, the intersection between the ADRS of the weak earthquake and capacity curve is found in the LE stage of the capacity curve. Therefore, little damage is expected. This is reflected by the maximum crack width of 0.05mm expected for both walls that can be considered negligible.

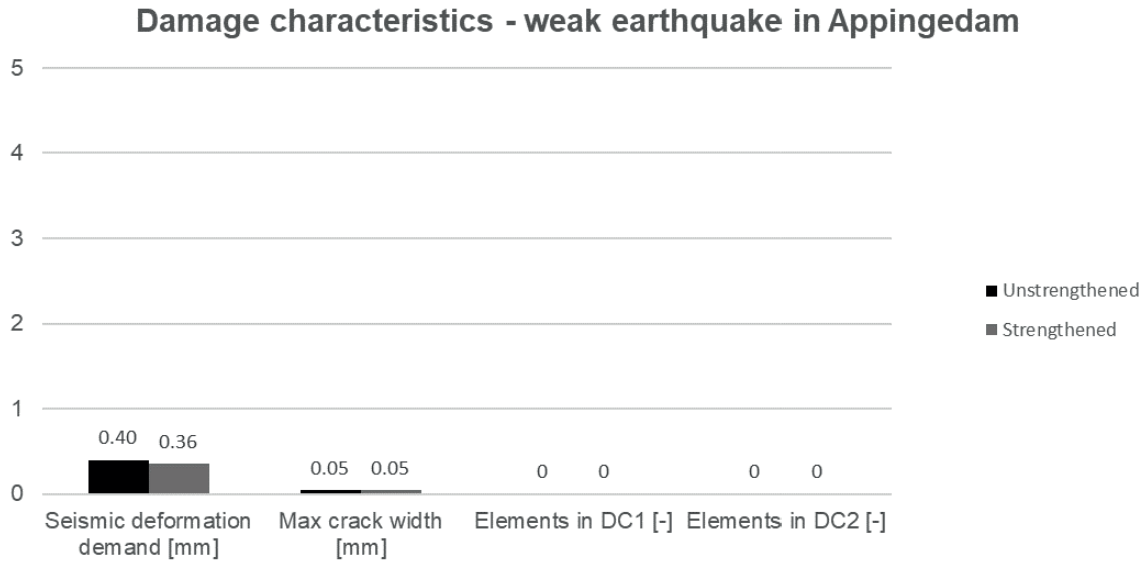

Figure 13.9: Extreme location - Damage analysis for the URM wall with a small window.

The effect of the structural window on the seismic performance of an URM wall with a small window located in the city of Appingedam can be concluded.

Based on figure 13.8, it can be concluded that strengthening with the structural window has a positive effect on the seismic force capacity. The contribution of the structural window to the total seismic force capacity increases with increasing imposed lateral displacements. At a lateral displacement of 8mm, the strengthened wall reaches 137% of the seismic force capacity obtained for the unstrengthened wall. However, both walls showed insufficient capacity to withstand a strong earthquake. Based on figure 13.9, it can be concluded that strengthening with the structural window has no effect on the expected damage resulting from a weak earthquake. Both walls are expected to remain practically undamaged.

13.3. Large window

Model geometry

Figure 13.10 shows the build-up for computational model of the URM wall with a large window.

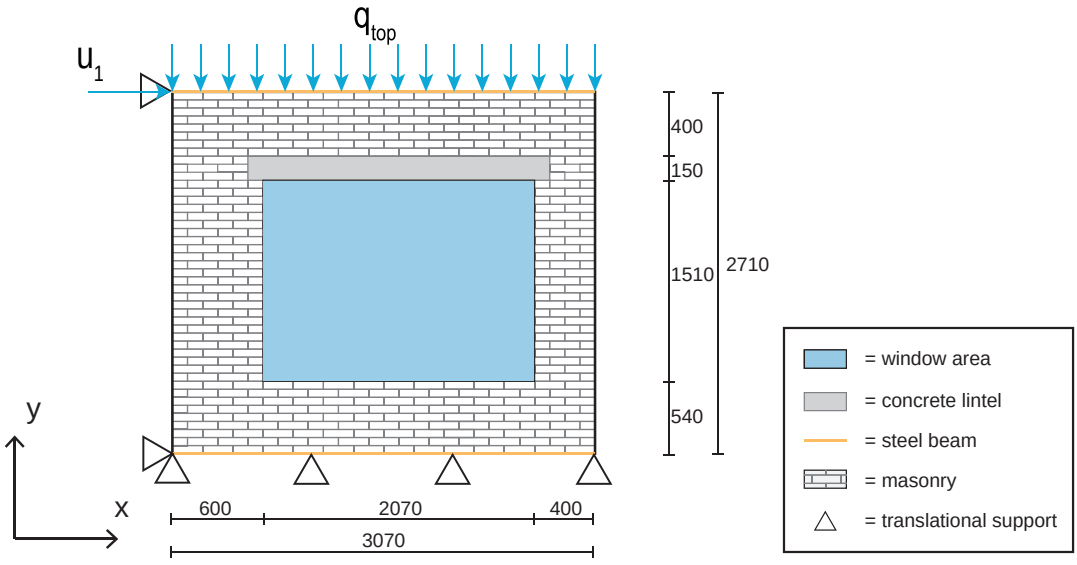

Figure 13.10: Build-up of the computational model used for the URM wall with a large window

In this case, the window area covers 38% of the total façade area. The results for a unstrengthened wall are compared with a strengthened wall, and theoretical upper bound model. For the strengthened wall and theoretical upper bound model, the structural window is placed adopting the component and superglue approach respectively.

Capacity curve

Figure 13.11 shows the obtained capacity curves for the URM wall with a large window. At a displacement of $8mm$, the strengthened wall has reached 300% of the seismic force capacity obtained for the unstrengthened wall. This is close to the theoretical upper bound model that has 356% of the seismic force capacity of the unstrengthened wall. It is observed that the initial stiffness is increased for the theoretical upper bound model and the strengthened wall compared to the unstrengthened wall. For the strengthened wall, the contribution of the structural window increases with increasing lateral displacements. At the end of the LE stage, around 1.0mm, the capacity curve of the strengthened wall is close to the unstrengthened wall. In contrast, at the end of the analysis, at 8mm, it is closer to the theoretical upper bound model.

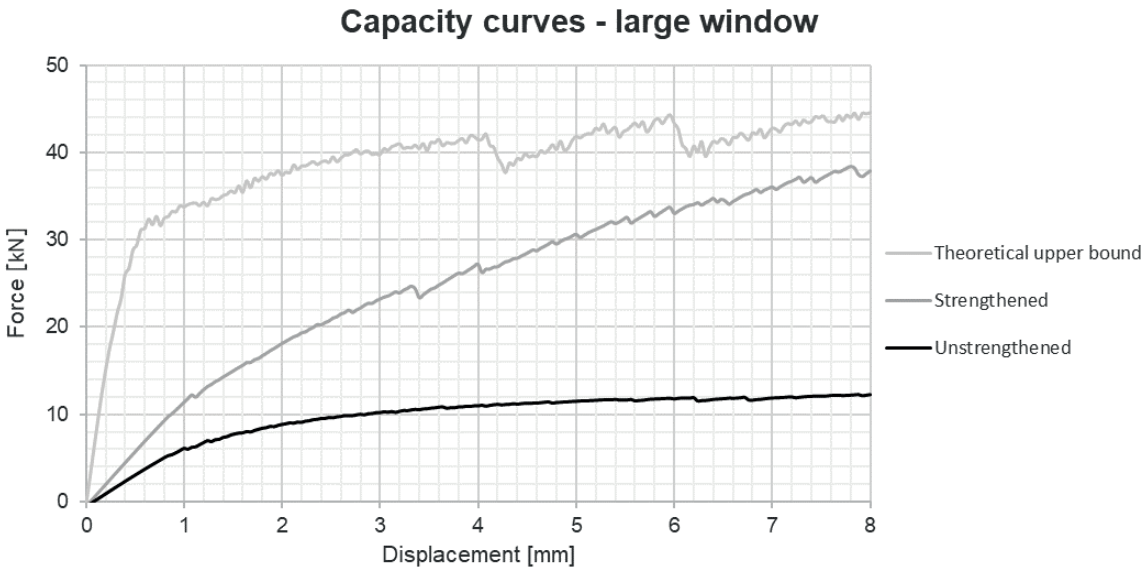

Figure 13.11: Capacity curves of seismic strengthening predictions for the URM wall with a large window.

Window stages

Figure 13.12 projects the window substages from section 11.6 on the capacity curve of the strengthened wall. It can be seen that the structural window remains in the first substage for the complete analysis up to a lateral displacement 8mm. This indicates that loads are transferred through the adhesive joint without tearing of the adhesive. In addition, no failure of the glass is expected for the analysis.

Figure 13.12: Projection of the window substages on the capacity curve of the strengthened URM wall with large window.

Crack patterns

The crack patterns give insight into the failure mechanism that occurs. The cracks at the final step of the numerical analysis, i.e. a lateral displacement of 8mm, are compared for the unstrengthened wall, strengthened wall, and the theoretical upper bound model in figure 13.13.

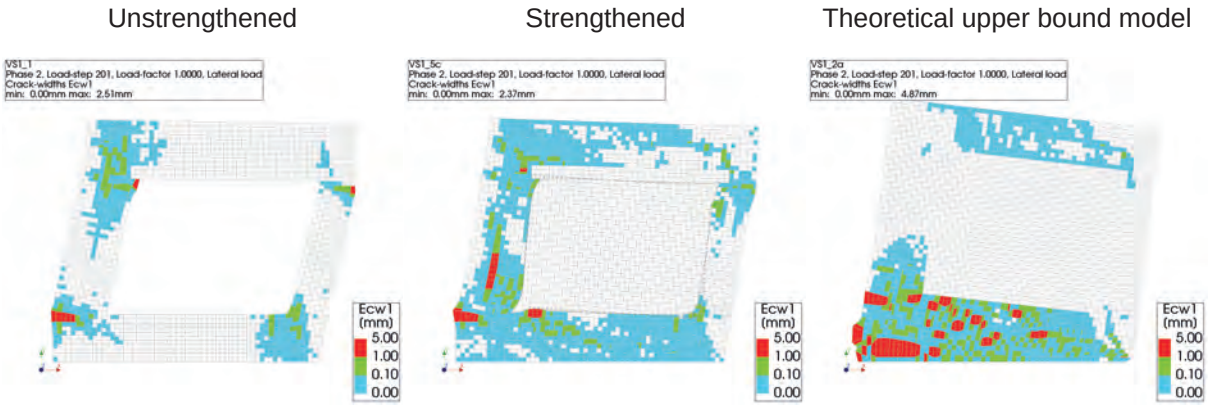

Figure 13.13: Crack patterns at a lateral displacement of 8mm for the URM wall with a large window. (DSF = 50)

It is observed that the structural window significantly affects the failure mechanism. The unstrengthened wall clearly shows the rocking mechanism with cracks concentrating at the top and bottom of both piers. For the theoretical upper bound model, the cracks concentrate mainly in the bottom spandrel. The strengthened wall shows a combination of the two models. For the strengthened wall, cracks do not only develop at the top and bottom of the piers but also in the bottom spandrel. In addition, vertical/diagonal cracks develop in the wide pier. The maximum crack width for the the theoretical upper bound model is significantly larger compared to the unstrengthened wall. In contrast, the strengthened wall results in a maximum crack width comparable to the unstrengthened. Lastly, it is observed that the total number of cracked elements is larger for the strengthened wall and the theoretical upper bound model compared to the unstrengthened wall.

Of course, it should be kept in mind that the seismic deformation demand depends on structural characteristics. The capacity curves show that these characteristics are different for the three models. Therefore, this comparison does not give any insight into the damage that is expected as a result of

a certain earthquake. The seismic performance including an evaluation of the expected damage as a result of different earthquakes is discussed in the next subsection.

Seismic performance

Based on the assumed effective mass of $16,000kg$ the seismic performance can be evaluated for a single-storey house. The seismic performance is evaluated for two locations: Groningen and Appingedam. This evaluation will compare the results for unstrengthened and strengthened wall. The theoretical upper bound model is disregarded as this model only served a theoretical purpose.

Average location - Groningen

The capacity curves of the unstrengthened and strengthened wall are plotted against the ADRS of a weak and strong earthquake in figure 13.14. It is observed both walls have sufficient capacity to withstand a weak earthquake. For a strong earthquake, it is observed that unstrengthened wall has insufficient capacity.

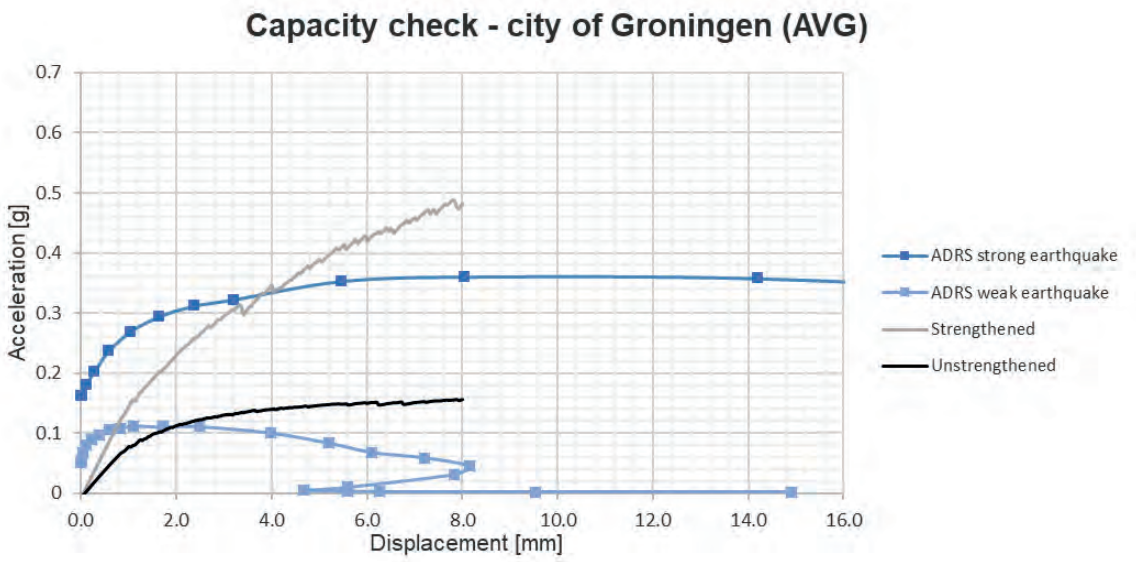

Figure 13.14: Average location - ADRS and obtained capacities for the URM wall with a large window.

A closer look is given to the expected damage as a result of the weak earthquake. First of all, the seismic deformation demand is determined by the intersection between the ADRS of the weak earthquake and the capacity curve. The expected damage resulting from a weak earthquake is evaluated by three damage characteristics: the maximum expected crack width, the number of elements in damage category 1, and the number of elements in damage category 2. Figure 13.15 compares these damage characteristics for the two walls. It is observed that the expected damage for the strengthened wall is significantly lower compared to the unstrengthened wall.

The effect of the structural window on the seismic performance of an URM wall with a large window located in the city of Groningen can be concluded.

Based on figure 13.14, it can be concluded that the stuctural window has a positive effect on the seismic force capacity. The contribution of the structural window to the total seismic force capacity increases with increasing imposed lateral displacements. At a lateral displacement of 8mm, the strengthened wall reaches 300% of the seismic force capacity of the unstrengthened wall. This increased force capacity proved to be important since only the strengthened wall showed sufficient capacity to withstand a strong earthquake. Based on figure 13.15, it can be concluded that strengthening with a structural window has a positive effect on the expected damage resulting from a weak earthquake. For example, the maximum crack width for the unstrengthened wall is expected to be 0.29mm, while for the strengthened wall a maximum crack width of only 0.03mm is expected.

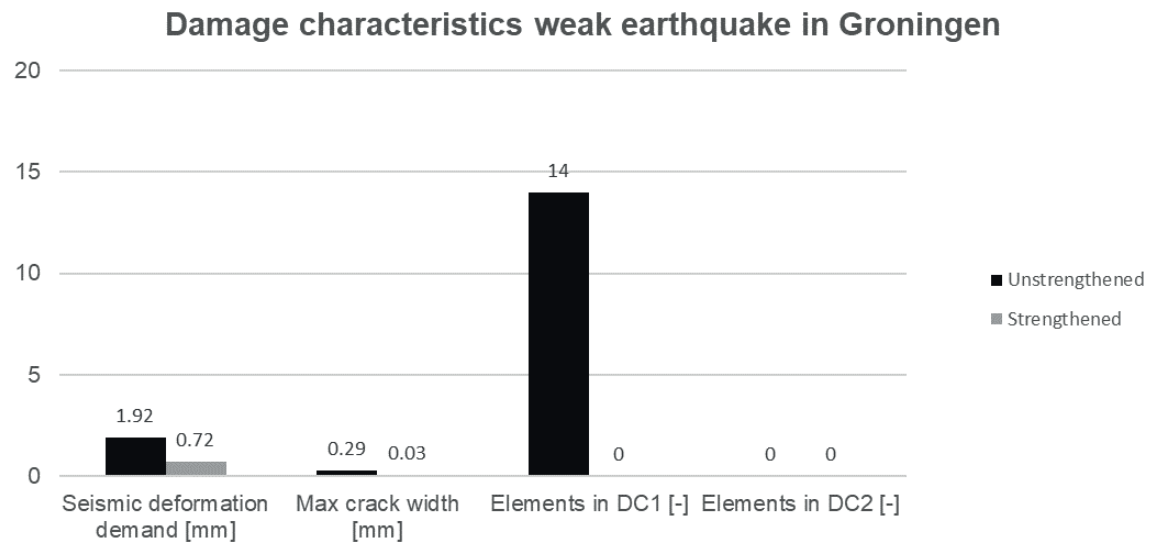

Figure 13.15: Average location - Damage analysis for the URM wall with a large window.

Extreme location - Appingedam

The capacity curves are plotted against the ADRS of a weak and strong earthquake in figure 13.16 for the location of Appingedam. It is observed that both walls have sufficient capacity for a weak earthquake. However, both walls show insufficient capacity to withstand a strong earthquake.

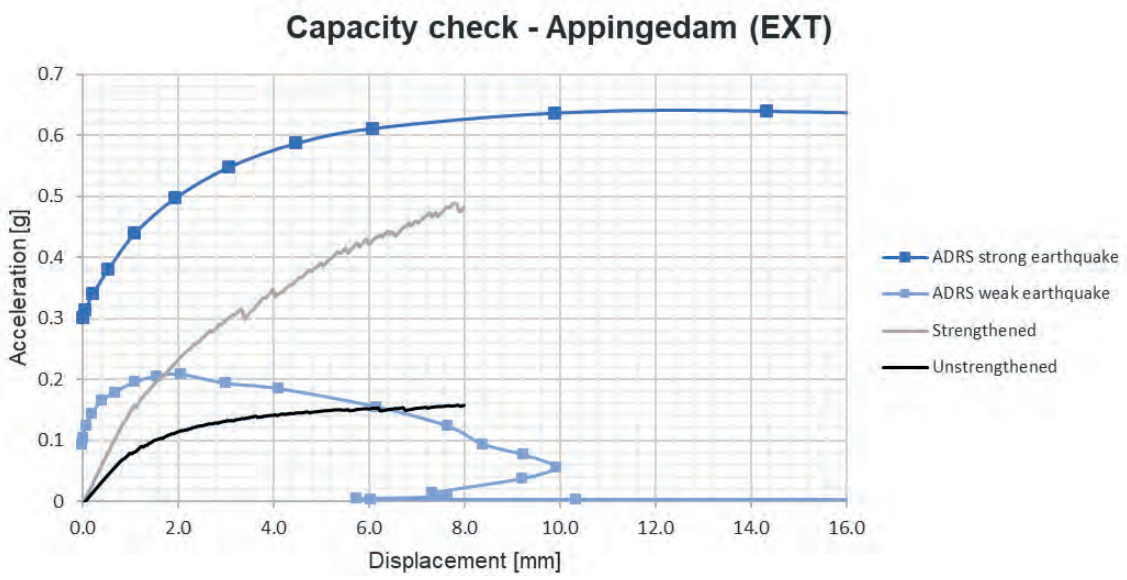

Figure 13.16: Extreme location - ADRS and obtained capacities for the URM wall with a large window.

Figure 13.17 gives an overview of the expected damage as a result of a weak earthquake in Appingedam. It is observed that the expected damage for the strengthened wall is significantly lower compared to the unstrengthened wall. For example, the maximum crack width for the unstrengthened wall is expected to be 1.86mm, while for the strengthened wall a maximum crack width of only 0.26mm is expected.

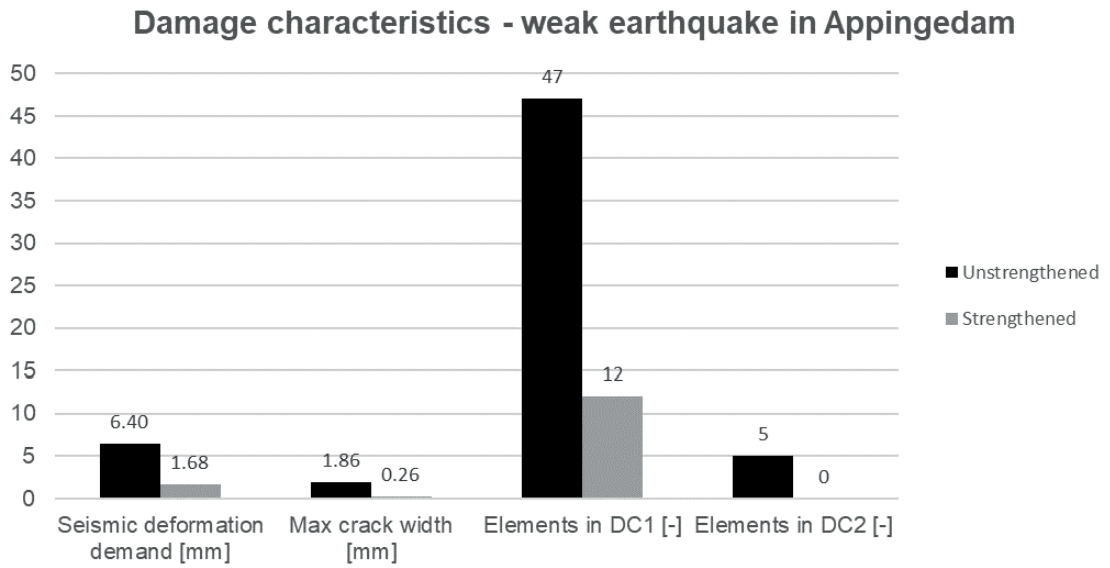

Figure 13.17: Extreme location - Damage analysis for the URM wall with a large window.

The effect of the structural window on the seismic performance of an URM wall with a large window located in the city of Appingedam can be concluded.

Based on figure 13.16, it can be concluded that strengthening with the structural window has a positive effect on the seismic force capacity. The contribution of the structural window to the total seismic force capacity increases with increasing imposed lateral displacements. At a lateral displacement of 8mm, the strengthened wall reaches 300% of the seismic force capacity obtained for the unstrengthened wall. However, both walls showed insufficient capacity to withstand a strong earthquake. Based on figure 13.17, it can be concluded that the structural window has positive effect on the expected damage resulting from a weak earthquake. For example, the maximum crack width for the unstrengthened wall is expected to be 1.86mm, while for the strengthened wall only 0.26mm.

13.4. Large window 3 sided

Model geometry

Figure 13.18 shows the build-up for computational model of the URM wall with a large window 3 sided.

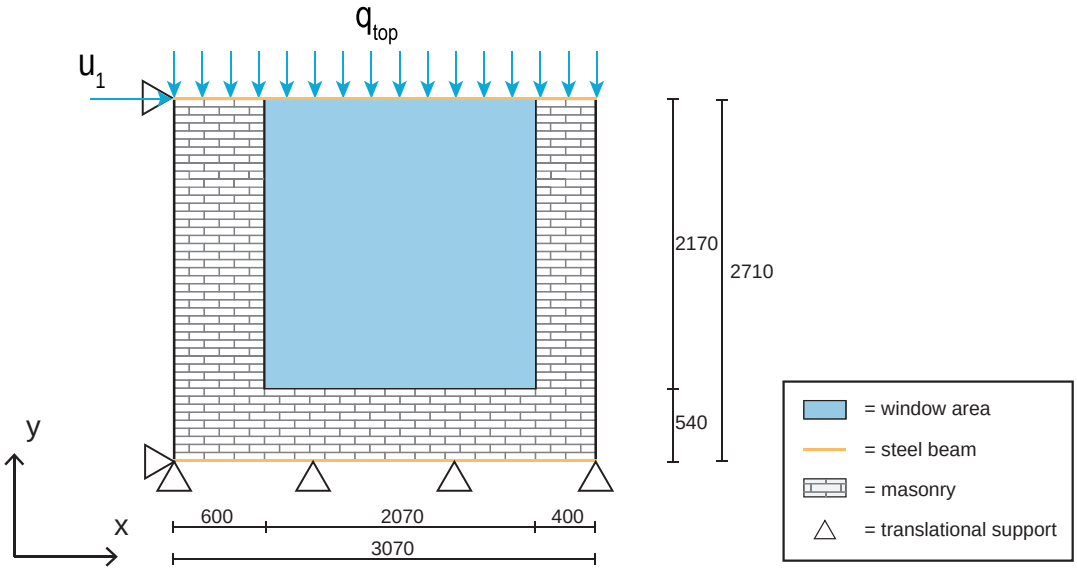

Figure 13.18: Build-up of the computational model used for the URM wall with a large window 3 sided.

In this case, the window area covers 54% of the total façade area. The results for a unstrengthened wall are compared with a strengthened wall, and theoretical upper bound model. For the strengthened wall and theoretical upper bound model, the structural window is placed adopting the component and superglue approach respectively.

Capacity curve

Figure 13.19 shows the obtained capacity curves for the URM wall with a large window. At a displacement of $8mm$, the strengthened wall has reached 367% of the seismic force capacity obtained for the unstrengthened wall. This is close to the theoretical upper bound model that has 433% of the seismic force capacity of the unstrengthened wall. It is observed that the initial stiffness is increased for the theoretical upper bound model and the strengthened wall compared to the unstrengthened wall. For the strengthened wall, the contribution of the structural window increases with increasing lateral displacements. At the end of the LE stage, around 1.0mm, the capacity curve of the strengthened wall is close to the unstrengthened wall. In contrast, at the end of the analysis, at 8mm, it is closer to the theoretical upper bound model.

Figure 13.19: Capacity curves of seismic strengthening predictions for the URM wall with a large window 3 sided.

Window stages

Figure 13.20 projects the window substages from section 11.6 on the capacity curve of the strengthened wall. It can be seen that the window remains in the first substage for the complete analysis up to $u_1 = 8mm$. This indicates that loads are transferred through the adhesive joint without tearing of the adhesive. In addition, no failure of the glass is expected for the analysis.

Figure 13.20: Projection of the window substages on the capacity curve of the strengthened URM wall with a large window 3 sided.

Crack patterns

The crack patterns give insight into the failure mechanism that occurs. The cracks at the final step of the numerical analysis are compared for the unstrengthened wall, strengthened wall, and the theoretical upper bound model in figure 13.21.

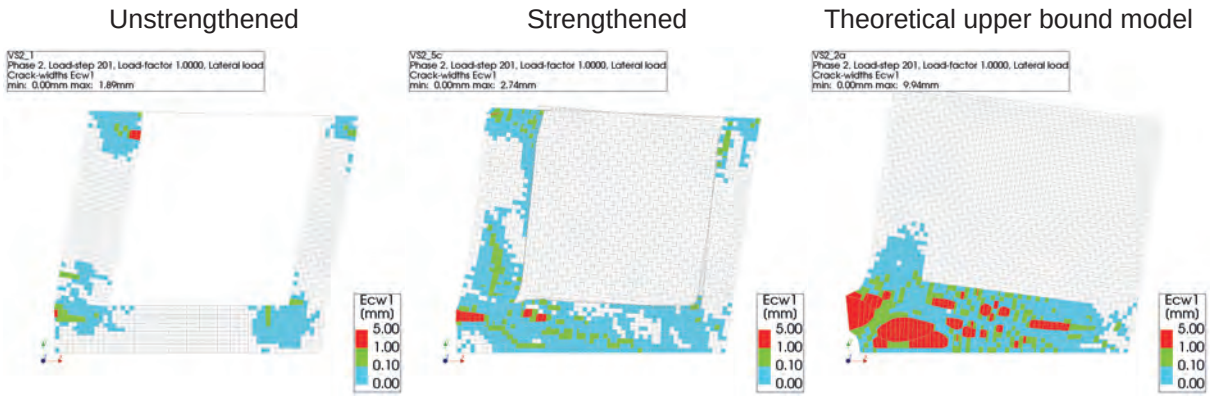

Figure 13.21: Crack patterns at a lateral displacement of 8mm for the URM wall with a large window 3 sided. (DSF = 50)

It is observed that the structural window significantly affects the failure mechanism. The unstrengthened wall clearly shows the rocking mechanism with cracks concentrating at the top and bottom of both piers. For the theoretical upper bound model, the cracks concentrate mainly in the bottom spandrel. The strengthened wall shows a combination of the two models. For the strengthened wall, cracks do not only develop at the top and bottom of the piers but also in the bottom spandrel. In addition, vertical/diagonal cracks develop in the wide pier. The maximum crack width for the theoretical upper bound model and strengthened wall are larger compared to the unstrengthened wall. Lastly, it is observed that the total number of cracked elements is higher for the strengthened wall and the theoretical upper bound model compared to the unstrengthened wall.

Of course, it should be kept in mind that the seismic deformation demand depends on structural characteristics. The capacity curves show that these characteristics are different for the three models. Therefore, this comparison does not give any insight into the damage that is expected as a result of a certain earthquake. The seismic performance including an evaluation of the expected damage as a result of different earthquakes is discussed in the next subsection.

Seismic performance

Based on the assumed effective mass of $16,000kg$ the seismic performance can be evaluated for a single-storey house. The seismic performance is evaluated for two locations: Groningen and Appingedam. This evaluation will compare the results for unstrengthened and strengthened wall. The theoretical upper bound model is disregarded as this model only served a theoretical purpose.

Average location - Groningen

The capacity curves of the unstrengthened and strengthened wall are plotted against the ADRS of a weak and strong earthquake in figure 13.22. It is observed both walls have sufficient capacity to withstand a weak earthquake. For a strong earthquake, it is observed that unstrengthened wall has insufficient capacity.

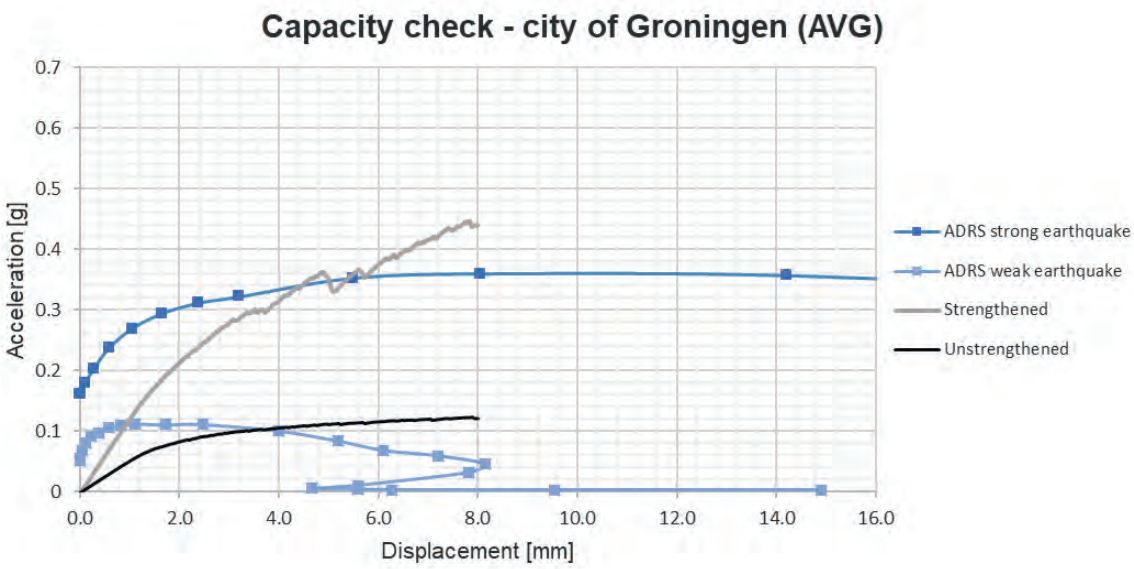

Figure 13.22: Average location - ADRS and obtained capacities for the URM wall with a large window 3 sided.

A closer look is given to the expected damage as a result of the weak earthquake. First of all, the seismic deformation demand is determined by the intersection between the ADRS of the weak earthquake and the capacity curve. The expected damage resulting from a weak earthquake is evaluated by three damage characteristics: the maximum expected crack width, the number of elements in damage category 1, and the number of elements in damage category 2. Figure 13.23 compares these damage characteristics for the two walls. It is observed that the expected damage for the strengthened wall is significantly lower compared to the unstrengthened wall. A weak earthquake is expected to result in 21 elements in damage category 1 with a maximum crack width of 0.68mm for the unstrengthened wall, while no damage is expected for the strengethened wall.

The effect of the structural window on the seismic performance of an URM wall with a large window 3 sided located in the city of Groningen can be concluded.

Based on figure 13.22, it can be concluded that the stuctural window has a positive effect on the seismic force capacity. The contribution of the structural window to the total seismic force capacity increases with increasing imposed lateral displacements. At a lateral displacement of 8mm, the strengthened wall reaches 367% of the seismic force capacity of the unstrengthened wall. This increased force capacity proved to be important since only the strengthened wall showed sufficient capacity to withstand a strong earthquake. Based on figure 13.23, it can be concluded that strengthening with a structural window has a positive effect on the expected damage resulting from a weak earthquake. For example, the maximum crack width for the unstrengthened wall is expected to be 0.68mm, while for the strengthened wall a maximum crack width of only 0.02mm is expected.

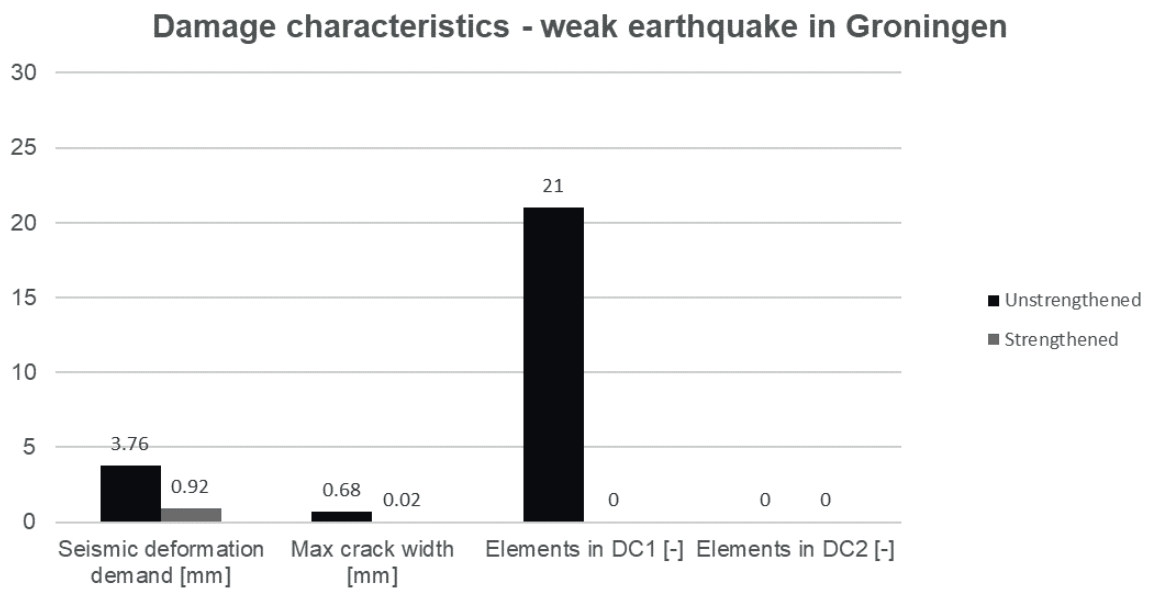

Figure 13.23: Average location - Damage analysis for the URM wall with a large window 3 sided.

Extreme location - Appingedam

The capacity curves are plotted against the ADRS of a weak and strong earthquake in figure 13.24 for the location of Appingedam. It is observed that both walls have sufficient capacity for a weak earthquake. However, both walls show insufficient capacity to withstand a strong earthquake.

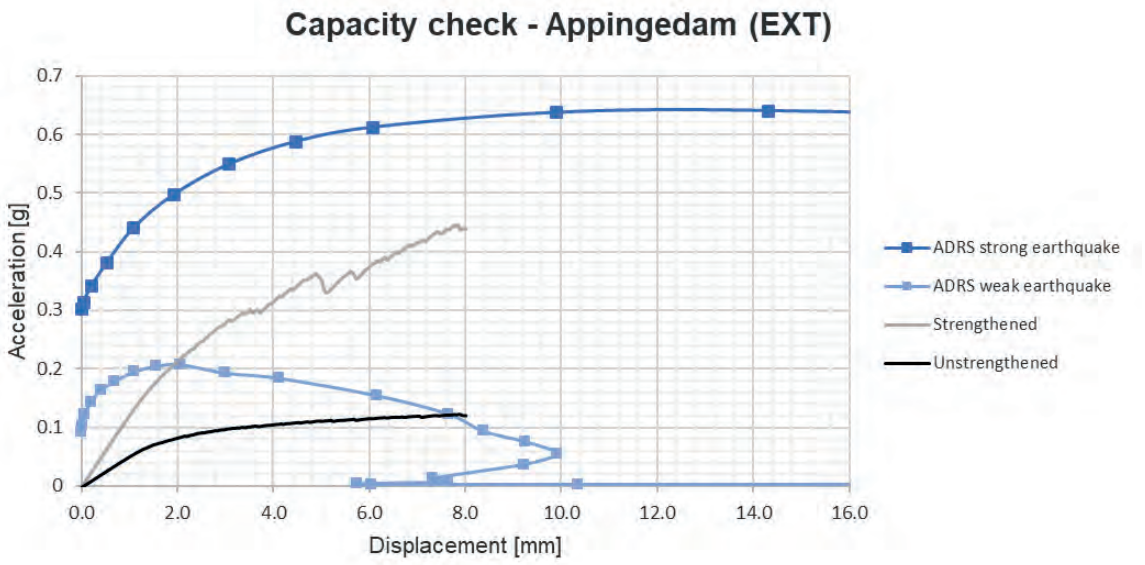

Figure 13.24: Extreme location - ADRS and obtained capacities for the URM wall with large window 3 sided.

Figure 13.25 gives an overview of the expected damage as a result of a weak earthquake in Appingedam. It is observed that the expected damage for the strengthened wall is significantly lower compared to the unstrengthened wall. A weak earthquake is expected to result in 33 elements in damage category 1 with a maximum crack width of 1.77mm for the unstrengthened wall, while only 4 elements in damage category 1 with a maximum crack width of 0.27mm is expected for the strengthened.

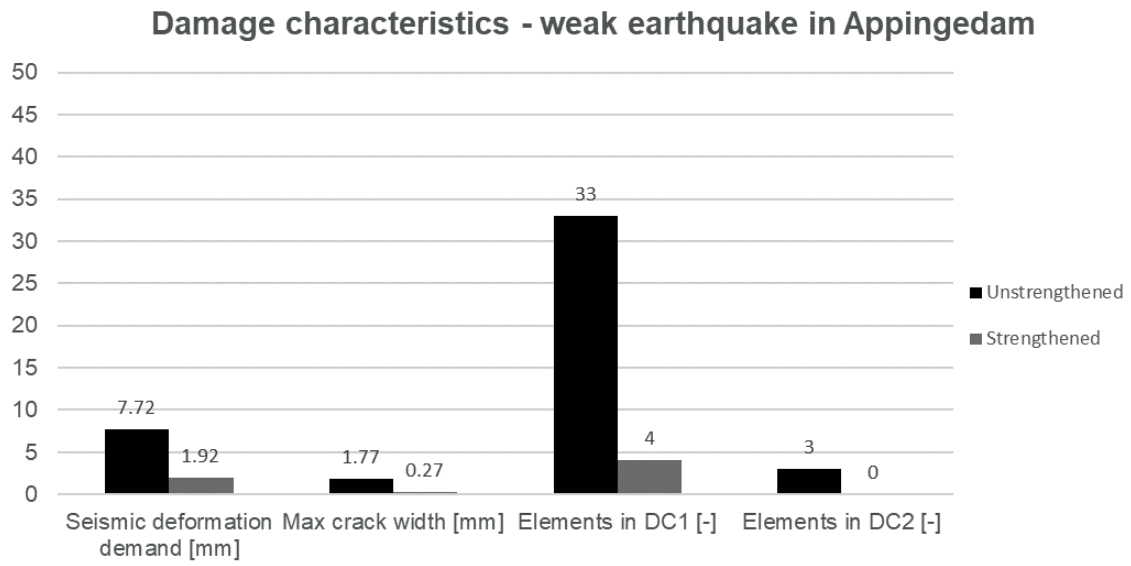

Figure 13.25: Extreme location - Damage analysis for the URM wall with a large window 3 sided.

The effect of the structural window on the seismic performance of an URM wall with a large window 3 sided located in the city of Appingedam can be concluded.

Based on figure 13.24, it can be concluded that strengthening with the structural window has a positive effect on the seismic force capacity. The contribution of the structural window to the total seismic force capacity increases with increasing imposed lateral displacements. At a lateral displacement of 8mm, the strengthened wall reaches 368% of the seismic force capacity obtained for the unstrengthened wall. However, both walls showed insufficient capacity to withstand a strong earthquake. Based on figure 13.25, it can be concluded that the structural window has positive effect on the expected damage resulting from a weak earthquake. For example, the maximum crack width for the unstrengthened wall is expected to be 1.77mm, while for the strengthened wall a maximum crack width of only 0.27mm is expected.

13.5. Conclusion chapter 13

The assessment of the seismic performance on the scale of a structural element focussed on a single-wythe wall of clay-brick masonry with one window. Three cases with different window sizes were considered. All model were subjected to a one-directional monotonic pushover load up to 8mm. The unstrengthened wall models leave an opening at the location of the window, while the strengthened wall models incorporate the designed structural window adopting the component approach. Additionally, a theoretical upper-bound solution is obtained adopting the superglue approach for the structural window. This theoretical upper-bound model showed to give an upper bound envelop for the capacity curve of the strengthened wall. Comparison of the result of the unstrengthened and strengthened wall gave insight into the structural potential of the designed structural window at the level of a structural element.

First of all, it was found that strengthening with the structural window has a positive effect on the seismic force capacity. Figure 13.26 shows that the strengthened walls reach between 137% and 367% of seismic force capacity of the corresponding unstrengthened wall. The structural potential was found highest for the two cases with a large window. This is mainly the result of the relatively low seismic force capacity found for the unstrengthened wall of these two cases. In contrast, it is observed that the window size has limited effect on the seismic force capacity of the strengthened wall. All strengthened walls have comparable seismic force capacity at a lateral displacement of 8mm.

Figure 13.26: Overview of seismic acceleration capacity[1] for the seismic strengthening predictions of the URM wall at $u_1 = 8mm$ and capacity check against strong earthquakes expected for Groningen and Appingedam.

Furthermore, figure 13.26 gives an overview of the capacity checks against strong earthquakes expected for the city of Groningen and Appingedam. For the location of Appingedam, it is observed that none of the unstrengthened and strengthened walls has sufficient capacity to withstand the strong earthquake. Therefore, the strengthening measure is not sufficiently effective for URM walls at the location of Appingedam for all cases considered. For the location of Groningen, it is observed that all strengthened walls have sufficient capacity to withstand the strong earthquake, while the unstrengthened walls show insufficient capacity withstand the strong earthquake for the two large window cases. Therefore, the strengthening measure is mainly effective for URM walls at the location of Groningen for the two cases with large window.

[1] Force and acceleration have been used interchangeably. These are directly proportional through the effective mass that is assumed to be a consant (independent of the window size and the installation of the structural window).

Secondly, it was found that strengthening with the structural window has positive effect on the expected damage caused by a weak earthquake. A significant reduction of the expected damage was found for the strengthened wall compared to the unstrengthened wall for the two large window cases. For example, a reduction from 1.86mm to 0.26mm was found for the maximum crack width for the large window case in Appingedam. However, this damage reduction is not observed for the small window case, because both the unstrengthened and strengthened wall are expected to remain practically undamaged. These observations were found for both the weak earthquake expected for the city Groningen, and Appingedam.

It can be concluded that the structural window has significant potential to improve the in-plane seismic performance of an URM wall both in terms of structural force capacity and expected damage.

14

Validation two-storey building model

A 3D two-storey building model made in DIANA FEA 10.2 will be validated with experimental results reported by Ravenshorst et al. [20]. Ravenshorst et al. [20] describes experiments on two-storey building consisting of CS brick masonry walls and solid concrete floors. The assembled structure represents a Dutch terraced house built in 1960-1980. The masonry walls represent the inner leaf of a cavity wall and any contribution of the outer leaf is neglected. In the experiment, the structure has been subjected to a two directional cyclic pushover loading scheme with equal forces at the two floor levels. Figure 14.1 shows the build-up of the two-storey building that has been tested. The goal of this study was to investigate structural characteristics of a typical Dutch terraced house up to failure.

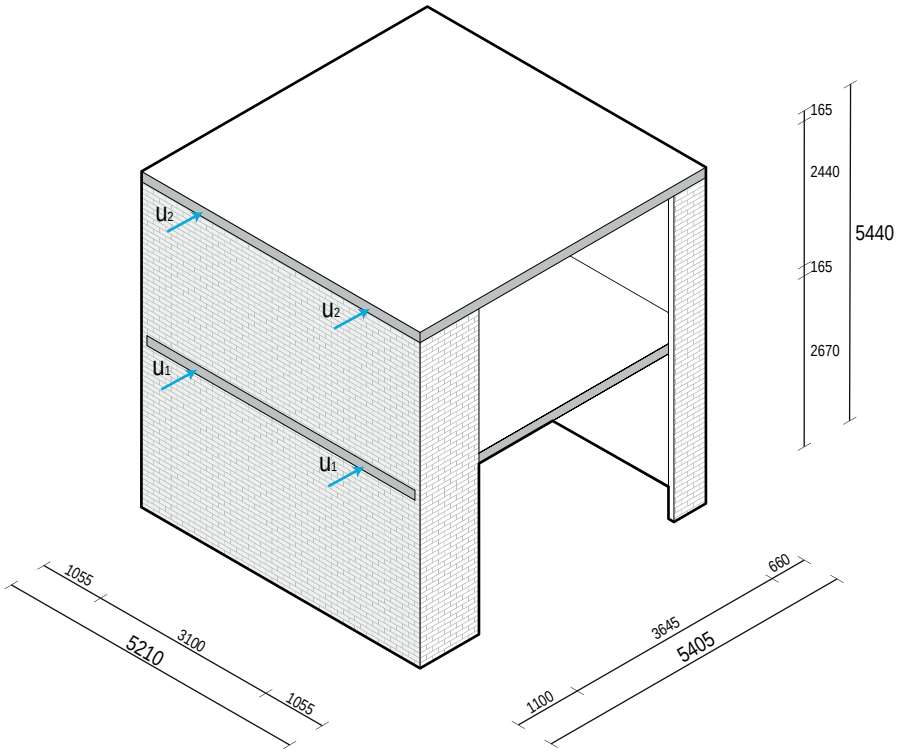

Figure 14.1: Build-up of the two-storey building that has been tested based on [20].

14.1. Model geometry

The numerical model is shown in figure 14.2. It is observed that both the geometry and loading conditions are line symmetric in the transverse direction. This symmetry line has been used in the model set-up saving computional time in the structural analysis. The model is supported in the global y-direction along this symmetry plane. At ground level, the structure is supported using tyings. All translational and rotational DOFs are fixed for the master node and the DOFs of the slave nodes are equalized.

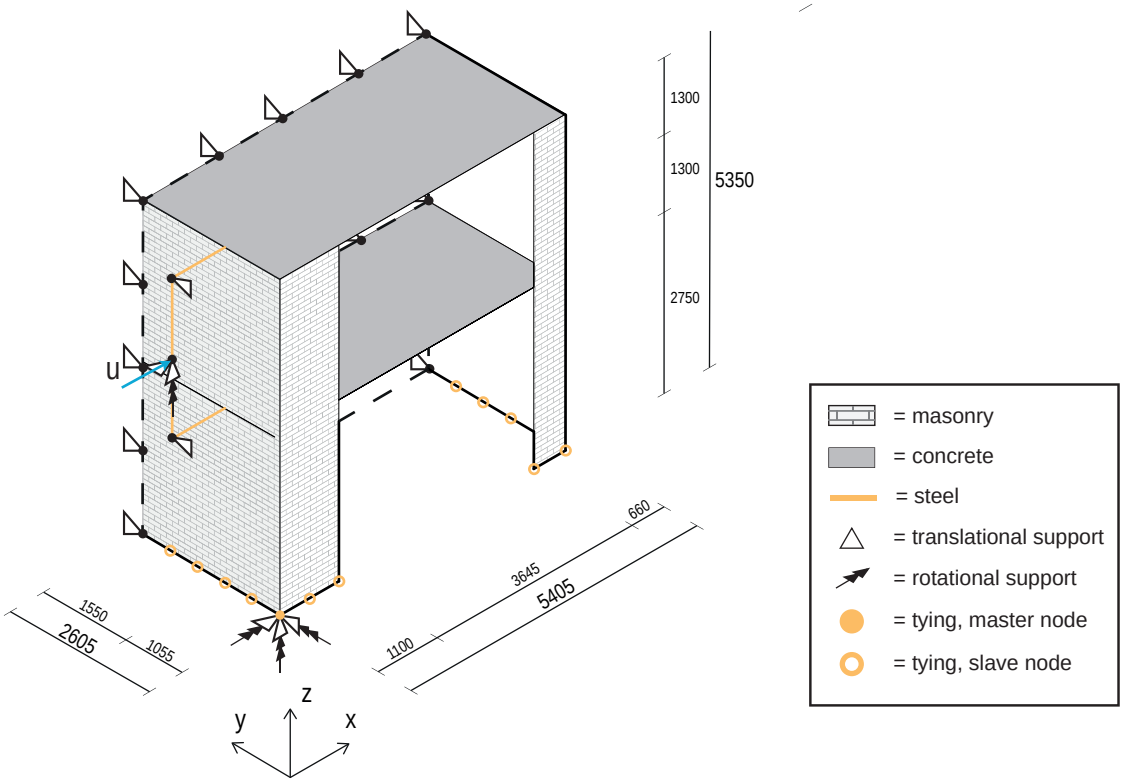

Figure 14.2: Build up of the symmetry model and steel loading structure used for mass proportional monotonic pushover analysis of the two-storey building model

The structure is loaded at the two floor levels by an auxiliary steel loading structure. This loading structure is composed of one vertical beam and two horizontal trusses. The vertical beam is loaded by an imposed deformation at its midpoint and its ends are hinged to the two horizontal trusses at the two floor levels. The vertical beam is able to rotate in the xz-plane around its midpoint equalizing the forces transferred at its ends. Therefore, this loading structure ensures a mass proportional loading scheme with equal forces at the two floor levels. The horizontal trusses ensure that the structure is loaded by horizontal forces only.

Figure 14.3 shows the connections between the masonry walls and concrete floor slabs. The floor to wall connections are modelled as rigid connections except for the anchor connections between the first floor and the façade wall. These anchor connections are marked with a dashed yellow line in figure 14.4.

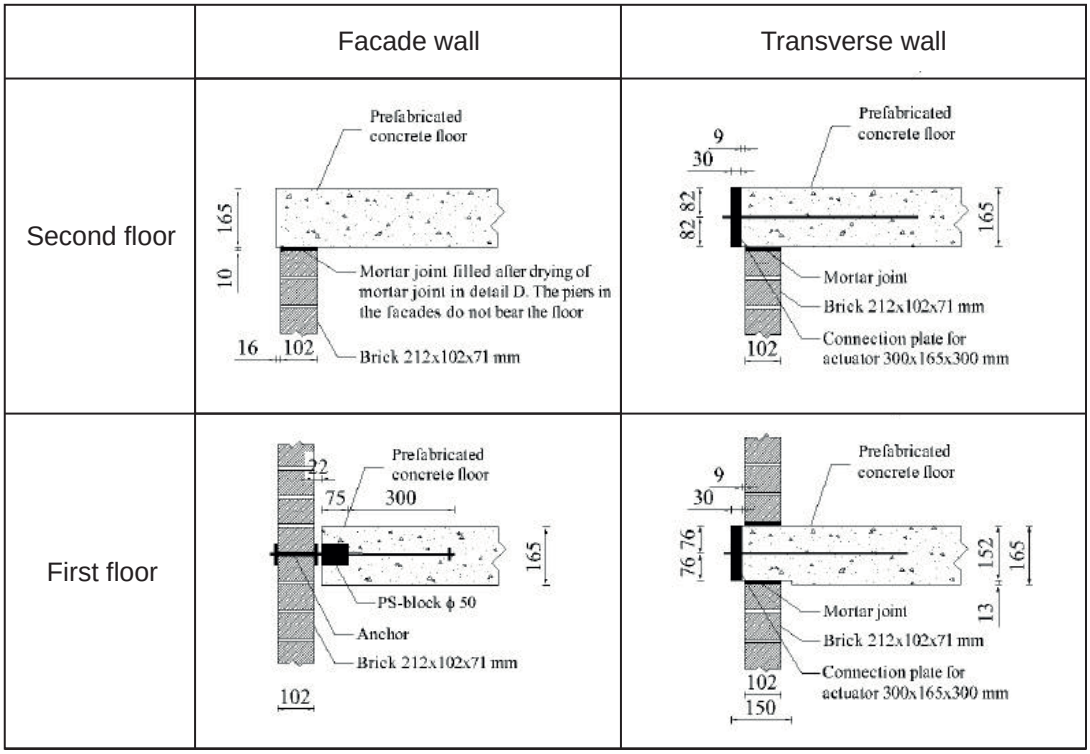

Figure 14.3: Connections between the masonry walls and two concrete floor slabs.

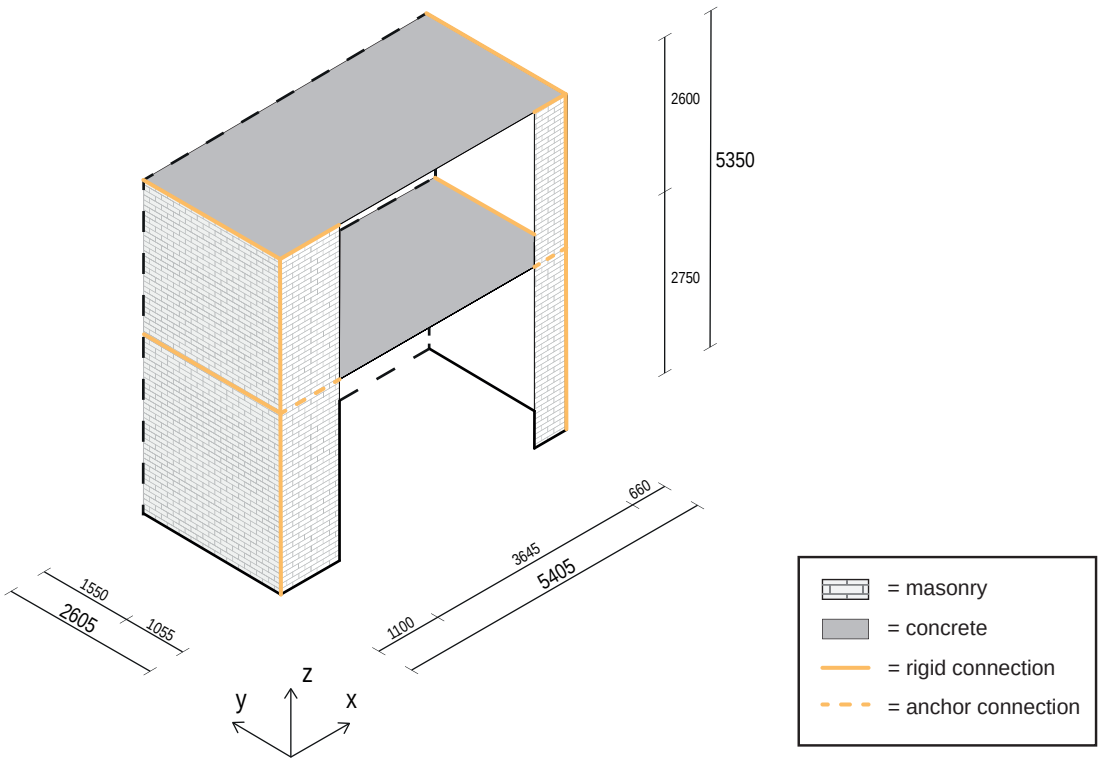

Figure 14.4: Modelling of the floor to wall connections of the two-storey building model.

14.2. Discretization

The structure that is composed of masonry walls and concrete floors is discretized by quadrilateral elements of 150mm x 150mm. Nonlinear behaviour is included for the masonry only. Curved shell elements are adopted to capture both in-plane and out-of-plane action. An overview of the discretization of the structure is given in figure 14.1. The orientation of the local axes of the masonry walls requires extra attention because of the orthotropic material properties of masonry. The local x-axis of the two piers corresponds to the global x-axis, while the local x-axis of the two transverse walls corresponds to the global y-axis.

Table 14.1: Discretization into elements for two-storey building model.

	Masonry walls	**Concrete floors**
Material model	Engineering Masonry Model	Linear elastic isotropic
Element type	Curved shells (CQ40S)	Curved shells (CQ40S)
DOFs	$u_x, u_y, u_z, \phi_x, \phi_y$	$u_x, u_y, u_z, \phi_x, \phi_y$
Integration scheme	2x2x3	2x2x3
Mesh size [mm]	150	150
Thickness [mm]	102	165

The loading structure is composed of one vertical beam and two horizontal trusses. Regular truss elements are adopted for the horizontal trusses to ensure a purely horizontal loading scheme on the masonry structure. An overview of the of the discretization of the loading structure is given in figure 14.2.

Table 14.2: Discretization of loading structure for two-storey building model.

	Vertical beam	**Horizontal trusses**
Material model	Linear elastic isotropic	Linear elastic isotropic
Element type	Class-III beams (CL18B)	Regular truss (L2TRU)
DOFs	$u_x, u_y, u_z, \phi_x, \phi_y, \phi_z$	u_x
Integration scheme	2-point Gauss	1-point direct
Mesh size [mm]	150	1,000
Cross-section [mm]	50,000 (100x500)	10,000 (100x100)

The anchor connection between the façade wall and the first floor is discretized into linear structural interface elements. An overview of the discretization of the loading structure is given in figure 14.3.

Table 14.3: Discretization of anchor connection into elements for two-storey building model.

	Anchor connection
Material model	Linear elasticity
Element type	Structural interface (CL24I)
DOFs	u_x, u_y, u_z
Integration scheme	3-point Newton-Cotes
Mesh size	150
Thickness [mm]	165

14.3. Material properties

The loading structure and concrete floors are modelled with linear elastic isotropic behaviour. An overview of their properties can be found in table 14.4. The horizontal trusses elements are given fictitious properties to minimise their effect on the results.

Table 14.4: Material properties for concrete floors and loading structure for two-storey building model.

Property	Parameter	Symbol	Unit	Concrete floors	Steel beam	Trusses
Elasticity	Young's modulus	E	MPa	35,500	210,000	1e+7
	Poisson's ratio	v	-	0.2	0.2	0.2
	Density	ρ	kg/m^3	2,400	7,800	1

.

The masonry is modelled with NLE elements. The engineering masonry model (EMM) is adopted. An overview of their properties can be found in table 14.5. These properties have been reported in [37] and [20]. The two presented Young's modulii have been evaluated between 0 and 1/3 of the maximum compressive stress. The shear modulus has been estimated based on the empirical relationship $G_{xy} = 0.4E_y$ reported in [36].

Table 14.5: Material properties for macro-modelling of CS masonry for two-storey building model according to Xu [37].

Property	Parameter	Symbol	Unit	Value
Elasticity	Young's modulus	E_x	MPa	2,212
		E_y	MPa	3,264
	Shear modulus	G_{xy}	MPa	1,306
	Density	ρ	kg/m^3	1,805
Cracking	Tensile strength	f_{ty}	MPa	0.19
	Tensile fracture energy	G_{ft}	N/mm	0.0127
	Diagonal crack orientation	α	rad	0.792
Crushing	Compressive strength	f_c	MPa	5.84
	Compressive fracture energy	G_c	N/mm	17.39
Sliding	Cohesion	c	MPa	0.14
	Fracture energy in shear	G_{fs}	N/mm	-
	Friction angle	ϕ	rad	0.406

The anchor connection between the façade wall and first floor are modelled with LE structural interface elements. Their properties are according to [37] can be found in table 14.6.

Table 14.6: Material properties for anchor connection between the façade walls and the first floor according to Xu [37].

Property	Parameter	Symbol	Unit	Value
Elasticity	Normal stiffness	$E_{n,y}$	MPa	0
	Shear stiffness	$E_{t,x}$	MPa	1,632
		$E_{t,z}$	MPa	0

.

14.4. Analysis method

An overview of the applied analysis method is shown in table 14.7. Both geometrical and physical nonlinearity are included. A phased analysis is adopted to prevent horizontal reaction forces as a result of the self-weight of the masonry structure. In the first phase, the loading structure is not included in the analysis to correctly calculate stresses in the masonry resulting from the self-weight. In the second phase, the loading structure is included and a monotonic pushover load is applied.

Table 14.7: Analysis method applied for two-storey building model.

Phase 1 Masonry structure only	**Load steps**	Load name	Self-weight
		Steps	0.1(10)
	Iterative procedure	Procedure	Regular Newton-Raphson
		Max. iterations	100
		Line search	Yes
	Convergence criterium	Norm	Energy
		Tolerance	0.001
		No convergence	Terminate
Phase 2 Complete model	**Start steps**	Start step	Use load of previous phase
	Load steps	Load name	Pushover load
		Load	60mm
		Steps	0.005(200)
	Iterative procedure	Procedure	Regular Newton-Raphson
		Max. iterations	100
		Line search	Yes
	Convergence criterium	Norm	Energy
		Tolerance	0.003
		No convergence	Continue

14.5. Results

Capacity curve

Figure 14.5 compares the capacity curve from the numerical model with the backbone curve of the experiment. The horizontal reaction force at ground floor level is plotted against the displacement at the second floor.

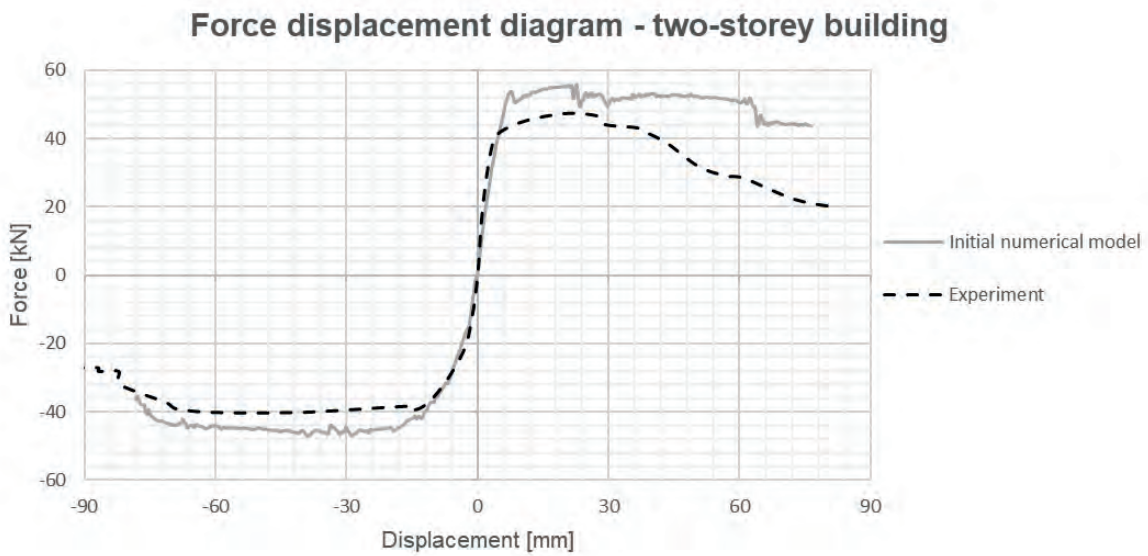

Figure 14.5: Comparison of the capacity curve with the backbone of the experimental results reported in [20].

The numerical results show differences with the numerical model for all important characteristics: initial stiffness, maximum force capacity, and softening behaviour. Table 14.8 compares these characteristics. The softening characteristic is determined by the reduction in force capacity, comparing the maximum value with the value at $70mm$.

Table 14.8: Comparison between characteristics of the experimental and numerical capacity curve for the two-storey building.

Characteristic	Unit	Experiment	Numerical model
Initial global stiffness	kN/mm	15.7	10.6
Maximum force capacity	kN	47.3	55.6
Softening behaviour	%	50	21

It is observed that both the initial stiffness and softening behaviour are underestimated by the numerical model, while the maximum force capacity is overestimated. Different suggestions for improving the numerical model are listed below:
- Detailed properties of the interface between the floors and walls, and between the longitudinal and transverse walls.
- Adopt a material model that includes cyclic damage accumulation and apply a cyclic loading scheme instead of a monotonic loading scheme.
- Adopt a (detailed) micro-modelling technique for the masonry walls.
- Adopt 3D solid elements instead of 2D curved shell elements.
- Sensitivity analyses on masonry material properties using the standard deviations obtained in material tests reported in [20].

It is chosen to only perform a sensitivity analysis on the elastic modulii of the masonry. The aim of this sensitivity analysis is to improve the initial global stiffness of the two-storey building since this is an important dynamic characteristic.

14.6. Calibration of results

Capacity curve

The elastic modulii given in table 14.5 are average values that have been evaluated between 0 and 1/3 of the maximum compressive stress. In addition, Ravenshorst et al. [20] also gives the average values for the elastic modulii that have been evaluated between 0 and 1/10 of the maximum compressive stress. These values have been adopted in the updated model and are given in bold in table 14.9.

Table 14.9: Updated material properties for macro-modelling of calcium silicate masonry for two-storey building model.

Property	Parameter	Symbol	Unit	Value
Elasticity	Young's modulus	E_x	MPa	**3,583**
		E_y	MPa	**4,788**
	Shear modulus	G_{xy}	MPa	**1,915**
	Density	ρ	kg/m^3	1,805
Cracking	Tensile strength	f_{ty}	MPa	0.19
	Tensile fracture energy	G_{ft}	N/mm	0.0127
	Diagonal crack orientation	α	rad	0.792
Crushing	Compressive strength	f_c	MPa	5.84
	Compressive fracture energy	G_c	N/mm	17.39
Sliding	Cohesion	c	MPa	0.14
	Fracture energy in shear	G_{fs}	N/mm	-
	Friction angle	ϕ	rad	0.406

Figure 14.6 compares the capacity curve of the updated numerical model with the initial numerical model and experiment. It can be seen that the updated numerical model gives only slightly different results compared to the initial numerical model.

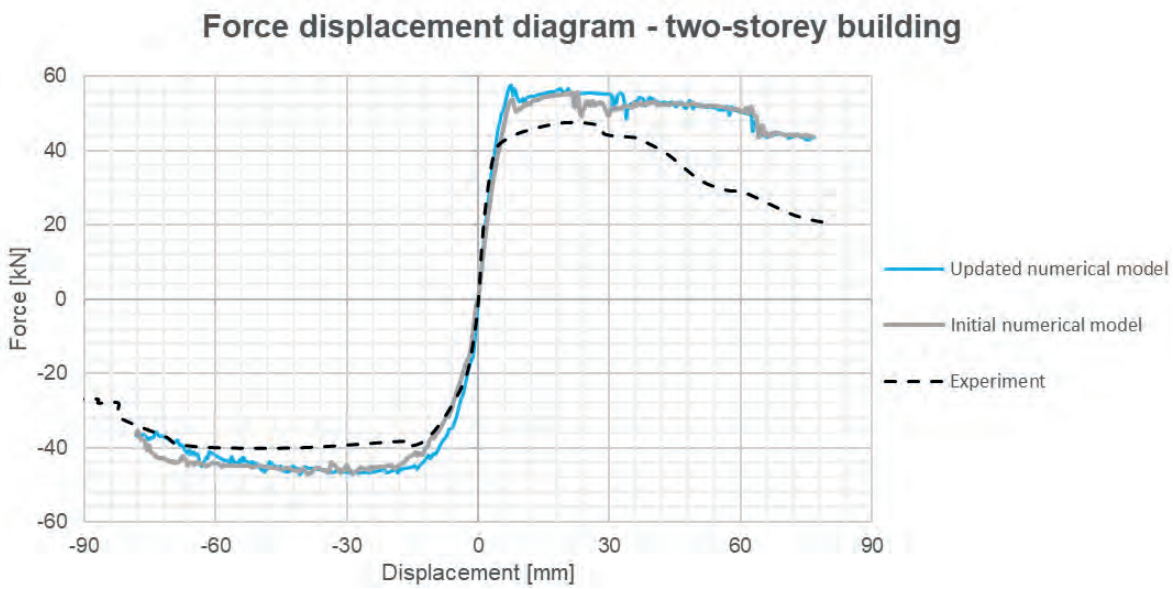

Figure 14.6: Capacity curve two-storey building model after stiffness calibration.

Table 14.10 compares important characteristics of the capacity curve obtained in the experiment and the numerical models. It is observed that the modification of elastic modulli of masonry improved the agreement between the numerical model and the experiment in terms of initial global stiffness. In contrast, the agreement in terms of force capacity was slightly decreased.

Table 14.10: Overview and comparison of capacity curve characteristics for updated numerical model of the two-storey building.

Characteristic	Unit	Experiment	Initial model	Updated model
Initial global stiffness	kN/mm	15.7	10.6	13.3
Maximum force capacity	kN	47.3	55.6	57.4
Softening behaviour	%	50	21	23

The updated numerical model is considered to be acceptable for the purpose of this study and the updated masonry material properties have been adopted in further studies.

Crack patterns

Figure 14.7 shows the damage evolution and force flow of the two-storey building. The model shows crack concentrations mainly at the top and bottom of the two piers indicating a rocking failure mechanism. This is in line with the governing failure mechanism observed in the experiment. However, diagonal/vertical crack patterns in the two transverse walls and piers observed in the experiment are not adequately captured by the model. The contour plots of the force flow show force concentrations in the wide pier, indicating that the wide pier has a large contribution to the total capacity of the two-storey building.

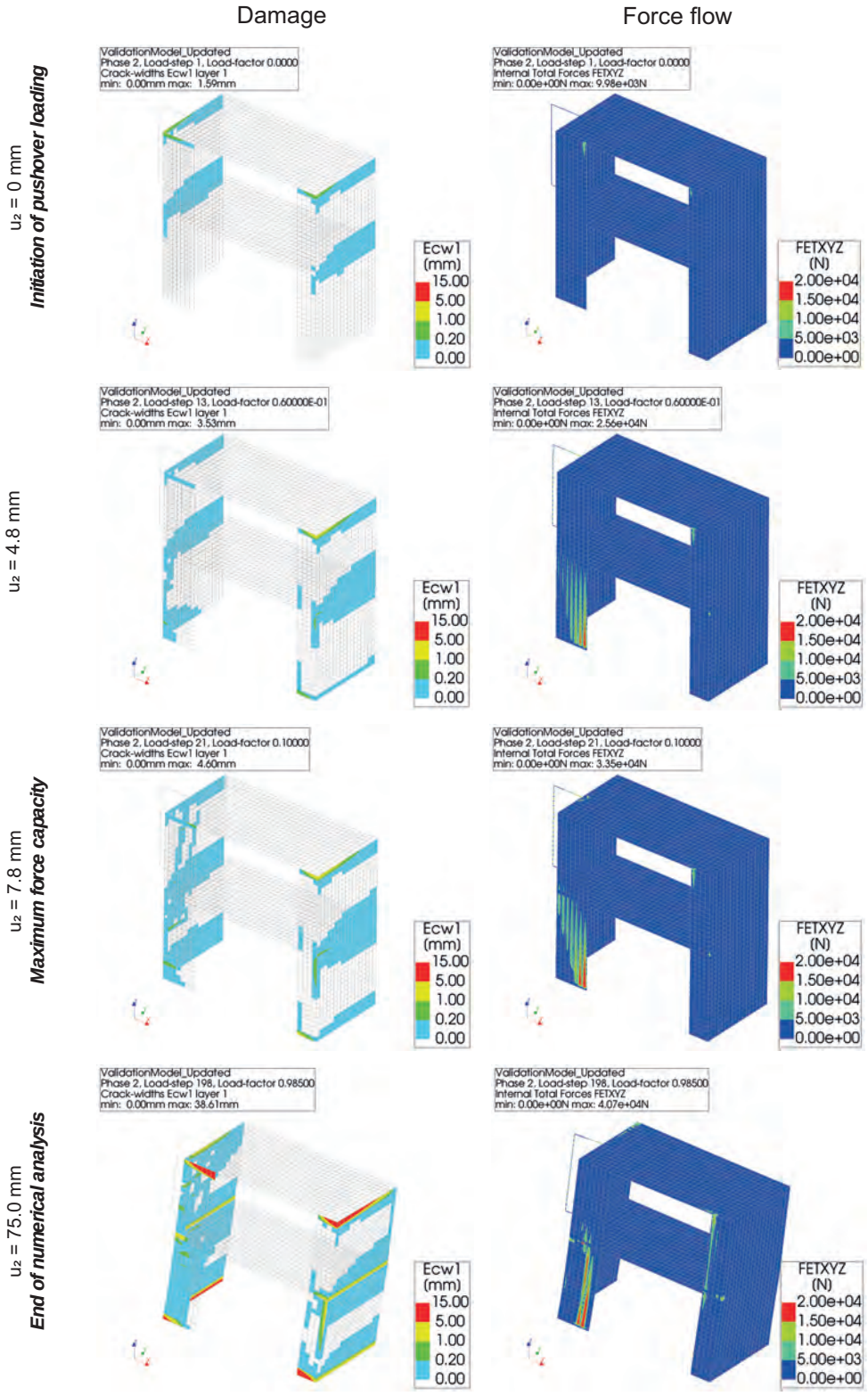

Figure 14.7: Damage evolution and force flow of the updated numerical model for the two-storey building. (DSF: 10)

14.7. Conclusions chapter 14

The capacity curve of a two-storey building consisting of CS masonry walls and concrete floors was reasonably well captured by a 3D finite element model in DIANA 10.2. Important characteristics of the capacity curve obtained by the numerical model have been compared with the backbone of the experimental results. Despite the differences that were found for all important characteristics of the capacity curve, the numerical results were considered acceptable for the purpose of this research after the modification of the stiffness properties of the masonry walls.

A rocking failure mechanism with crack concentrations at the top and bottom of the two masonry piers has been found to be governing in the numerical model which is in agreement with the experiment. However, crack patterns and corresponding crack widths prove to be difficult to capture correctly. Propagation of vertical/diagonal cracks in the transverse masonry walls and piers has not been observed in the numerical model while these have been observed in the experiment.

Several suggestions have been made to improve the numerical model. First of all, the damage characteristics are likely to improve by adopting a more detailed modelling approach, e.g. 3D solid elements or a micro-modelling approach for the masonry elements. Secondly, the capacity curve is likely to improve by replacing the assumed rigid connections between masonry walls and concrete floors by a more detailed description using interface elements. However, these modifications are considered to be outside of the scope and aim of this thesis.

It is concluded that the calibrated numerical model provides an acceptable starting point for seismic strengthening predictions in which structural windows are included in the numerical model.

15

Seismic strengthening predictions terraced house

The seismic strengthening predictions of a terraced house combines the validated window model with the validated two-storey building model and extrapolates the results. In this chapter, numerical results for strengthened houses are compared with unstrengthened houses. The unstrengthened models leave an opening at the location of the window, while the strengthened models incorporate the designed structural window adopting the component approach. Additionally, a theoretical upper-bound solution is obtained adopting the superglue approach for the structural window. The strengthening predictions will focus on a terraced house with two large windows. This corresponds to a category 1 terraced house described in section 2.1. Relative window sizes found in the front façade of an actual terraced house have been projected on the front façade of the validated two-storey building model. Two cases are considered that utilise different percentages of the total window area as structural windows with the aim to investigate the effect of allowing for ventilation possibilities. The terraced house is subjected to a one-directional monotonic pushover loading scheme with equal forces at the two floor levels. The seismic performance assessment addresses the capacity curve, window substages, and expected damage characteristics.

15.1. General settings

The properties and geometry of the validated two-storey building model are adopted. Additional information about the build-up of the front façade wall of the terraced house, and additional settings required for the inclusion of the structural window are given in this section. These settings are the same for both cases considered.

Model geometry

The build-up of the front façade of the terraced house shown in figure 15.1 is projected on the geometry of the two-storey building model.

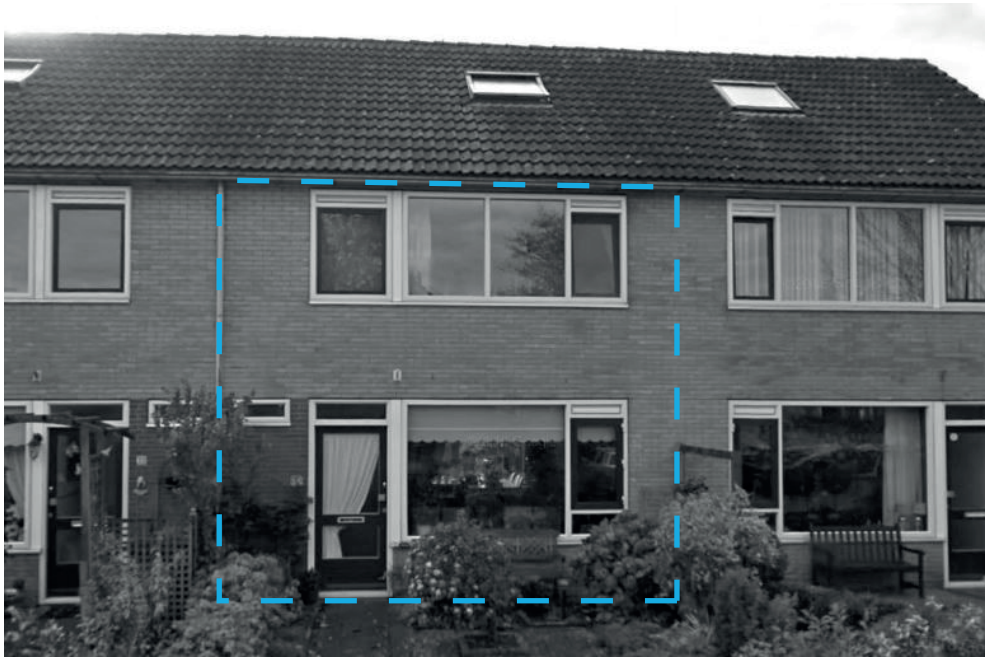

Figure 15.1: Front façade of the actual terraced house that has been adopted for the strengthening predictions of the terraced house. (image based on [20])

The result of this projection is shown in figure 15.2. A timber door frame with hinged corners has been placed at the location of the door. The horizontal door elements at the top are rigidly connected to the masonry, while the vertical door elements at the sides are connected to the masonry by slide interface elements that allow sliding in global z-direction. This sliding interface at the sides of the door frame allows the masonry to deform and crack freely without interference of the door frame. The unstrengthened model includes the door frame and leaves openings at the location of the two windows.

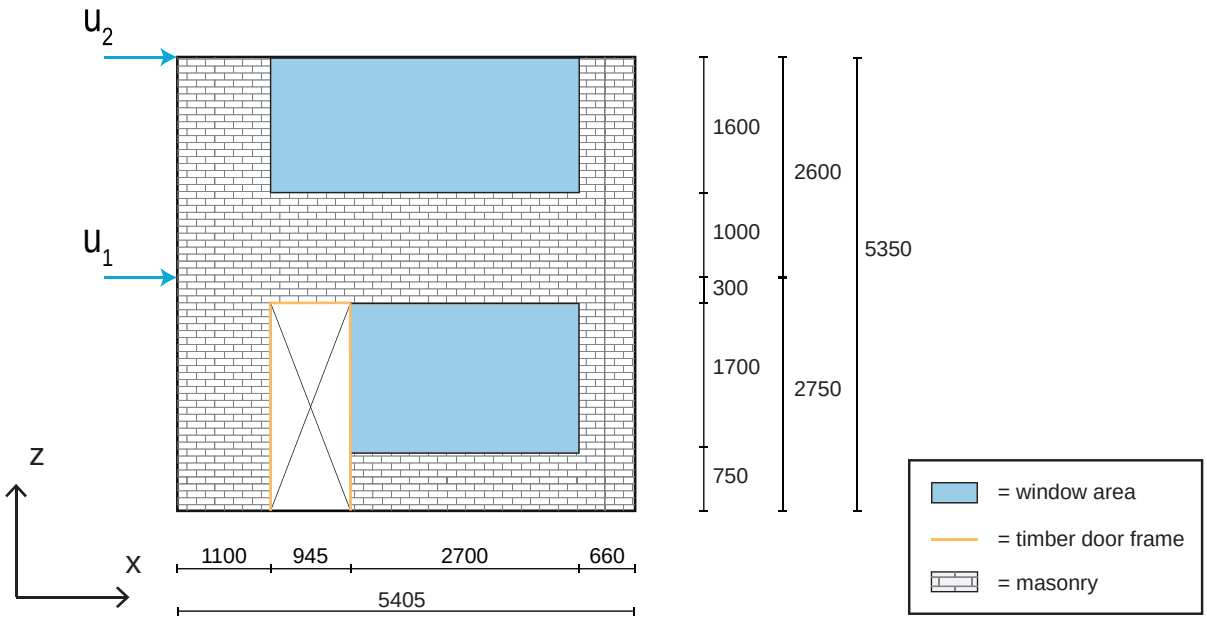

Figure 15.2: Geometry of the front façade of the 3D model for the seismic strengthening predictions of the terraced house.

It is underlined that line symmetry in geometry is not very likely to be present for the terraced house. Despite this, it is expected that a symmetry model composed of the front façade wall and half of the transverse walls will give reasonable results.

Additional finite elements

The glass pane and timber frame are both modelled with LE elements. The timber frame elements are used for the door, and two windows. An overview of their properties is given in table 15.1.

Table 15.1: Discretization into elements for glass pane and timber frame

	Glass pane	**Timber frame**
Material model	Linear elastic isotropic	Linear elastic isotropic
Element type	Curved shells (CQ40S)	Class-III beams (CL18B)
DOFs	$u_x, u_y, u_z, \phi_x, \phi_y$	$u_x, u_y, u_z, \phi_x, \phi_y, \phi_z$
Integration scheme	2x2	2-point Gauss
Mesh size [mm]	150	150
Thickness [mm]	20	-
Cross-section [mm^2]	-	2,000 (50x40)

.

The component approach requires structural interfaces between frame/glass (interface 1) and masonry/frame (interface 2). Both interfaces are modelled with nonlinear 3D line interface elements. An overview of their properties is given in table 15.2. The orientation of the local axes of the interfaces requires extra attention. The in-plane shear and in-plane normal direction should correspond with the local x-axis and y-axis respectively. The local z-axis should corresponds to the out-of-plane shear direction. This out-of-plane shear direction gives an extra DOF compared to the interfaces adopted in the 2D models of the URM wall.

Table 15.2: Discretization into elements for interfaces between frame/glass and masonry/frame

	Interface 1	**Interface 2**
Material model	Nonlinear elasticity	Nonlinear elasticity
Element type	3D line interface (CL24I)	3D line interface (CL24I)
DOFs	u_x, u_y, u_z	u_x, u_y, u_z
Integration scheme	3-point Newton-Cotes	3-point Newton-Cotes
Mesh size [mm]	150	150
Thickness [mm]	20	102
NLE properties input	diagrams	diagrams

.

Additional material properties

The LE material properties of the glass and the birch plywood are given in table 15.3.

Table 15.3: Material properties for glass pane and timber frame

Property	**Parameter**	**Symbol**	**Unit**	**Glass pane**	**Birch plywood**
Elasticity	Young's modulus	E	MPa	70,000	9,000
	Poisson's ratio	v	-	0.23	0.40
	Density	ρ	kg/m^3	2,400	680

.

Interface 1 represents a PU adhesive with a thickness of 5mm between the glass and frame. The NLE diagrams for this interface in the local x-direction and local y-direction are according to the diagrams given in section 11.7 and are not repeated in this section. No diagram is defined for this interface in the local z-direction assuming a rigid connection in the out-of-plane shear direction.

Interface 2 represents an injection mortar connection between the masonry and frame. The NLE diagrams for this interface in the local x-direction and local y-direction are given in figure 15.3. The properties of this interface are related to those of the adjacent masonry elements. The stiffness of these adjacent masonry elements is calculated in equation 15.1 and 15.2.

$$k_n = \frac{E}{l} = \frac{4788}{150} \approx 30N/mm^3 \tag{15.1}$$

$$k_t = \frac{G}{l} = \frac{1915}{150} \approx 10N/mm^3 \tag{15.2}$$

The normal stiffness of the interface is chosen to be large in the compressive direction ($\approx 100 * k_n$), while small in the tensile direction ($\approx 0.01 * k_n$) compared to the normal stiffness of the masonry elements. The shear stiffness of the interface in both directions is chosen to be comparable to the shear stiffness ($\approx k_t$) of the masonry elements. Failure of interface 2 is not included since failure of the adjacent masonry is assumed to be governing. Failure of the adjacent masonry element automatically limits the stress that is transferred by interface 2.

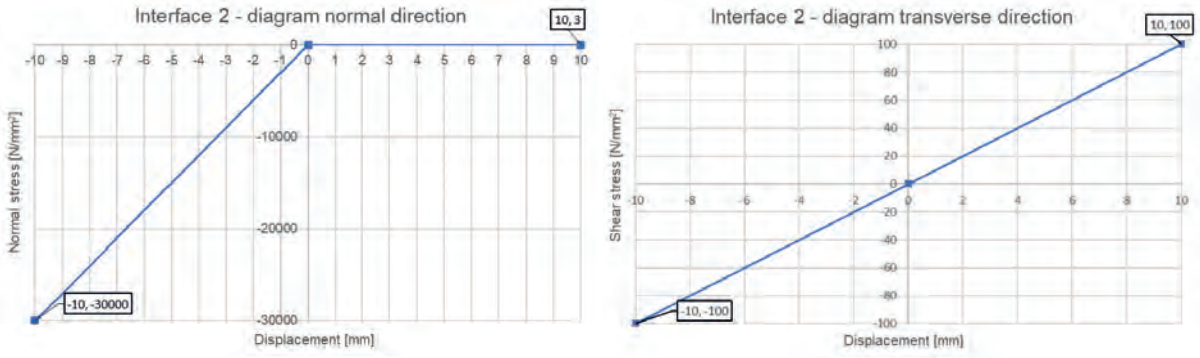

DUSTNY (u_y σ_y):
[-10 -30,000; 0 0; 10 3]

DUSTSX (u_x τ_x)
[-10 -100; 0 0; 10 100]

Figure 15.3: Interface 2: Assumed diagrams for the the masonry/frame connection.

No diagram is defined for this interface in the local z-direction assuming a rigid connection in the out-of-plane shear direction.

Phased analysis

For the unstrengthened and theoretical upper bound models, the applied analysis method is according to the validation study that was given in table 14.7. For the strengthened models, the convergence tolerance and load step size has been adjusted to improve the convergence performance. An overview of the applied analysis method for the strengthened models is shown in table 15.4.

For all models, both geometrical and physical nonlinearity are included and a phased analysis adopted. In phase 1, the self-weight is applied on the masonry structure consisting of the masonry walls, concrete floors, door frame and anchor connections. In phase 2, the loading structure, and window components are included and a monotonic pushover load is applied.

Table 15.4: Adjusted analysis method applied for the strengthened models of the seismic strengthening predictions for the terraced house.

Phase 1 Masonry structure only	**Load steps**	Load name	Self-weight
		Steps	0.1(10)
	Iterative procedure	Procedure	Regular Newton-Raphson
		Max. iterations	100
		Line search	Yes
	Convergence criterium	Norm	Energy
		Tolerance	0.001
		No convergence	Terminate
Phase 2 Complete model	**Start steps**	Start step	Use load of previous phase
	Load steps	Load name	Pushover load
		Load	60mm
		Steps	0.00125(160) 0.005(160)
	Iterative procedure	Procedure	Regular Newton-Raphson
		Max. iterations	100
		Line search	Yes
	Convergence criterium	Norm	Energy
		Tolerance	0.005
		No convergence	Continue

15.2. Windows without openable window sections

Model geometry

Figure 15.4 shows the build-up for the strengthened model for the case of a terraced house without openable window sections. In this case, the full window area is utilised as structural window. Results for the unstrengthened house are compared with the strengthened house, and the theoretical upper bound model. For the strengthened house and theoretical upper bound model, the structural window is placed adopting the component and superglue approach respectively.

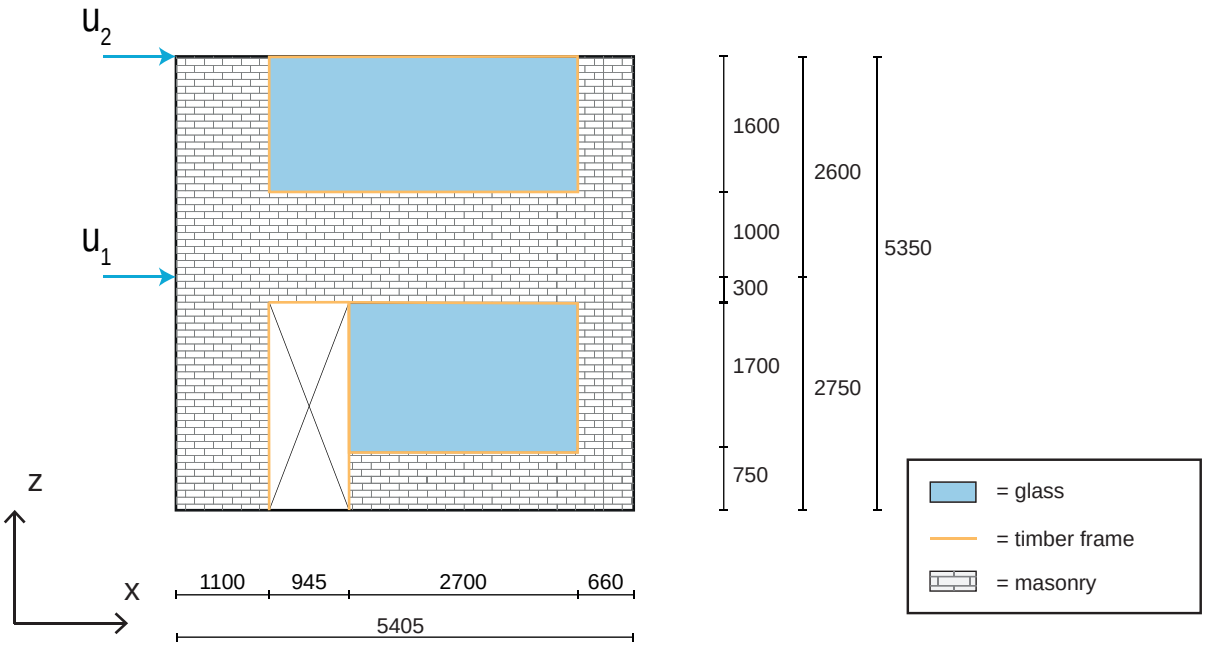

Figure 15.4: Build-up of the strengthened model used for the terraced house without openable window sections

It should be noted that this figure does not show the loading structure and supports. These are incorporated to conform to the two-storey building validation model and can be found in figure 14.2.

Capacity curve

Figure 15.5 shows the obtained capacity curves for the terraced house without openable window sections. It is observed that the structural windows significantly increases the global initial stiffness and seismic force capacity of the terraced house. For the strengthened house, the contribution of the structural windows increases with increasing lateral displacements. At the end of the LE stage, around 2mm, the capacity curve of the strengthened house is closer to the unstrengthened house, while after a displacement of 30mm the curve is overlapping with the theoretical upper bound model. At a lateral displacement of 70mm, the strengthened house has reached 240% of the seismic force capacity obtained for the unstrengthened house. After reaching a displacement of 30mm, the strengthened house and the theoretical upper bound model have a comparable seismic force capacity. This indicates that the theoretical upper bound model indeed gives a upper bound envelop for the capacity curve of the strengthened house.

In addition, it is observed that the strengthened house has a different shape of capacity curve compared to the unstrengthened house and theoretical upper bound model. The unstrengthened house and theoretical upper bound model roughly show a two-staged capacity curve, while a three-staged capacity curve is observed for the strengthened house. After the LE stage, the unstrengthened house and theoretical upper bound model almost immediately reach a plateau with constant force capacity. In contrast, the capacity curve of the strengthened house also shows an intermediate stage between the LE stage and the plateau.

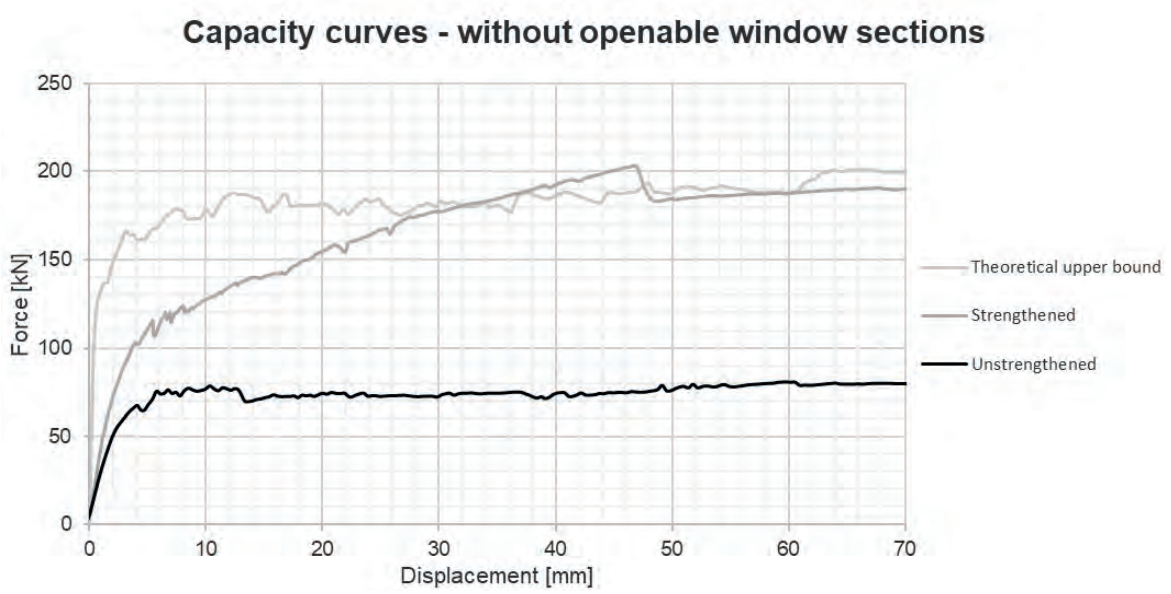

Figure 15.5: Capacity curves of seismic strengthening predictions for the terraced house without openable window sections.

Window stages

Figure 15.6 projects the window substages that were found in section 11.6 on the capacity curve of the strengthened terraced house. In the first substage, loads are transferred through the adhesive joint without tearing. This substage ends at u_2 = 9.3mm when the maximum relative normal interface displacements reaches +2.5mm and tearing of the adhesive is initiated. The second substage proceeds to u_2 = 26.5mm and the maximum relative normal interface displacement reaches a value of -5.0mm indicating that frame/glass contact occurs. The third substage continues until the end of the analysis indicating that glass cracking is not expected. The stress levels in the glass pane range between -12.60 N/mm^2 and +1.91 N/mm^2 at u_2 = 70.0mm. This is well below the stress levels at the onset of glass cracking found in section 11.6.

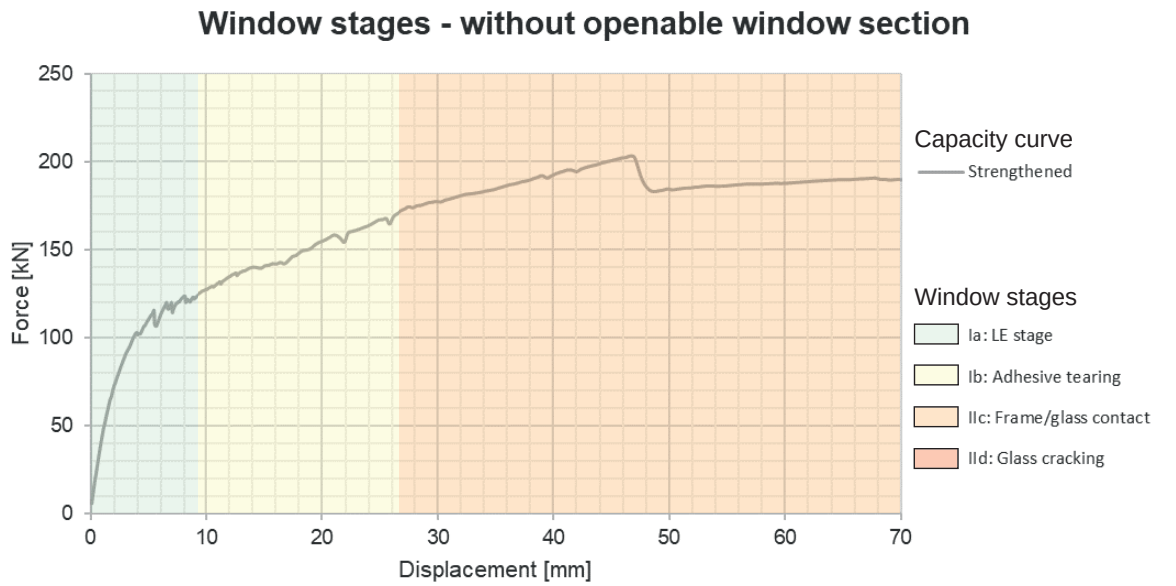

Figure 15.6: Projection of the window substages on the capacity curve of the strengthened terraced house without openable window sections.

Crack patterns

The crack patterns give insight into the failure mechanisms that occur. The cracks patterns at a lateral displacement of 6mm and 30mm are compared for the unstrengthened house, strengthened house, and theoretical upper bound model in figure 15.7.

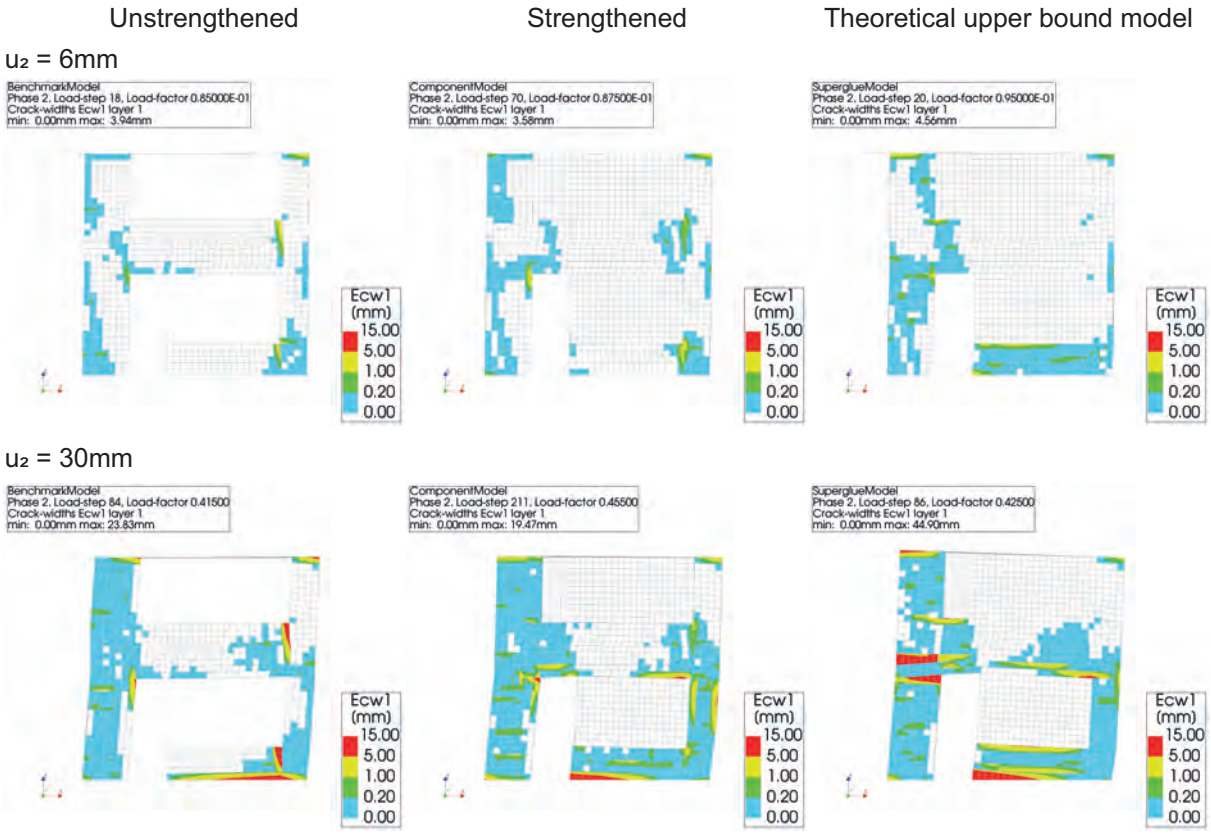

Figure 15.7: Crack patterns in front façade at u_2=6mm and u_2=30mm for seismic strengthening predictions of the terraced house without openable window sections. (DSF = 10)

It can be seen that the different models show more complex crack patterns compared to the validation model of the two-storey building. The unstrengthened house mainly shows crack concentrations at the top and bottom of the two piers, and at the connections between the piers and spandrels.

For the theoretical upper bound model, rocking failure mechanisms seem to develop for both floor levels. For the ground floor, crack concentrations are found at the TRC of the bottom half of the wide pier and BLC of the spandrel under the window. For the first floor, cracks concentrate at the BLC of the top half of the wide pier.

The strengthened house mainly shows similarities to the unstrengthened house at u_2=6mm. In contrast, at u_2=30mm the crack pattern observed for the strengthened house shows more similarities to the theoretical upper bound model.

Seismic performance

Based on the assumed effective mass of $40,000kg$ the seismic performance can be evaluated for a terraced house without openable window sections. The seismic performance is evaluated for two locations: Groningen and Appingedam. This evaluation will compare the results for unstrengthened and strengthened terraced house. The theoretical upper bound model is disregarded as this model only served a theoretical purpose.

Average location - Groningen

The capacity curves of the unstrengthened and strengthened terraced house are plotted against the ADRS of a weak and strong earthquake in figure 15.8. It is observed that both houses have sufficient capacity for the strong earthquake.

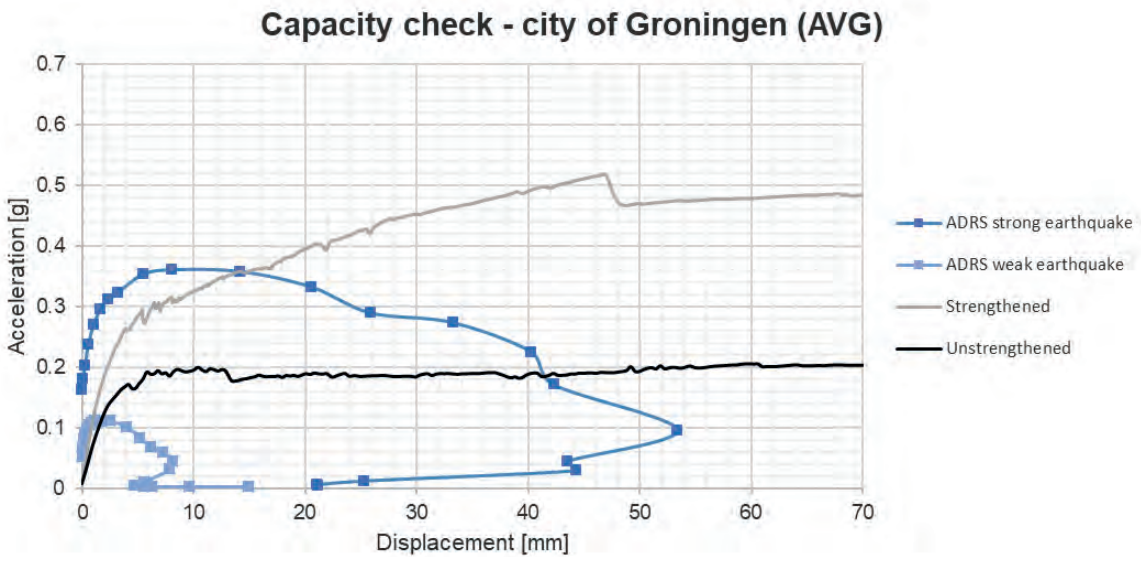

Figure 15.8: Average location - ADRS and obtained capacities for the terraced house without openable window sections.

However, the balance between two seismic load components caused by a strong earthquake varies significantly for the two terraced houses. For the unstrengthened house, the seismic load is composed of a seismic deformation load of 41mm in combination with a seismic force load of 0.19g. For the strengthened house model, the seismic load is composed of a significantly lower seismic deformation load of 14mm in combination with a significantly larger seismic force load of 0.35g.

Figure 15.9 gives an overview of the expected damage to the load-bearing superstructure of the terraced house caused by a weak earthquake in the city of Groningen. It is observed that all damage characteristics are lower for the strengthened house compared to the unstrengthened house. For example, a reduction from 2.15mm to 1.72mm for the maximum crack width is expected as a result of strengthening the terraced house with structural windows.

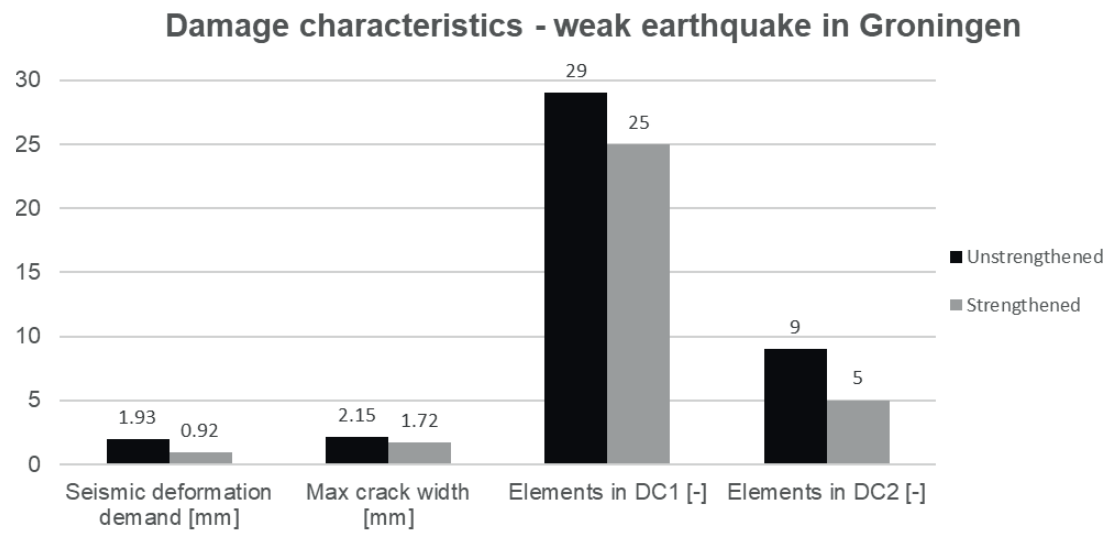

Figure 15.9: Average location - Damage analysis of terraced house without openable window sections.

The effect of the structural window on the seismic performance of a terraced house without openable window sections can be concluded for the location of the city of Groningen.

Based on figure 15.8, it can be concluded that the structural window has a positive effect on the seismic force capacity. The contribution of the structural window to the total force capacity increases with increasing imposed lateral displacements. At a lateral displacement of 70mm, the strengthened house reaches 240% of the seismic force capacity of the unstrengthened house. It was found that both houses showed sufficient capacity to withstand a strong earthquake. However, it should be noted that strengthening of the terraced house results in a significant shift in the balance between the two seismic load components. This shift will have consequences for connected structural elements, e.g. foundation elements, and connected non-structural elements, e.g. walls with no load bearing function. However, this is not considered within the scope of this thesis. Based on figure 15.9, it can be concluded that strengthening with a structural window has a positive effect on the expected damage to the load-bearing superstructure of the terraced house caused by a weak earthquake. For example, a reduction from 2.15mm to 1.72mm for the maximum crack width is expected as a result of strengthening the terraced house with structural windows.

Extreme location - Appingedam

The capacity curves of the unstrengthened and strengthened terraced house are plotted against the ADRS of a weak and strong earthquake in figure 15.8. It is observed that both houses have sufficient capacity for the strong earthquake. However, the balance between two seismic load components caused by a strong earthquake varies significantly for the two terraced houses. For the unstrengthened house, the seismic load is composed of a seismic deformation load of 54mm in combination with a seismic force load of 0.19g. For the strengthened house model, the seismic load is composed of a significantly lower seismic deformation load of 38mm in combination with a significantly larger seismic force load of 0.49g.

Figure 15.9 gives an overview of the expected damage to the load-bearing superstructure of the terraced house caused by a weak earthquake in the city of Appingedam. It is observed that all damage characteristics are lower for the strengthened house compared to the unstrengthened house. For example, a reduction from 3.34mm to 2.08mm for the maximum crack width is expected as a result of strengthening the terraced house with structural windows.

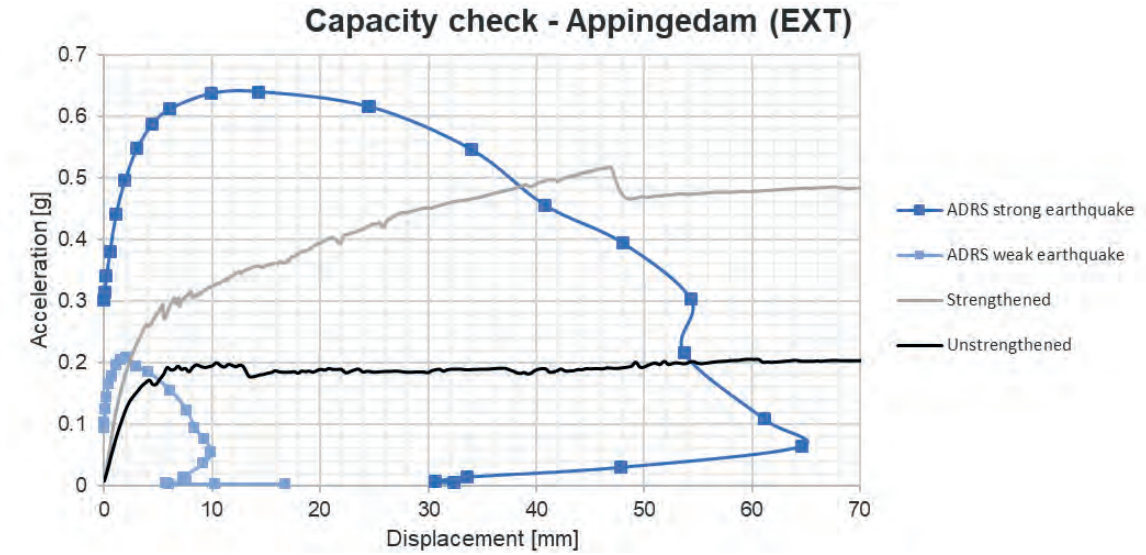

Figure 15.10: Extreme location - ADRS and obtained capacities for the terraced house without openable window sections.

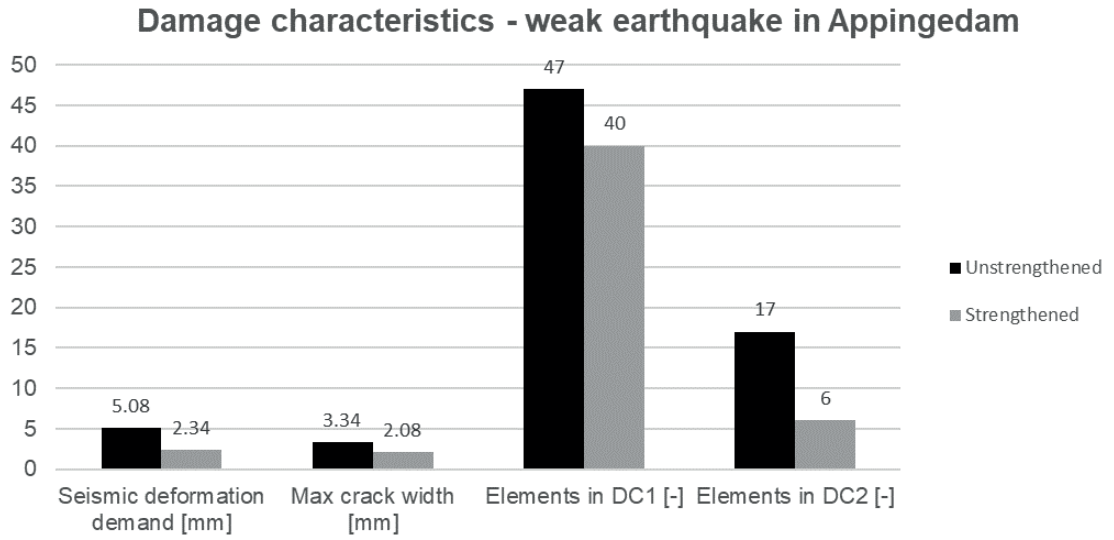

Figure 15.11: Extreme location - Damage analysis for the terraced house without openable window sections.

The effect of the structural window on the seismic performance of a terraced house without openable window sections can be concluded for the location of the city of Appingedam.

Based on figure 15.10, it can be concluded that the structural window has a positive effect on the seismic force capacity. The contribution of the structural window to the total force capacity increases with increasing imposed lateral displacements. At a lateral displacement of 70mm, the strengthened house reaches 240% of the seismic force capacity of the unstrengthened house. It was found that both houses showed sufficient capacity to withstand a strong earthquake. However, it should be noted that strengthening of the terraced house results in a significant shift in the balance between the two seismic load components. This shift will have consequences for connected structural elements, e.g. foundation elements, and connected non-structural elements, e.g. walls with no load bearing function. However, this is not considered within the scope of this thesis. Based on figure 15.11, it can be concluded that strengthening with a structural window has a positive effect on the expected damage for the load-bearing superstructure of the terraced house caused by a weak earthquake. For example, a reduction from 3.34mm to 2.08mm for the maximum crack width is expected as a result of strengthening the terraced house with structural windows.

15.3. Windows with openable window sections

Model geometry

Figure 15.12 shows the build-up for strengthened model of the terraced house with openable window sections. In this case, only part of the window area is utilised as structural window. At the remaining parts of the window area a gap is modelled. These gaps represent a window that can be opened for ventilation purposes. The location and size of these openable window sections are chosen according to figure 15.1. Results for the strengthened terraced house are compared with the unstrengthened house, and the strengthened house without openable window sections.

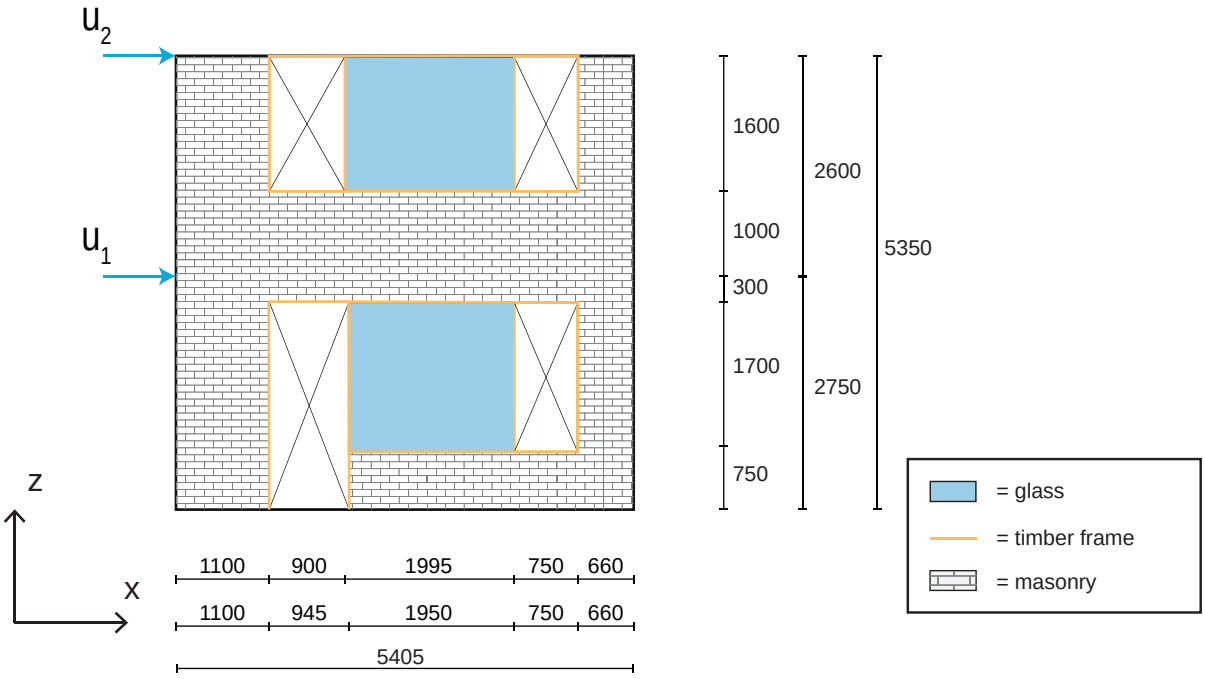

Figure 15.12: Build-up of the strengthened model used for the terraced house with openable window sections.

It should be noted that this figure does not show the loading structure and supports. These are incorporated to conform to the two-storey building validation model and can be found in figure 14.2.

Capacity curve

Figure 15.13 shows the obtained capacity curve for the terraced house with openable window sections. This capacity curve is compared to capacity curves of the unstrengthened terraced house, and the terraced house without openable window sections that were found in previous section.

It is observed that the strengthened terraced house with openable window sections shows a three-staged capacity curve. This is similar to the strengthened terraced house without openable window sections. At a lateral displacement of 70mm, the strengthened terraced house with openable window sections has reached seismic force capacity of 160kN. This seismic force capacity is 30kN lower compared to the strengthened terraced house without openable window sections. Nonetheless, strengthening with structural windows including openable window sections remains to have significant structural potential for a terraced house. At a lateral displacement of 70mm, the seismic force capacity of a strengthened terraced house with openable window sections is about 205% of the seismic force capacity obtained for the unstrengthened terraced house.

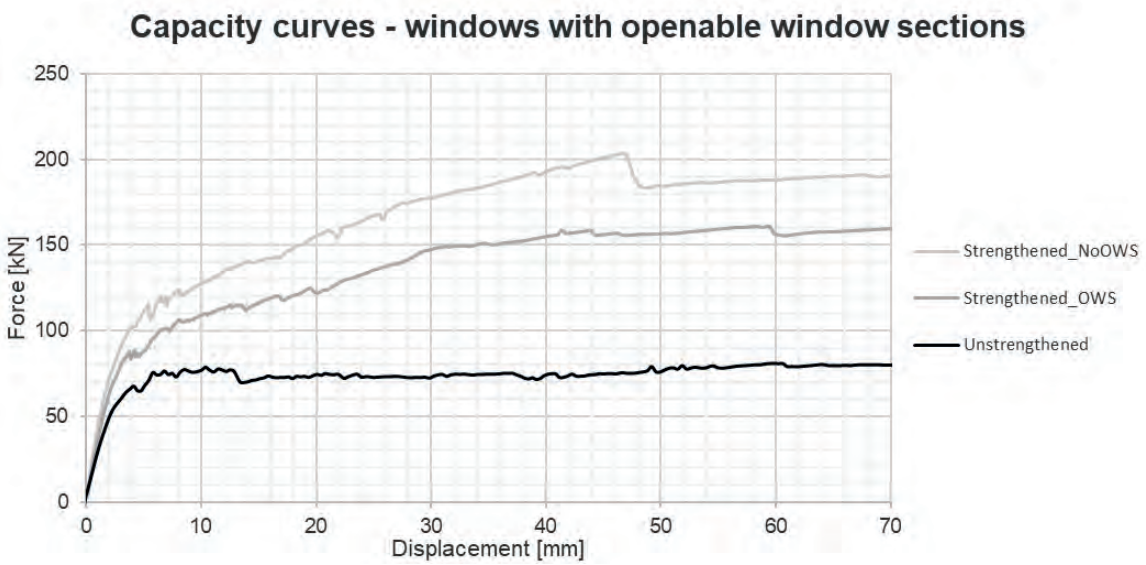

Figure 15.13: Capacity curves of seismic strengthening predictions for the terraced house with openable window sections.

Window stages

Figure 15.14 projects the window substages that were found in section 11.6 on the capacity curve of the strengthened terraced house with openable window sections. In the first substage, loads are transferred through the adhesive joint without tearing. This substage ends at u_2 = 13.2mm when the maximum relative normal interface displacements reaches +2.5mm and tearing of the adhesive is initiated. The second substage proceeds to u_2 = 32.4mm and the maximum relative normal interface displacement reaches a value of -5.0mm indicating that frame/glass contact occurs. The third substage continues until the end of the analysis indicating that glass cracking is not expected. At a lateral displacement of 70.0mm, the stress levels in the glass pane range between -11.18 N/mm^2 and +1.32 N/mm^2. This is well below the stress levels at the onset of glass cracking found in section 11.6.

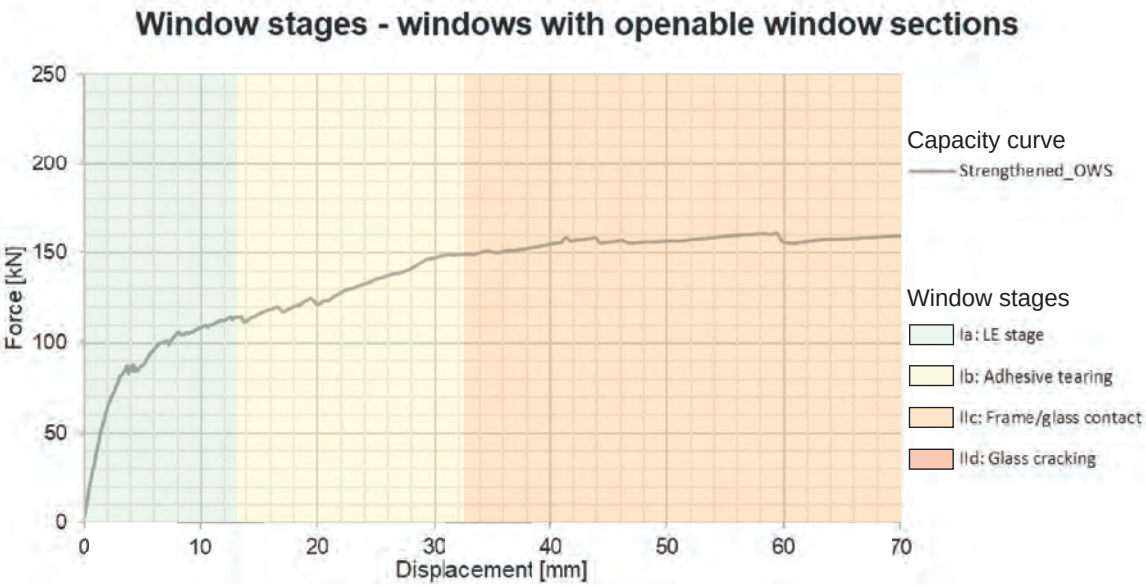

Figure 15.14: Projection of the window substages on the capacity curve of the strengthened terraced house with openable window sections.

Seismic performance

Based on the assumed effective mass of $40,000kg$ the seismic performance can be evaluated for the case of a terraced house with openable window sections. This evaluation will compare the results for the strengthened terraced house with unstrengthened terraced house, and the strengthened terraced house without openable window sections. The seismic performance is evaluated for two locations: Groningen and Appingedam.

Average location - Groningen

The capacity curves of the unstrengthened and strengthened terraced house are plotted against the ADRS of a weak and strong earthquake in figure 15.15. Additionally, the capacity curve of the strengthened terraced house without openable window sections is shown. It is observed that all terraced houses have sufficient capacity for the strong earthquake.

Furthermore, it is observed that the inclusion of openable window sections has an effect on the magnitude of the shift in the two seismic load components. Compared to the unstrengthened terraced house, both strengthening cases result in a lower seismic deformation demand in combination with a larger seismic force demand caused by a strong earthquake. However, this shift is less strong for the case with openable window sections compared to the case without openable window sections.

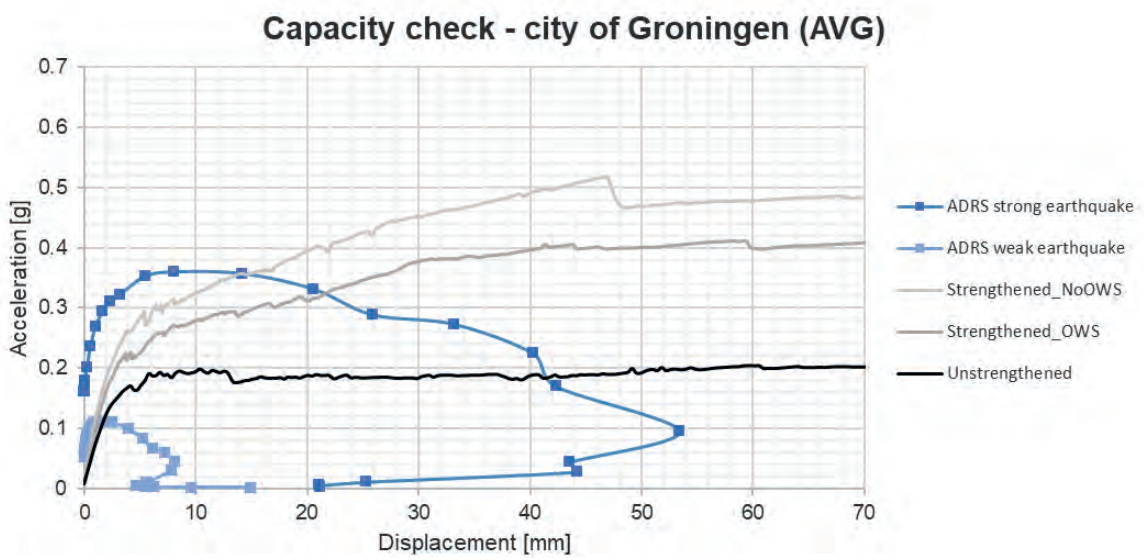

Figure 15.15: Average location - ADRS and obtained capacities for the terraced house with openable window sections.

Figure 15.16 gives an overview of the expected damage to the load-bearing superstructure of the terraced house caused by a weak earthquake in the city of Groningen. All damage characteristics are lower for the strengthened house compared to the unstrengthened house. Furthermore, the openable window sections have limited effect on the expected damage. The damage characteristics for the strengthening case with openable window sections are comparable to the case without openable window sections.

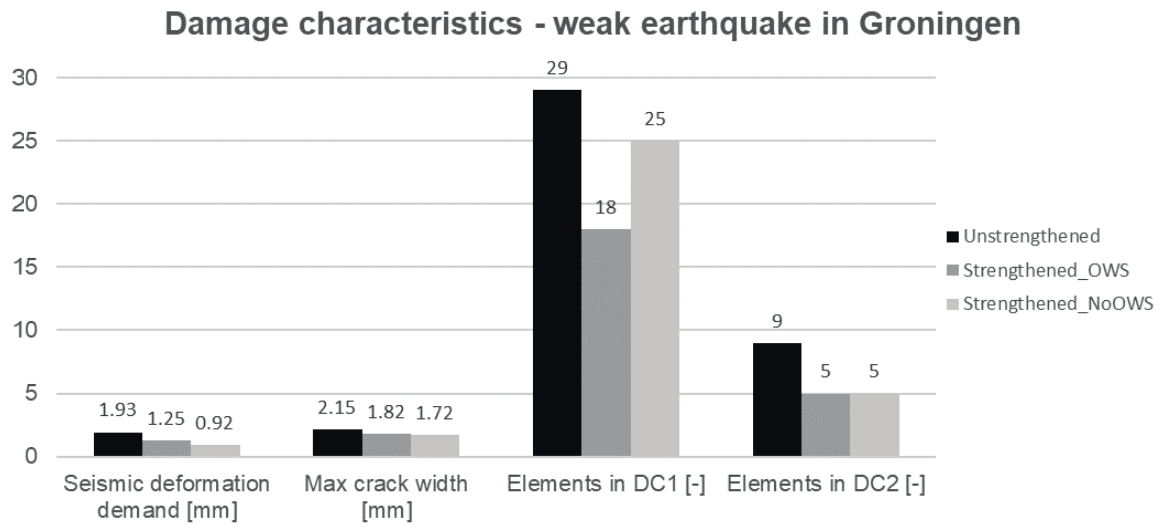

Figure 15.16: Average location - Damage analysis of terraced house with openable window sections.

Extreme location - Appingedam

The capacity curves of the unstrengthened and strengthened terraced house are plotted against the ADRS of a weak and strong earthquake in figure 15.17. Additionally, the capacity curve of the strengthened terraced house without openable window sections is shown. It is observed that all terraced houses have sufficient capacity to withstand the strong earthquake.

Furthermore, it is observed that the inclusion of openable window sections has an effect on the magnitude of the shift in the two seismic load components. Compared to the unstrengthened terraced house, both strengthening cases result in a lower seismic deformation demand in combination with a larger seismic force demand caused by a strong earthquake. However, this shift is less strong for the case with openable window sections compared to the case without openable window sections.

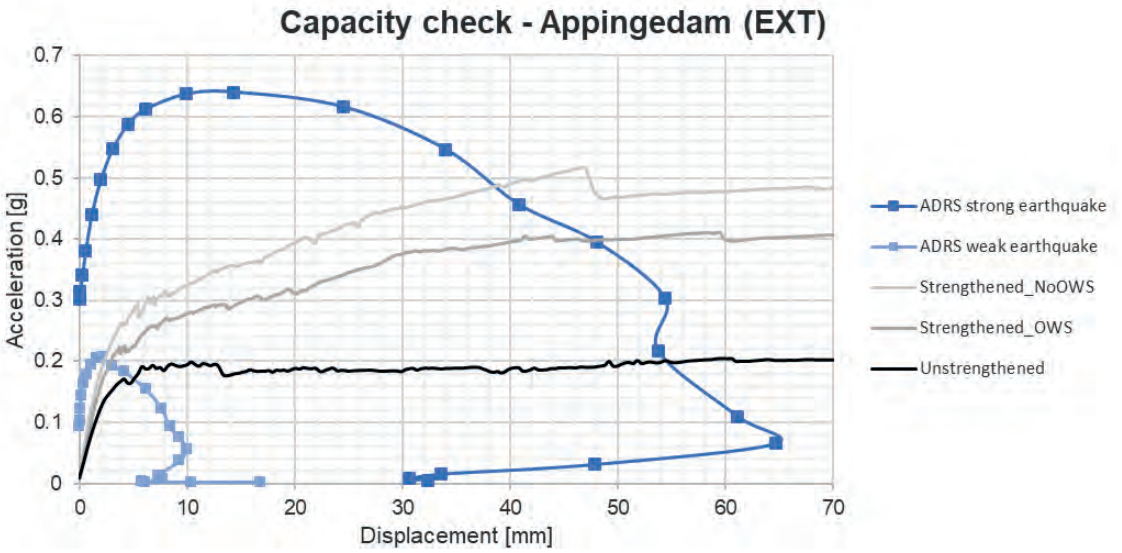

Figure 15.17: Extreme location - ADRS and obtained capacities for the terraced house with openable window sections.

Figure 15.18 gives an overview of the expected damage to the load-bearing superstructure of the terraced house caused by a weak earthquake in the city of Groningen. For the strengthened terraced

house, all damage characteristics are lower compared to the unstrengthened house. Furthermore, the openable window sections have limited effect on the expected damage. The damage characteristics for the strengthening case with openable window sections are comparable to the case without openable window sections.

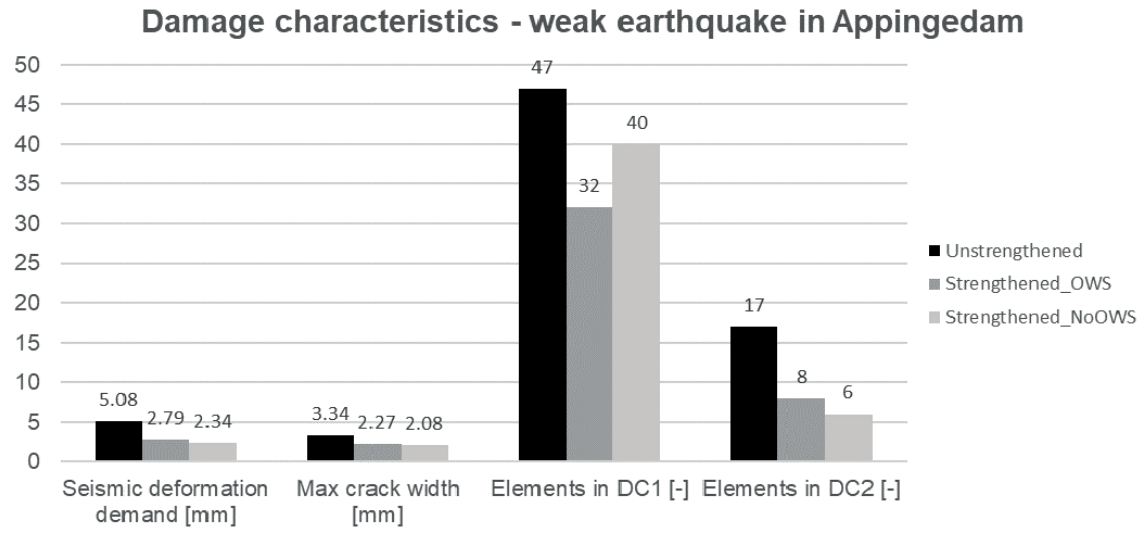

Figure 15.18: Extreme location - Damage analysis of terraced house with openable window sections.

15.4. Sensitivity analysis

A sensitivity analysis is performed to investigate the influence of the material properties for masonry on the results for unstrengthened terraced house, and strengthened terraced house with openable window sections. The influence of the material properties for masonry on the stress levels in the glass panes are of specific interest. The weak and strong set of material properties for masonry have been derived mostly based on standard deviations reported by Ravenshorst et al. [20] and empirical formulations reported by Schreppers et al. [36]. An overview of the material sets that have been adopted in the sensitivity analysis is given in table 15.5.

Table 15.5: Sets of material properties for masonry adopted in the sensitivity analysis for the terraced house.

Property	Weak	Standard	Strong	Explanation
E_x [1]	2,437	3,583	5,267	Based on CoV
E_y [1]	3,495	4,788	6,560	Based on CoV
G_{xy} [2]	1,398	1,915	2,624	Based on $G_{xy} = 0.4E_y$
ρ	1,805	1,805	1,805	No variation
f_{ty} [*1]	0.18	0.19	0.38	Based on mean value and CoV
G_{ft}	0.0116	0.0127	0.0502	Softening line parallel to standard material set
α	0.792	0.792	0.792	No variation
f_c [1]	5.34	5.84	6.38	Based on CoV
G_c	15.66	17.39	19.62	Softening line parallel to standard material set
c [*2]	0.14	0.14	0.57	Strong value derived based on $c = 1.5f_{ty}$
G_{fs}	-	-	-	No variation
ϕ [*2]	0.4	0.406	0.6	Based on $c = 0.4 - 0.6$

[*] Standard value was already low.
[1] Reported by Ravenshorst et al. [20]
[2] Reported by Schreppers et al. [36]

It is pointed out that some of the material properties of the standard set were already relatively low. Therefore, values for the tensile strength, cohesion, friction angle of the weak set are comparable to the values of the standard set.

Weak masonry properties

Figure 15.19 compares the capacity curves of the terraced houses with the set of weak and standard masonry properties. Both the influence on the capacity curve of the unstrengthened terraced house, and the strengthened terraced house with openable window sections is shown. The weak masonry properties prove to have limited effect on the capacity curve of the unstrengthened, and strengthened terraced house.

Furthermore, it is found that the set of weak masonry properties has limited effect on the stress levels in the glass pane. At a lateral displacement of 70mm, the stress levels in the glass pane are comparable to the stress levels that were found with the standard masonry properties. Therefore, glass cracking is not expected for the weak material set.

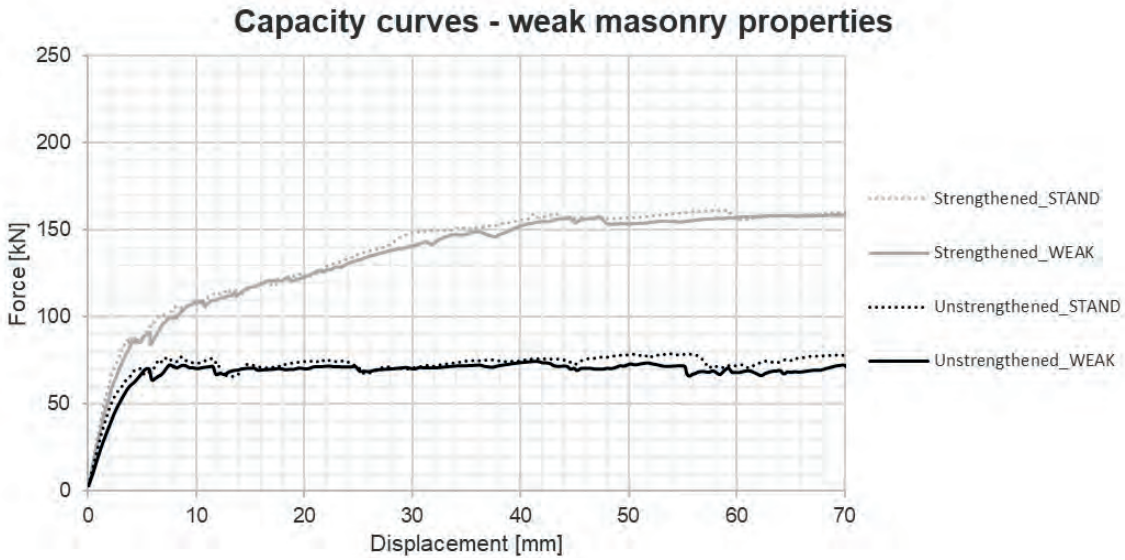

Figure 15.19: Influence of weak masonry properties on capacity curves for the terraced house with openable window sections.

Strong masonry properties

Figure 15.20 compares the capacity curves of the terraced houses with the set of strong and standard masonry properties. Both the influence on the capacity curve of the unstrengthened terraced house, and the strengthened terraced house with openable window sections is shown. It can be seen that the initial stiffness, and seismic force capacity of both the unstrengthened, and strengthened terraced house are increased as a results from the strong masonry properties. However, the strong masonry properties seem to have limited effect on the structural potential of the structural window. The increase in seismic force capacity seems even higher for the terraced house with strong masonry properties compared to the standard masonry properties.

Furthermore, it is found that the set of strong masonry properties has limited effect on the stress levels in the glass pane. At a lateral displacement of 70mm, the stress levels in the glass pane are comparable to the stress levels that were found with the standard masonry properties. Therefore, glass cracking is not expected for the strong material set.

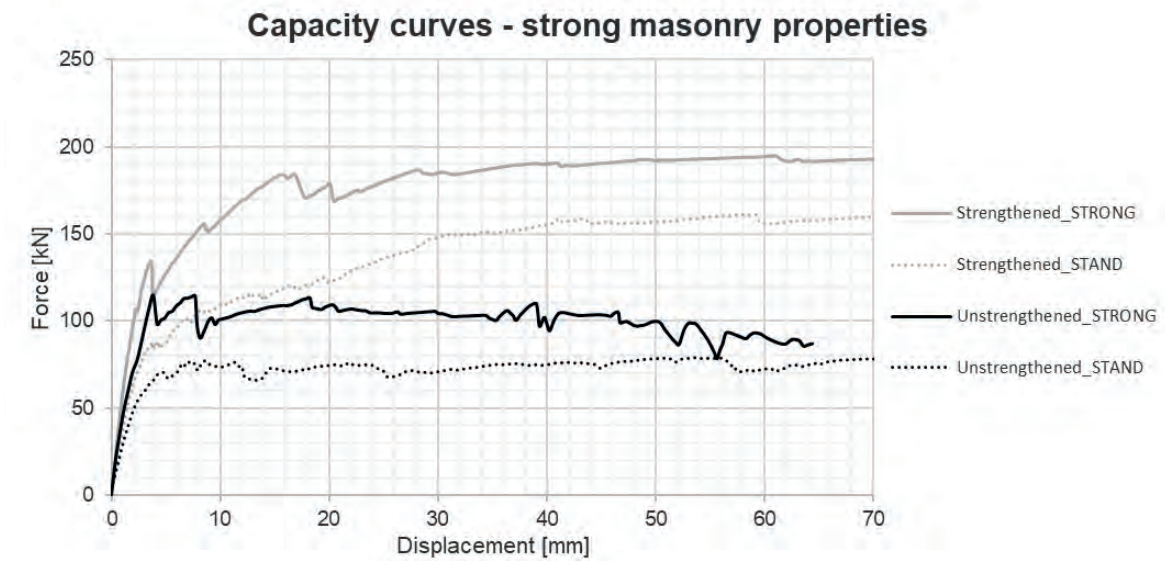

Figure 15.20: Influence of strong masonry properties on capacity curves for the terraced house with openable window sections.

15.5. Conclusion chapter 15

The assessment of the seismic performance on the scale of a structure focussed on a terraced house consisting of CS-brick masonry walls, solid concrete floors with two large windows in the front façade wall. Two strengthened terraced houses were considered that utilise different percentages of the total window area as structural windows. The first case utilised the full window area as structural window, while the second case included openable window sections. All model were subjected to a one-directional monotonic pushover load up to 60mm. The unstrengthened terraced house left openings at the location of the windows, while the two strengthened terraced house incorporated the designed structural window adopting the component approach. Comparison of the result of the unstrengthened and two strengthened terraced house gave insight into the structural potential of the designed structural window at the level of a structure. Additionally, comparison between the two strengthened terraced houses gave insight into the effect of incorporating ventilation possibilities.

First of all, it was found that strengthening with the structural window has a positive effect on the seismic force capacity of the terraced house. Figure 15.21 shows that the strengthened terraced houses without openable window sections has 240% of seismic force capacity of the unstrengthened terraced house. It can be seen that including openable window sections reduces the seismic force capacity. Nonetheless, strengthening with structural windows with openable window sections remains to have significant structural potential. The strengthened terraced houses with openable window sections has 205% of seismic force capacity of the unstrengthened terraced house.

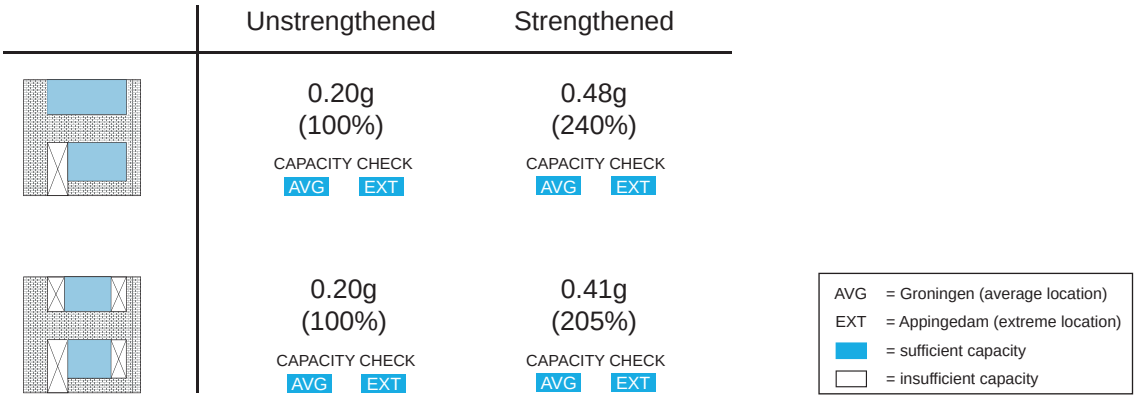

Figure 15.21: Overview of seismic acceleration capacity[1] for the seismic strengthening predictions of the terraced house at u_2=70mm and capacity check against strong earthquakes expected for Groningen and Appingedam.

Furthermore, it is observed that all terraced houses have sufficient capacity for all earthquakes considered. However, the balance between the two seismic load components acting upon the terraced house is expected to shift significantly by the structural window. The strengthened terraced house has to withstand a significantly smaller seismic deformation demand, but significantly larger seismic force demand compared to the unstrengthened terraced house. This shift in the seismic demand components is expected to have consequences for connected structural elements, e.g. foundation elements, and connected non-structural elements, e.g. walls with no load bearing function. However, this is not considered within the scope of this thesis

Secondly, it was found that strengthening with the structural window has positive effect on the expected damage caused by a weak earthquake. A reduction of the expected damage was found for the two strengthened houses compared to the unstrengthened houses. These observations were found for both the weak earthquake expected for the city Groningen, and Appingedam.

It can be concluded that the structural window has significant potential to improve the in-plane seismic performance of a terraced house both in terms of structural force capacity and expected damage.

[1] Force and acceleration have been used interchangeably. These are directly proportional through the effective mass that is assumed to be a consant (independent of the window size and the installation of the structural window).

16

Conclusions part III

The potential of the structural window for in-plane seismic strengthening of URM structures was investigated based on numerical studies in DIANA FEA 10.2. These numerical studies were divided into validation studies and seismic strengthening predictions. In the validation studies, results from numerical models were compared, and validated to experimental results found in literature. These validation studies were used as a valuable starting point for the seismic strengthening predictions that investigated the potential of the structural window design for in-plane seismic strengthening of URM structures.

The validation studies were performed in a step-wise approach with increasing scale at each step. First of all, a window model was validated with experiments by Huveners [18]. Huveners [18] investigated the structural potential of a steel-glass composite wall with a semi-rigid adhesive joint, *Sikaflex-252*, with a thickness of 5mm. The capacity curve of the steel-glass composite wall was adequately captured by a 2D model. Furthermore, it was found that the capacity curve of a squared steel-glass composite wall can be divided into four subsequent substages: LE stage, adhesive tearing, frame/glass contact, and glass cracking. The stress levels at the initiation of glass cracking were found to be between -73.53 N/mm^2 and 5.72 N/mm^2. Secondly, a clay-brick URM wall model was validated with experiments by Korswagen et al. [19]. The capacity curve and governing failure mechanism were adequately captured by the numerical model. In contrast, the exact crack patterns and crack widths proved to be more difficult to capture correctly. Lastly, a two-storey building model was validated with experiments by Ravenshorst et al. [20]. The two-storey building consisted of CS-brick masonry walls with two solid concrete floors. The capacity curve and governing failure mechanism were reasonably well captured by the 3D numerical model.

The seismic strengthening predictions on the scale of a structural element focussed on a single-wythe wall of clay-brick masonry with one window. These predictions combined the validated window model with the validated URM wall model. Three cases with different window sizes were considered. For all cases, the full window area was utilised for the designed structural window leaving no gaps for ventilation. All models were subjected to a one-directional monotonic pushover load up to 8mm. The unstrengthened wall models left an opening at the location of the window, while the strengthened wall models incorporated the designed structural window adopting the component approach. It was found that the structural window has significant potential to improve the in-plane seismic performance of an URM wall both in terms of structural force capacity and expected damage. The strengthened walls reached between 137% and 367% of the seismic force capacity of the corresponding unstrengthened wall. The largest increase in seismic force capacity was found for the two cases with a large window. However, it was observed that the window size has limited effect on the seismic force capacity of the strengthened wall. All strengthened walls showed a comparable seismic force capacity at a lateral displacement of 8mm. The expected damage for the strengthened wall was found significantly reduced compared to the unstrengthened wall for the two large window cases. For example, a reduction from 1.86mm to 0.26mm was found for the maximum crack width expected for the large window case in Appingedam.

The seismic strengthening predictions on the scale of a structure focussed on a terraced house consisting of CS-brick masonry walls, and solid concrete floors with two large windows in the front façade wall. This predictions combined the validated window model with validated two-storey building model. Two cases were considered with the aim to investigate the influence of incorporating ventilation possibilities. All models were subjected to a one-directional mass proportional monotonic pushover load up to 60mm. It was found that the structural window has significant potential to improve the in-plane seismic performance of a terraced house both in terms of structural force capacity and expected damage. First of all, it was found that strengthening with the structural window has a positive effect on the seismic force capacity of the terraced house. The strengthened terraced houses without openable window sections showed 240% of the seismic force capacity of the unstrengthened terraced house. Additionally, strengthening with structural windows including openable window sections remained to have significant structural potential. The strengthened terraced houses with openable window sections had 205% of the seismic force capacity of the unstrengthened terraced house. Secondly, it was found that strengthening with the structural window had a positive effect on the expected damage caused by a weak earthquake. A reduction of the expected damage was found for the two strengthened houses compared to the unstrengthened houses. Lastly, it was found that glass cracking is not to be expected. At a lateral displacement of 70.0mm, the stress levels in the glass pane ranged between -11.18 N/mm^2 and +1.32 N/mm^2. This is well below the stress levels at the onset of glass cracking that were found for the validated window model. A sensitivity analysis showed that these stress levels in the glass pane were barely influenced by adopting weak or strong masonry properties.

17

Conclusions and recommendations

17.1. Conclusions

Seismic performance assessment

The seismic performance of the unstrengthened and strengthened masonry structure is assessed by the seismic force capacity, a capacity check, and a damage evaluation of the load-bearing superstructure. Additionally, failure of the structural adhesive, and glass pane were checked for the strengthened masonry structure. The capacity check is performed for the strong earthquake (NC limit state), while the damage evaluation is performed for the more frequent weak earthquake (DL limit state). The strong and weak earthquakes were defined as earthquakes with return periods of 95 and 2475 years, respectively. The damage evaluation addressed three damage characteristics: the maximum crack width, the number of finite elements with a crack width between 0.1mm and 1mm (damage category 1), and the number of finite elements with a crack width between 1mm and 5mm (damage category 2). Furthermore, the seismic performance was assessed for the city of Groningen and Appingedam. These locations were selected as an average and extreme location based on the spatial distribution of terraced houses, and the PGA contour map.

Structural window design

Frame-glass composite walls were studied for the design of the structural window. These frame-glass composite walls contain two traditional components of a window, i.e. a frame and a glass pane. Furthermore, several authors demonstrated the potential of these frame-glass composite walls to act as a stabilising element. The in-plane capacity is generated by the glass panes through a circumferentially adhesive bonded joint. This circumferentially adhesive bonded joint connects the glass panes with the frame.

The structural window was designed with the aim to increase the in-plane seismic force capacity of an existing URM structure by utilising the glass pane as a structural element. The structural window is composed of a timber frame, a semi-rigid adhesive, and double glazing unit. The structural layer of the double glazing unit has a thickness of 20mm and is composed of two laminated annealed glass panes with equal thickness. The prefabricated structural window is placed in-plane with the existing load-bearing inner leaf of the cavity wall. The prefabricated structural window is connected to the existing structure by an injection mortar joint that fills a gap up to 25mm at all sides of the prefabricated structural window.

The components of the structural window design were effectively modelled with beam elements for the frame, 2D continuum elements for the glass pane, and nonlinear interface elements for the structural adhesive. The nonlinear material properties of the structural adhesive do not only incorporate adhesive failure, but also an increased stiffness at glass/frame contact. Glass/frame contact occurs when the structural adhesive is completely pushed in, i.e. the relative normal interface displacement in the negative direction reaches the thickness of the structural adhesive.

The capacity curve of a frame-glass composite wall can be divided in four subsequent substages. These window substages are: a linear elastic stage, adhesive tearing, glass/frame contact, and glass cracking. It was found that the stress levels in the glass pane ranged between -73.53 N/mm^2 and +5.72 N/mm^2 at the initiation of glass cracking.

Numerical studies

The potential of the designed structural window for in-plane seismic strengthening of URM structures was investigated through numerical studies using DIANA FEA 10.2. The potential of the designed structural window was assessed at the level of a structural element and an entire structure. The assessment of the seismic performance at the level of a structural element focussed on a single-wythe wall of clay-brick masonry with one window. The assessment of the seismic performance at the level of an entire structure focussed on a terraced house consisting of CS-brick masonry walls and solid concrete floors. The scope of this thesis was limited to only one type of terraced house with two rigid floors, masonry spandrels, and two large windows in the façade wall. Only the front half of the terraced house was modelled, assuming line symmetry in the geometry.

Strengthening predictions at wall level

The numerical predictions indicated that the structural window has significant potential to improve the in-plane seismic performance of an URM wall. Three cases with different window sizes were considered. It was found that a strengthened URM wall performed better both in terms of seismic force capacity, and expected damage compared to an unstrengthened URM wall.

The strengthened masonry walls reach 137%, 300% and 367% of the seismic force capacity of the corresponding unstrengthened wall, depending on the window size. The largest increase in seismic force capacity was found for the case with the largest window size. The results revealed that the window size mainly has an effect on seismic force capacity of the unstrengthened wall. For the unstrengthened wall, a large window size resulted in a significantly lower seismic force capacity. In contrast, it is observed that the window size has limited effect on the seismic force capacity of the strengthened wall. All strengthened walls showed a comparable seismic force capacity at the end of the pushover analysis.

The damage evaluation focussed on the damage to the URM wall. For the two large window cases, a substantial reduction of the expected damage was found for the strengthened wall compared to the unstrengthened wall. For example, a reduction from 1.86mm to 0.26mm was found for the maximum crack width for the case with a large window at the location of Appingedam. For the small window case, both the unstrengthened and strengthened wall remained practically undamaged.

For all cases, it was found that the structural window remained in the first substage, up to the end of the pushover analysis. This indicates that loads are transferred through the adhesive joint without tearing of the adhesive. In addition, no failure of the glass is expected for the analysis.

Strengthening predictions at building level

The numerical predictions indicated that the structural window has significant potential to improve the seismic performance of a terraced house in the longitudinal direction. Two cases were considered. The first case utilised the full window area as structural window, while the second case incorporated openable window sections and only part of the window area was utilised as structural window. For both cases, it was found that the strengthened terraced house performed better both in terms of seismic force capacity and expected damage compared to an unstrengthened terraced house.

It was found that the strengthened terraced house with openable window sections has 205% of the seismic force capacity of the unstrengthened terraced house. This is lower compared to the strengthened terraced house without openable window sections that showed 240% of seismic force capacity of the unstrengthened terraced house. Nonetheless, it can be concluded that strengthening with structural windows with openable window sections remains to have substantial structural potential.

Furthermore, it was observed that all terraced houses have sufficient capacity for all earthquakes considered. However, the balance between the two seismic load components acting upon the terraced house is expected to shift significantly by the structural windows. The strengthened terraced houses have to withstand a significantly smaller seismic deformation demand, but significantly larger seismic force demand compared to the unstrengthened terraced house.

The damage evaluation focussed on the damage to the load-bearing superstructure of the terraced house. For both cases, a reduction of the expected damage was found for the two strengthened houses compared to the unstrengthened houses. For example, a reduction from 3.34mm to 2.27mm was found for the maximum crack width for the case with openable window sections at the location of Appingedam. Furthermore, it was observed that the presence of openable window sections has limited effect on the damage expectation of the strengthened terraced house.

It was demonstrated that the structural window remained in the third window stage, up to the end of the pushover analysis. This indicates that no failure of the glass panes is expected. At the end of the pushover analysis, the stress levels in the glass panes ranged between -11.18 N/mm^2 and +1.32 N/mm^2. This is well below the stress levels that were found at the onset of glass cracking. A sensitivity analysis showed that the stress levels in the glass pane were barely influenced by adopting weak, and strong masonry properties. In contrast, failure of the adhesive is expected as a result of the two strong earthquakes. This is expected to occur locally at the corners of the structural window. For the two weak earthquakes, the structural windows are expected to remain in the first window substage and no failure of the structural adhesive is expected.

17.2. Recommendations

Experimental validation steps

The numerical predictions are promising. Therefore, it is recommended to validate the numerical predictions with an experimental testing campaign. It is suggested to adopt a step-wise and pragmatic approach from small to large scale, and from monotonic to cyclic loading with prototype testing. The seismic performance under cyclic loading conditions is an important next step to assess the residual capacity after multiple earthquakes and the influence of pre-damage. A valuable starting point for the set-up for this experimental campaign can be found in Ber et al. [44]. Ber et al. [44] provides a valuable framework for the monotononous, cyclic and dynamic testing of timber-glass composite walls that can potentially be extended to testing strengthened masonry structures.

Specifically, this experimental campaign could investigate certain aspects that were either not included in the numerical model or included based on assumptions that have to be checked:

- Strength degradation in masonry under repeated loading. This feature was not included in the numerical model. The amount of strength degradation depends on, among other factors, the mode of failure and is difficult to predict a priori. The amount of strength degradation can be determined in an experimental campaign.
- Influence of pre-damage to the existing masonry structure on the residual capacity. This pre-damage could be caused by other load types, e.g. differential settlements or restrained shrinkage.
- Material properties of the connection between the existing masonry inner leaf and frame of the prefabricated structural window. It is recommended to determine the stiffness properties and check if failure of this connection is indeed not governing.
- Material properties of the structural adhesive. It is recommended to investigate the effect of loading rate, load duration, and repetitive loading on the material properties of structural adhesive.

Seismic performance assessment

Several suggestions to improve the seismic performance assessment are listed below:

- Include connected (non-)structural elements in the damage evaluation. In this thesis, the damage evaluation only included the load-bearing superstructure. However, it was found that strengthening with a structural window results in a significantly smaller seismic deformation demand, but significantly larger seismic force demand. The increased seismic force demand is expected to result in more damage to connected structural elements, e.g. foundation elements. In contrast, the reduced seismic deformation demand is expected to result in less damage to connected non-structural elements, e.g. the outer leaf of the cavity wall.
- Combine the damage characteristics into a single scalar damage parameter. This increases the ease of comparing the damage condition of the unstrengthened and strengthened masonry structure. An example of this can be found in Korswagen et al. [19].
- Investigate the influence of the effective mass of the terraced house on the seismic performance. In this thesis, an effective mass of 40,000kg was assumed. However, Crowley et al. [8] reported a range of 32,000-47,000kg for the effective mass of residential terraced houses in the Groningen area.
- Perform the damage evaluation for a strong earthquake. In this thesis, the damage evaluation was performed for a weak earthquake at the two selected locations. However, the strong earthquake results in more damage and it is expected that this increases the difference between the damage to the unstrengthened and strengthened structure. Therefore, this evaluation is likely to give more insight in the effect of strengthening with a structural window on the damage expectation.

Structural window design

Several suggestions to further develop the structural window design are listed below:

- Extend the performance assessment with a quantification the performance on traditional functions of a window, e.g. thermal insulation, water tightness and air permeability. In this thesis, the focus was on the structural performance and the potential of the structural window has been demonstrated. Therefore, a logical next step would be to investigate and improve of the performance on traditional functions. An overview of the traditional functions of a window is given in table 2.1.
- Extend the performance assessment with additional practical requirements, e.g. durability and maintenance.
- Development of prototypes for the structural window in collaboration with a manufacturer for experimental testing. Furthermore, an installation process proposal could be developed in collaboration with contractors that could be tested in the experimental testing campaign. For the installation proposal and experimental testing, it is recommended to further examine the practical feasibility of the wet joint focussing on the possible risk of leakage.
- Investigate possibilities to take other measures that improve the sustainability of the building in combination with placing the structural window, e.g. improve the insulation in the cavity wall.

Numerical modelling

The numerical models adopted the macro-modelling approach for the masonry elements. In the validation study of the masonry wall and the two-storey building, it was found that the exact crack patterns, and corresponding crack widths were difficult to capture correctly. Therefore, it could be investigated if the damage characteristics improve with a more detailed modelling approach, e.g.:

- Adopt a (detailed) micro-modelling approach for the masonry elements.
- Adopt 3D solid elements instead of 2D elements.

It is underlined that these detailed modelling approaches are computationally expensive. Therefore, it is recommended to test on the scale of the URM wall first. If these tests prove to be successful, it could be considered to adopt a more detailed modelling approach for the terraced house.

Additionally, several suggestions for the numerical predictions of the terraced house are listed below:

- Specify properties for the interfaces between the floors and walls, and between the longitudinal and transverse walls. In this thesis, these interfaces were assumed to be rigid.
- Extend the numerical model with the other half of the terraced house. In this thesis, only the front half of the terraced house was modelled. Thus, the front and back facade walls of the terraced house were assumed to be identical in terms of the location and size of the window(s) and door. However, this assumption is not very likely for most terraced houses. Unequal façade walls are expected to cause torsional forces as a result of stiffness differences between the front and back facade wall. Nonetheless, the symmetry model could be very useful to prevent these torsional forces. The symmetry model could be used to equalize the stiffness of the front and back half of the terraced house by adjusting openable window part sizes.
- Adopt a masonry material model that includes strength degradation under repeated loading (e.g. see Srinidhi [38]) in combination with a cyclic or repetitive loading scheme. This will give insight into the residual capacity after multiple earthquakes.
- Run numerical analyses in the negative global x-direction. The capacity curve of the validated two-storey building was found to be asymmetric. Therefore, the structural potential of the structural might be different in the negative global x-direction.
- Investigate the potential of the structural window for variations within the terraced house building typology, e.g. by adopting the window sizes of the two remaining categories of terraced houses that were defined in section 2.1

Future studies could also investigate the potential of the structural window for other building typologies that were defined in section 2.1, e.g. detached and semi-detached houses.

Bibliography

[1] KNMI, "Aardbevingscatalogus geinduceerde bevingen," , 2018. URL https://www.knmi.nl/kennis-en-datacentrum/dataset/aardbevingscatalogus.

[2] Spetzler, J., and Dost, B., "Probabilistic Seismic Hazard Analysis for Induced Earthquakes in Groningen, Update June 2017," Tech. rep., KNMI, De Bilt, 2017. URL https://cdn.knmi.nl/system/readmore_links/files/000/000/408/original/20170615_Technisch_rapport_hazardkaart_Groningen_2017.pdf?1497511525.

[3] NEN, "Webtool expected response spectrum Groningen," , 2018. URL http://seismischekrachten.nen.nl/ers.php.

[4] NAM, "Totaal uit Groningen-gasveld gewonnen gas," , 2019. URL https://www.nam.nl/feiten-en-cijfers/gaswinning.html#iframe=L2VtYmVkL2NvbXBvbmVudC8_aWQ9Z2Fzd2lubmluZw.

[5] Rijksoverheid, "Kabinet: einde aan gaswinning in Groningen," , 2018. URL https://www.rijksoverheid.nl/onderwerpen/gaswinning-in-groningen/nieuws/2018/03/29/kabinet-einde-aan-gaswinning-in-groningen.

[6] Spetzler, J., Dost, B., and Evers, L., "Seismic Harzard Assessment of Production scenarios in Groningen," Tech. rep., Royal Netherlands Meteorological Institute, De Bilt, 2018. URL https://www.knmi.nl/over-het-knmi/nieuws/minder-gaswinning-groningen-minder-seismische-dreiging.

[7] NCG, "Halfjaar rapportage - december 2018," Tech. Rep. december, Nationaal Coordinator Groningen, 2019. URL https://www.nationaalcoordinatorgroningen.nl/onderwerpen/voortgangsrapportages.

[8] Crowley, H., Pinho, R., Polidoro, B., and Stafford, P., "Development of v2 Partial Collapse Fragility and consequence functions for the Groningen Field," Tech. Rep. November, NAM, 2015. URL https://www.sodm.nl/documenten/publicaties/2016/06/21/advies-sodm-winningsplan-groningen-2016.

[9] Krijgsman, H., "Krachten of verplaatsingen?" *Bouwen met Staal*, Vol. 255, 2017, pp. 34–39. URL https://www.abt.eu/bestanden/Afbeeldingen/Actueel/Publicaties/5721-1/Krachten_of_verplaatsingen_BORG_groningen_ABT.pdf.

[10] Dagblad van het Noorden, "Huiseigenaren Opwierde Zuid in Appingedam ontevreden met versterkingsmaatregelen," , 2017.

[11] NCG, "Residents of the neighbourhood Opwierde-Zuid in Appingedam prefer a new building to retrofitting of the existing building," , 2018. URL https://www.nationaalcoordinatorgroningen.nl/actueel/nieuws/2018/1/17/bewoners-opwierde-zuid-kiezen-voor-nieuwbouw.

[12] Sucuoglu, H., and Vallabhan, C., "Behaviour of window glass panels during earthquakes," *Engineering Structures*, Vol. 19, No. 8, 1997, pp. 685–694. doi:10.1016/S0141-0296(96)00130-7, URL https://www.researchgate.net/publication/222626013_Behaviour_of_window_glass_panels_during_earthquakes.

[13] Stepinac, M., Rajcic, V., and Zarnic, R., "Timber-structural glass composite systems in earthquake environment," *Journal of the Croatian Association of Civil Engineers*, Vol. 68, No. 03, 2016, pp. 211–219. doi:10.14256/JCE.1505.2015, URL http://casopis-gradjevinar.hr/archive/article/1505.

[14] Bilgin, H., and Korini, O., "Seismic capacity evaluation of unreinforced masonry residential buildings in Albania," *Natural Hazards and Earth System Science*, Vol. 12, No. 12, 2012, pp. 3753–3764. doi:10.5194/nhess-12-3753-2012, URL https://www.researchgate.net/publication/267763641_Seismic_capacity_evaluation_of_unreinforced_masonry_residential_buildings_in_Albania.

[15] Foraboschi, P., "Coupling effect between masonry spandrels and piers," *Materials and Structures/Materiaux et Constructions*, Vol. 42, No. 3, 2009, pp. 279–300. doi:10.1617/s11527-008-9405-7.

[16] Park, J., Towashiraporn, P., Craig, J. I., and Goodno, B. J., "Seismic fragility analysis of low-rise unreinforced masonry structures," *Engineering Structures*, Vol. 31, No. 1, 2009, pp. 125–137. doi:10.1016/j.engstruct.2008.07.021, URL http://dx.doi.org/10.1016/j.engstruct.2008.07.021.

[17] NEN, "NPR 9998 - Assessment of structural safety of buildings in case of erection, reconstruction and disapproval - Basic rules for seismic actions: induced earthquakes," Tech. rep., Koninklijk Nederlands Normalisatie-instituut, Delft, 2017.

[18] Huveners, E. M. P., "Circumferentially Adhesive Bonded Glass Panes for Bracing Steel Frames in Façades," Tech. rep., Technische Universiteit Eindhoven, Eindhoven, 2009. doi:10.6100/IR657800, URL https://pure.tue.nl/ws/files/3022741/200613161.pdf.

[19] Korswagen, P. A., Meulman, E., Longo, M., and Rots, J. G., "Light Crack Initiation and Propagation in Unreinforced Masonry Specimens Subjected to Repeated Loading Such as Earthquake Vibrations - Laboratory and Computational Analyses," Tech. rep., Delft University of Technology, Delft, 2018.

[20] Ravenshorst, G., Esposito, R., Schipper, R., Messali, F., Tsouvalas, A., Lourens, E.-M., and Rots, J. G., "Structural behaviour of a calcium silicate brick masonry assemblage: quasi-static cyclic pushover and dynamic identification test." Tech. rep., Delft University of Technology, Delft, 2016.

[21] Google, "Google Maps image of front facade of terraced house in Appingedam," , 2009. URL https://www.google.com/maps/place/Kastanjelaan+31,+9902+PJ+Appingedam/@53.3112308,6.8660649,3a,75y,196.89h,89.27t/data=!3m7!1e1!3m5!1sD-mihoudnEuQAgjQC-X6iw!2e0!6s%2F%2Fgeo2.ggpht.com%2Fcbk%3Fpanoid%3DD-mihoudnEuQAgjQC-X6iw%26output%3Dthumbnail%26cb_clien.

[22] Arup BV, "Groningen 2013: Implementation Study," Tech. rep., NAM, 2013. URL http://www.rijksoverheid.nl/documenten-en-publicaties/rapporten/2014/01/17/arup-rapport.html.

[23] Crowley, H., Polidoro, B., Pinho, R., and van Elk, J., "Framework for Developing Fragility and Consequence Models for Local Personal Risk," *Earthquake Spectra*, Vol. 33, No. 4, 2017, pp. 1325–1345. doi:10.1193/083116EQS140M, URL http://earthquakespectra.org/doi/10.1193/083116EQS140M.

[24] Google, "Google Maps images of selection of different front facade configurations of terraced houses in the province of Groningen," , 2019.

[25] Hakker, B., van Muijen, H., Reymers, H., Reitsma, A., and van Tol, A., *Jellema 4C: Omhulling - Gevelopeningen*, 1st ed., ThiemeMeulenhoff, Utrecht, 2000.

[26] Nieman, H., *SBR-referentie details woningbouw (studenten editie 2007)*, 6th ed., ThiemeMeulenhoff, Utrecht, 2007.

[27] Giardina, G., Marini, A., Hendriks, M. A. N., Rots, J. G., and Rizzardini, F., "Experimental analysis of a masonry façade subject to tunnelling-induced settlement," *Engineering Structures*, Vol. 45, 2012, pp. 421–434. doi:10.1016/j.engstruct.2012.06.042, URL http://dx.doi.org/10.1016/j.engstruct.2012.06.042.

[28] Barraza, J. A. C., “Numerical Model for Nonlinear Analysis of Masonry Walls,” Tech. rep., RWTH Aachen University, Aachen, 2012.

[29] Bournas, D. A., “Concurrent seismic and energy retrofitting of RC and masonry building envelopes using inorganic textile-based composites combined with insulation materials: A new concept,” *Composites Part B: Engineering*, Vol. 148, No. December 2017, 2018, pp. 166–179. doi:10.1016/j.compositesb.2018.04.002, URL https://doi.org/10.1016/j.compositesb.2018.04.002.

[30] van Wijnbergen, E., “Exploration and analysis of low-cost seismic retrofit measures to improve box-action for traditional brick masonry houses in Nepal,” Tech. rep., TU Delft, Amsterdam, 2016.

[31] Yi, T., “Experimental Investigation and Numerical Simulation of an Unreinforced Masonry Structure with Flexible Diaphragms,” Tech. Rep. February, Georgia Institute of Technology, 2004.

[32] Lourenco, P., “Computational strategies for masonry structures,” Tech. rep., TU Delft, Delft, 1996.

[33] Lagomarsino, S., Penna, A., Galasco, A., and Cattari, S., “TREMURI program: An equivalent frame model for the nonlinear seismic analysis of masonry buildings,” *Engineering Structures*, Vol. 56, 2013, pp. 1787–1799. doi:10.1016/j.engstruct.2013.08.002, URL http://dx.doi.org/10.1016/j.engstruct.2013.08.002.

[34] Esposito, R., “Tests for the Characterization of Replicated Masonry and Wall Ties,” Tech. Rep. April, Delft University of Technology, Delft, 2016. URL https://nam-feitenencijfers.data-app.nl/download/rapport/a71866d5-8ce8-4ef6-8b8a-8523bfc4bda6?open=true.

[35] Messali, F., Ravenshorst, G., Esposito, R., and Rots, J., “Large-scale testing program for the seismic characterization of Dutch masonry walls,” Tech. rep., Delft University of Technology, Delft, 2017. URL https://repository.tudelft.nl/islandora/object/uuid%3A7f4baaa0-b1d4-49ad-b41c-584f324c102e.

[36] Schreppers, G., Garofano, A., Messali, F., and Rots, J., “DIANA Validation report for Masonry modelling,” Tech. rep., DIANA FEA B.V., 2017.

[37] Xu, T., “Modeling the seismic response of a two-storey calcium silicate brick masonry structure with nonlinear pushover and time-history analyses,” Tech. rep., TU Delft, Delft, 2018.

[38] Srinidhi, B., “A Hyperbolic model for Degradation in Tension mode-I Fracture of Masonry,” Ph.D. thesis, Delft University of Technology, 2018.

[39] Chakrabarti, A., Menon, D., Sengupta, A. K., Central Public Works Department, and Indian Building Congress, *Handbook on seismic retrofit of buildings*, April, Narosa Publishing House Pvt. Ltd., New Delhi, 2008.

[40] American Society of Civil Engineers, *Seismic rehabilitation of existing buildings*, American Society of Civil Engineers, Reston, Viginia, 2007.

[41] CVW, VIIA, and BORG, “Groninger Maatregelen Catalogus,” , 2019. URL https://www.maatregelencatalogus.nl/.

[42] Huveners, E. M. P., Van Herwijnen, F., Soetens, F., and Hofmeyer, H., “Glass panes acting as shear wall,” *Heron*, Vol. 52, No. 1-2, 2007, pp. 5–29. URL http://heronjournal.nl/52-12/1.pdf.

[43] Ber, B., Premrov, M., Štrukelj, A., and Kuhta, M., “Experimental investigations of timber-glass composite wall panels,” *Construction and Building Materials*, Vol. 66, 2014, pp. 235–246. doi:10.1016/j.conbuildmat.2014.05.044.

[44] Ber, B., Sustersic, I., Premrov, M., Strukelj, A., and Dujic, B., “Testing of timber–glass composite walls,” *Structures and Buildings*, Vol. 168, No. SB7, 2015, pp. 500–513. URL https://www.icevirtuallibrary.com/doi/pdf/10.1680/stbu.13.00105.

[45] Bos, F., and Louter, C., “Mechanical modelling of in-plane loaded glass panes,” *Challenging Glass 2*, 2010.

[46] Haldimann, M., Luible, A., and Overend, M., “Structural Use of Glass,” Tech. rep., International association for bridge and structural engineering, Zurich, 2008.

[47] Laufs, W., and Luible, A., “Introduction on use of glass in modern buildings,” Tech. Rep. January, École Polytechnique Fédérale de Lausanne, Lausanne, 2003.